

TOWARD THE UNDERSTANDING OF COMPLEX BIOCHEMICAL SYSTEMS: THE
SIGNIFICANCE OF GLOBAL PROTEIN STRUCTURE AND
THOROUGH PARAMETRIC ANALYSIS

Except where reference is made to the work of others, the work described in this dissertation is my own or was done in collaboration with my advisory committee. This dissertation does not include proprietary or classified information.

Robert Moore

Certificate of Approval:

Holly Ellis
Associate Professor
Chemistry and Biochemistry

Douglas Goodwin, Chair
Associate Professor
Chemistry and Biochemistry

Evert Duin
Associate Professor
Chemistry and Biochemistry

German Mills
Associate Professor
Chemistry and Biochemistry

George Flowers
Acting Dean
Graduate School

TOWARD THE UNDERSTANDING OF COMPLEX BIOCHEMICAL SYSTEMS: THE
SIGNIFICANCE OF GLOBAL PROTEIN STRUCTURE AND
THOROUGH PARAMETRIC ANALYSIS

Robert Moore

A Dissertation

Submitted to

the Graduate Faculty of

Auburn University

in Partial Fulfillment of the

Requirements for the

Degree of

Doctor of Philosophy

Auburn, Alabama
August 10, 2009

TOWARD THE UNDERSTANDING OF COMPLEX BIOCHEMICAL SYSTEMS: THE
SIGNIFICANCE OF GLOBAL PROTEIN STRUCTURE AND
THOROUGH PARAMETRIC ANALYSIS

Robert Moore

Permission is granted to Auburn University to make copies of this dissertation at its discretion, upon the request of individuals or institutions and at their expense. The author reserves all publication rights.

Signature of Author

Date of Graduation

VITA

Robert Lee Moore was born to Robert Lynn Moore and Margaret Dale Moore on September 6, 1981. Robert graduated from the Alabama School of Mathematics and Science in Mobile, AL in 1998. From there, Robert attended Huntingdon College in Montgomery, AL where he earned Bachelor of Arts degrees in mathematics, chemistry, and cell biology in 2002. While at Huntingdon College, Robert was inducted into the Kappa Mu Epsilon mathematics honor society, Beta Beta Beta biology honor society, and Alpha Beta national honor society. Robert married his wife Emilia Anna Luśnia, whom he met at Huntingdon College, on July 19, 2003. Shortly after marrying, he began employment in the Department of Chemistry and Biochemistry at Auburn University as a lab technician for the general chemistry labs. Robert joined the graduate program in 2004 and began work on his Ph.D. in biochemistry.

DISSERTATION ABSTRACT

TOWARD THE UNDERSTANDING OF COMPLEX BIOCHEMICAL SYSTEMS: THE
SIGNIFICANCE OF GLOBAL PROTEIN STRUCTURE AND
THOROUGH PARAMETRIC ANALYSIS

Robert Moore

Doctor of Philosophy, August 10, 2009
(B.A. Chemistry, Huntingdon College, 2002)
(B.A. Cell Biology, Huntingdon College, 2002)
(B.A. Mathematics, Huntingdon College, 2002)

178 Typed Pages

Directed by Douglas Goodwin

Enzymes are a highly diverse set of macromolecules, and, given their size and biocatalytic significance, each is an extremely complex system to study. As such, many assumptions must be made to simplify these systems to a manageable level to study. Unfortunately, the more complex the system, the more simplifications need to be introduced. Most simplifications entail two different types of assumptions: structural assumptions, and parametric assumptions. Since catalysis is generally limited to a small region of the enzyme (the active site), most non-active site structures are ignored if there is no evidence for substrate binding or allosteric control. In regards to parametric analysis, the assumption is that as long as one variable is held constant, that variable will have the same effect on a system regardless of changes to other variables. Catalase-peroxidases provide an ideal system to analyze these assumptions. Although having an active site identical to monofunctional peroxidases, catalase-peroxidases have significant catalase activity. Differentiation between which catalytic cycle is utilized appears to be linked to the pH of the environment. The commonly held assumption was that by varying the pH at substrate-saturating conditions, the pH

optima of the two activities could be determined. Here, that assumption is dissected by varying pH and substrate concentrations simultaneously. This revealed substrate-dependent inhibition that had resulted in misidentification of the pH optima and possible misinterpretations of structural data. Another assumption was that by only providing the enzyme with the substrates required for one activity, the two different catalytic cycles could be studied and understood separately. Here, by placing the system in an environment where both activities could occur, it became clear that the two activities are synergistic and result in broadening the catalase pH range of the enzyme. Furthermore, the synergy of the two catalytic cycles rather than competition emphasized that the classical representation of catalase-peroxidase activity could not be true, leading to the proposal of a new mechanism. Previous studies have shown that an entire domain absent in monofunctional peroxidases is necessary for any catalysis in catalase-peroxidases. Here, by creating variants of residues 25 Å (and further) away from the active site in two hydrogen bonding networks at the interface of the two domains, the significance of these non-active site networks is shown to be as great as some of the active site structures.

ACKNOWLEDGMENTS

I could not begin to pretend that any of my achievements could have been possible without being influenced and surrounded by virtually innumerable, incredibly giving people. Listed here are only a few of those.

My advisor, Dr. Douglas Goodwin, has established the ideal setting for growing independent researchers. He is clearly conscientious about his role as a mentor, not only to aspiring scientists, but also to future mentors. Dr. Holly Ellis has taken time to preview and comment every manuscript I have written, and has appreciated as much as anyone my sarcasm and humor. Dr. Evert Duin has been of great assistance with EPR, and is a model of genuine friendliness. It is obvious that his role as an educator is not limited to his students, but encompasses who he is. I have shared many conversations with Dr. German Mills about my research, science, academia, and beyond - and in every one his passion is evident. I always walked away thinking how much fun it was to talk, and more inspired and passionate about my work.

My laboratory predecessors and contemporaries (Drs. Li, Varnado, Baker-Hartfield, and Cook) were always very giving and patient in training me, and seeing how they approached research and how they matured as scientists gave me references to place standards and expectations for myself. Dr. Carma Cook provided KatG^C and KatG^N data and the undergraduates Luke Powell and Rachel Williams assisted me in the pH profiling of KatG and preparation of the Y111A KatG mutant.

More personally, I absolutely must recognize my parents who opened every door they could possibly open for me, and never shut a single one.

My amazing wife, Emilia: no one has been more supportive of me than you. Everything I do, you are right beside me. I am blessed beyond measure. This work is dedicated to our sons Isen Benjamin and Montana Drew.

Style manual or journal used Biochimica et Biophysica Acta (together with the style known as “aums”).

Computer software used The document preparation package T_EX (specifically L^AT_EX) together with the departmental style-file `aums.sty`, Microsoft Excel for data analysis, GraphPad Prism 4.0c for graph preparations, Swiss-PdbViewer 3.7 and MegaPOV 1.2.1 for protein structures, ChemDraw 10.0 and WinDrawChem 1.6.2 for reaction schemes and molecular structures, and Microsoft Powerpoint 2003 and Gnu Image Manipulation Program 2.4.4 for image conversions.

TABLE OF CONTENTS

LIST OF TABLES		xii
LIST OF FIGURES		xiii
1 LITERATURE REVIEW		1
1.1 Proteins		1
1.2 Enzymes		2
1.2.1 Structural Features		4
1.2.2 Analysis Techniques		15
1.2.3 Therapeutics		37
1.3 Catalase-peroxidases		41
1.3.1 Reactive Oxygen Species		41
1.3.2 Monofunctional Catalases		43
1.3.3 Monofunctional Peroxidases		45
1.3.4 Catalase-peroxidases		48
2 COMPLEXITY OF KATG KINETICS REVEALED BY pH ANALYSIS		56
2.1 Introduction		56
2.2 Materials and Methods		57
2.2.1 Materials		57
2.2.2 Expression and Purification of wtKatG		57
2.2.3 Peroxidase Activity Assays		61
2.2.4 Catalase Activity Assays		61
2.2.5 Circular Dichroism Spectroscopy		62
2.2.6 pK_a Determination		62
2.3 Results		66
2.3.1 Kinetic Parameters for Peroxidase Activity of KatG		66
2.3.2 Kinetic Parameters for Catalase Activity of KatG		72
2.3.3 Kinetic Parameters and pK_{as}		76
2.4 Discussion		78
2.4.1 Optimal Peroxidase Activity and ABTS-dependent Inhibition		78
2.4.2 Different pH Optima for Binding and Activity in Catalase Cycle		82
3 PRESENCE OF REDUCING SUBSTRATES BROADENS CATALASE ACTIVITY pH RANGE		84
3.1 Introduction		84
3.2 Materials and Methods		85
3.2.1 Materials		85

3.2.2	Expression, Purification, and Reconstitution of <i>EcKatG</i>	85
3.2.3	Activity Assays	85
3.2.4	End-point Assays and UV-visible Spectra	86
3.3	Results	87
3.3.1	Effect of Reducing Substrates on Oxygen Production	87
3.3.2	Evaluation of Role of pH on Activation Effects	89
3.3.3	Effect of Reducing Substrate Presence on Reacted Enzyme Spectra	92
3.4	Discussion	95
4	GENERATION OF MIXED SPIN-STATE POPULATION VIA Y111A SUBSTITUTION	101
4.1	Introduction	101
4.2	Materials and Methods	103
4.2.1	Materials	103
4.2.2	Cloning	103
4.2.3	Expression and Purification	104
4.2.4	Absorption Spectra and Activity Assays	104
4.2.5	Stopped-flow	105
4.2.6	Magnetic Circular Dichroism	105
4.2.7	Electron Paramagnetic Resonance	106
4.3	Results and Discussion	106
4.3.1	UV-visible Absorption	106
4.3.2	Cyanide Binding	107
4.3.3	Magnetic Circular Dichroism	110
4.3.4	Electron Paramagnetic Resonance	113
4.3.5	Steady-state Kinetics	113
4.4	Discussion	115
5	COMPREHENSIVE ANALYSIS OF INTERDOMAIN INTERFACE SINGLE VARIANTS	120
5.1	Introduction	120
5.2	Materials and Methods	121
5.2.1	Materials	121
5.2.2	Cloning of R117A, R479A, D482A, and D597A	121
5.2.3	Expression and Purification	122
5.2.4	UV-visible Absorption Spectra and Activity Assays	122
5.2.5	Circular and Magnetic Circular Dichroism	123
5.2.6	Electron Paramagnetic Resonance Spectroscopy and Spin Quantification	123
5.3	Results	123
5.3.1	Mutagenesis, Expression, and Purification of KatG Interdomain Variants	123
5.3.2	UV-visible Spectroscopy	124
5.3.3	Magnetic Circular Dichroism	130
5.3.4	Electron Paramagnetic Resonance	130
5.3.5	Steady-state Kinetics	133
5.4	Discussion	133

6	SUMMARY	139
6.1	Assumption: pH-profiling at Saturating Substrate Concentrations	140
6.2	Assumption: Catalysis Can Be Differentiated by pH and Substrate Availability	141
6.3	Assumption: Global Features Play Structural Roles, Active Site Features Play Functional Roles	142
6.4	Conclusion	143
	BIBLIOGRAPHY	144

LIST OF TABLES

1.1	Examples of Non-heme Iron Cofactors.	7
1.2	Enzyme Commission Classes.	17
1.3	Antibiotic Classes.	40
2.1	Lowest Concentration of ABTS at Each pH Where Inhibition Was Observed.	70
2.2	Observed Kinetic Parameters for <i>E. coli</i> KatG Reducing Substrates.	74
2.3	Approximated Rate Constants for <i>E. coli</i> KatG.	79
4.1	Spectral Features of Ferric and Ferrous Wild Type and Y111A KatG.	109
4.2	Apparent Catalase Kinetic Parameters of Wild Type and Y111A KatG.	116
4.3	Apparent Peroxidase Kinetic Parameters of Wild Type and Y111A KatG.	116
5.1	Ratios of Various EPR Signals Observed in wtKatG and Variants.	132
5.2	Apparent Catalase Kinetic Parameters of wtKatG and Interdomain Interface Variants.	134
5.3	Apparent Peroxidase Kinetic Parameters of wtKatG and Interdomain Interface Variants.	135
5.4	Ratio of Catalase to Peroxidase Activity Relative to Wild Type.	138

LIST OF FIGURES

1.1	Heme.	9
1.2	Various Heme <i>b</i> Ligand Environments.	11
1.3	Effects of Ligands on Fe ^{III} <i>d</i> -electrons.	20
1.4	Electronic Transitions Observed in Heme Peroxidases.	22
1.5	Electron Paramagnetic Absorption.	23
1.6	EPR Absorption Derivatives.	25
1.7	Origin of MCD Signals: A-term.	27
1.8	Origin of MCD Signals: C-term.	29
1.9	Origin of MCD Signals: B-term.	30
1.10	Relative Concentrations of S, P, E, and ES During Reaction Progression.	33
1.11	Comparison of Catalase-peroxidase Active Site to Monofunctional Catalase and Peroxidases.	50
1.12	Identification of Interhelical Insertions and C-terminal Domain in Catalase-peroxidase.	51
1.13	Classic Catalase-peroxidase Scheme.	55
2.1	Peroxidase Cycle Scheme with pH Dependence.	58
2.2	Catalase Cycle Scheme with pH Dependence.	59
2.3	Initial Velocity of Peroxidase Activity Under Saturating Substrate Conditions.	67
2.4	Observed Peroxidase Kinetic Parameters Under Saturating ABTS Conditions.	69
2.5	Evidence of ABTS Inhibition.	70
2.6	Observed Peroxidase Kinetic Parameters Versus pH: Constant [ABTS].	71

2.7	Observed Peroxidase Kinetic Parameters Versus pH: Constant $[H_2O_2]$	73
2.8	Evidence of Protein Unfolding at Low pH.	75
2.9	Observed Catalase Kinetic Parameters Versus pH.	77
3.1	Effects of Reducing Substrate on Catalase Activity at pH 5.0.	88
3.2	Evidence of Peroxidatic Consumption of Reducing Substrates.	90
3.3	pH-dependence of Activation with ABTS Compared to Catalase and Peroxidase Activities.	91
3.4	Effect of ABTS on Apparent K_M for H_2O_2 at pH 5.0.	93
3.5	Effect of ABTS on Linearity of Catalase Initial Rates.	94
3.6	“Dead-end” Species Does Not Accumulate When ABTS Is Present.	96
3.7	A Proposed Scheme Accounting for Differentiation Between Catalase and Peroxidase Prior to Substrate Interaction.	98
4.1	Interactions Between the N-terminal BC Interhelical Loop and C-terminal Domain of KatG.	102
4.2	UV-visible Absorption Spectra of Native and Reduced Y111A KatG.	108
4.3	Stopped-flow Cyanide Binding Shows Two Distinct Species in Y111A KatG.	111
4.4	Prediction of Y111A KatG Ferrous Heme MCD Spectrum.	112
4.5	EPR Spectrum of Y111A KatG Compared to wtKatG.	114
4.6	Y111A KatG Catalase Activity.	117
4.7	Y111A KatG Peroxidase Activity.	118
5.1	Far-UV Circular Dichroism of wtKatG and Interdomain Interface Variants.	125
5.2	UV-vis Spectra of wtKatG, KatG ^N , and Interdomain Interface Variants: Ferric Heme.	126
5.3	UV-vis Spectra of wtKatG, KatG ^N , and Interdomain Interface Variants: Ferrous Heme.	127
5.4	MCD Spectra of KatG ^N , wtKatG, and Interdomain Interface Variants: Ferrous Heme.	128

5.5	MCD Spectrum of R479A KatG Ferric Heme Compared to wtKatG and KatG ^N	129
5.6	EPR Spectra of wtKatG, KatG ^N , and Interdomain Interface Variants.	131
5.7	Simulation of Y111A KatG Spectrum.	132

CHAPTER 1
LITERATURE REVIEW

1.1 Proteins

DNA is colloquially referred to as the blueprint of the cell. Comparing two organisms' DNA is a means of quantifying how closely related the two are, and has even been employed in determining approximately how long ago two species diverged from a common ancestor. Like a blueprint, DNA is only information. The true difference between organisms arises in their proteomes, or the protein content of the cell - a direct consequence of differences in DNA.

Proteins are a diverse group of biological molecules composed of a linear sequence of amino acids (directed by the DNA) joined by peptide linkage. This is known as the primary structure. Stretches of amino acids can form ordered structures such as alpha-helices, beta-sheets, and random (not to be confused with disordered) coils. These are known as secondary structural features. The tertiary structure is the overall three-dimensional fold of a protein that is achieved spontaneously after expression. Proteins that are composed of multiple subunits not linked through the primary structure are considered to have quaternary structure. Variations on all four structural levels give rise to the diversity in protein function.

The primary types of proteins based on their function are structural proteins, proteins involved in cell signaling, transport proteins, and catalysts or enzymes. Keratin in hair and fingernails, collagen in connective tissues, and tubulin in the cytoskeleton are examples of structural proteins. The role of antibodies in immune response and insulin in glucose uptake control are examples of cell signaling by proteins. Transport proteins include hemoglobin,

which is responsible for transporting oxygen in the blood, and ion channels, which are responsible for transporting ions across the cell membranes. Transport proteins are frequently grouped with cell signaling proteins, as transport and cell signaling often refer to the same thing, such as the ligand-gated ion channels involved in muscular action.

1.2 Enzymes

The catalytic group of proteins, or enzymes, is the working force of the cell, driving all the chemical reactions without which life would not occur. Enzymes have significant advantages over more common small-molecule catalysts. They do not require extreme temperatures, pH, or pressure to be fully functional, but instead are commonly adapted to function optimally at the conditions of an organism's ecosystem. In spite of functioning under commonly experienced conditions, enzyme action is still tightly controlled within the cell through expression regulation, post-transcriptional modification, and through substrate, inhibitor, or cofactor availability. Enzymes catalyze reactions with high specificity, frequently distinguishing between stereoisomers and recognizing entire molecules rather than just functional groups.

Enzymology is a major aspect of biochemistry. Understanding the mechanisms by which enzymes gain their specialization and how they undertake their task is crucial in our fundamental knowledge of the chemistry of life. Yet the diversity achieved in the specialization is astounding considering that proteins are all made from the same 22 amino acids and are all coded from DNA that has only a four-letter alphabet.

Inherent in any mechanistic elucidation is relating the function of the enzyme to its structure (internal effects) and environment (external effects). Knowledge of the structure can reveal electronic, chemical, and steric information regarding an enzyme's active site (the site where activity occurs) and how it translates into function. It is also not uncommon to study what is known as second-sphere effects, that is, the role of amino acids not inside the active site but still in proximity to or in contact with active site amino acids. Attempting to relate structural information from sites on the enzyme distant from the active site to

function is more difficult and rarely observed in literature. Still, distant features are clearly significant. Small molecule active site mimics rarely demonstrate catalytic ability comparable to a full enzyme, and early life organisms could ill-afford tying up so much energy and resources in developing large molecules if smaller molecules could have sufficed. Learning to relate features seemingly distant from the relevant portions of an enzyme to its function is a daunting, but crucial step in enzymology.

The scope of external effects on function is even broader than that of the internal effects. The presence of substrates, inhibitors, and cofactors all have obvious roles and are typically the first to be evaluated in a new characterization. Parameters not directly involved in the overall reaction, however, frequently are just as important. For example, temperature can affect folding and stability of an enzyme, and pH can affect the protonation of active site acids or bases as well as possible pH-induced structural changes. It is common to study most of these parameters one variable at a time, but this assumes that the effects of the variables are independent of each other (i.e., that varying A will not change the effects of B on function). This is indubitably an oversimplification of external effects that can lead to many pitfalls, but due to the large number of environmental parameters, it is possibly an inevitable simplification. With current techniques, even varying two parameters such as pH and substrate concentration is extremely time intensive to get sufficient data points. The more complex the system gets (multiple substrates, multiple functions, more parameters to vary), the time required to eliminate this assumption grows exponentially. This is not to say that there has been no attempt to resolve this disparity between assumption and reality. Much has been progressed in methods of data collection and analysis of multisubstrate systems and pH effects, such as the efforts of W. W. Cleland [1]. Still, the application of this progress could stand to be propagated in practice more widely than it has been, and needs to be further developed to account for more variables.

In order to increase our ability to relate the function of an enzyme to its internal and external affecters, we will first lay the groundwork by looking in more depth at general structural features and enzymological analysis techniques. From there, we will consider a

model of a complex biochemical system, the multi-functional catalase-peroxidase (KatG), and demonstrate how limited parametric analysis has led to misidentification of KatG functional characteristics and how features in the global structure are as crucial to activity as many active site features.

1.2.1 Structural Features

Active Sites

The region of the enzyme where activity occurs is referred to as the active site. The minimal requirements of an active site are a substrate recognition and binding mechanism and a mechanism for catalytic activity. Both of these are typically achieved by the arrangement and identity of amino acids inside the active site.

The current theory of substrate binding is called the “induced-fit model”. A flexible active site will interact with a substrate to optimize binding upon interaction. This can lower the activation energy needed for the reaction by binding the substrate in a conformation closer to the transition state, by stabilizing the transition state through polar interactions, decreasing entropy by properly orienting the substrate for reaction, or by providing an alternate pathway that may not be available without the presence of a catalyst.

Once binding has occurred, the reaction can occur via acid-base catalysis, covalent catalysis (where the substrate is temporarily covalently attached to the enzyme), by bringing molecules together that would be less likely to find each other in solution, or by using cofactors. Most of these reactions can occur in solution chemistry; but by using an active site, the enzyme decreases the concentration needed and effectively eliminates any variability in collision orientation and kinetic energy.

Cofactors

Some enzymes require the presence of certain molecules called cofactors for activity, and use them for the transferring of functional groups or electrons. The role of the cofactor is dependent upon how it is bound or interacts with the enzyme and the structure of the

active site around. Cofactors that are loosely bound are called coenzymes and those that are tightly bound are called prosthetic groups. Although the boundary between loosely and tightly bound is fuzzy, a simplified definition is tightly bound cofactors are those that cannot leave the active site once incorporated. Some prosthetic groups are even covalently bound to the enzyme. An enzyme that requires a cofactor that has yet to associate is an apoenzyme. Conversely, an enzyme with an incorporated cofactor is termed holoenzyme.

Cofactors are divided into two categories, non-metallo or organic cofactors and metallo cofactors. Many organic cofactors are vitamins (such as biotin) or use vitamins as precursors (such as FAD from B₂ or NAD⁺ from B₃). ATP and S-adenosyl methionine are common organic cofactors that are not vitamin derivatives. Metallo cofactors are metal ions that can be either directly ligated to the enzyme or have an organic component that also interacts with the enzyme. This category of cofactors is highly variegated from mononuclear centers such as the iron in Rieske dioxygenases [2], to binuclear centers (both homonuclear [3] and heteronuclear [4]), to metal clusters (such as the iron-sulfur clusters found in numerous enzymes [5] or the large FeMo-co clusters in nitrogenases [6]), and to the large class of tetrapyrrole-based metallo cofactors [7] including the porphyrins (such as iron-containing hemes), the nickel-containing F₄₃₀, the cobalt-containing cobalamin, and the magnesium containing chlorophylls.

The identity of the cofactor can frequently be used to determine part of the function or mechanism of an enzyme, but even those with nearly exclusive roles cannot be assured of that role without investigation. For example, ATP is commonly used as an energy source during a reaction by transferring a phosphate group. In the biosynthesis of another cofactor, S-adenosyl methionine, ATP transfers the adenosine moiety [8]. Similarly, S-adenosyl methionine is most associated as the methyl donor cofactor for methyltransferases, but it also has biosynthetic precursor roles and is a source of 5'-deoxyadenosyl radicals used in the synthesis of L-methionine and 5'-deoxyadenosine [9].

Metallo cofactors can hardly be considered to have “exclusive” roles like many organic cofactors. The nature of the d-orbitals in transition metals, particularly, allows for multiple

oxidation states and a broad range of reduction potentials - both of which are primarily determined by the ligand environment. The major advantage transition metals (especially iron, copper, and manganese) have is the ability to catalyze oxygen requiring reactions that would be spin-forbidden with most organic compounds or cofactors. Molecular (or di-) oxygen exists in a triplet ground state, that is, two unpaired electrons in antibonding orbitals; but most organic compounds exist in the singlet ground state. This parity problem is fortuitous in that it prevents oxygen from spontaneously oxidizing all organic compounds it encounters, but is also the reason that nature requires transition metals that can reach multiple oxidation states and reduction potentials to aid in the catalysis of many essential biochemical reactions.

Iron is possibly the most versatile of these transition metals cofactors. A summary of non-heme iron centers and some of the representatives and reactions catalyzed is shown in Table 1.1 [2–6, 10–13]. Table 1.1 lists only resting oxidation states, but $\text{Fe}^{\text{IV}}=\text{O}$ (ferryl iron) is also seen in many intermediates. Reduction potentials for the various cofactors can range from as low as -500 mV in 2Fe2S ferredoxins [13] to as high as 1.1 V in the diiron(III) intermediate in toluene/*o*-xylene monooxygenase hydroxylase [3], illustrating how broad the electronic states are that iron and iron derived cofactors can reach.

Heme iron is distinct from other iron cofactors in that it contains an organic component in the form of a porphyrin ring. This supplies the iron with four nitrogen ligands and leaves two iron binding sites available for ligation by the protein, solvent, or substrate. Oxidation states are stabilized and reduction potentials are set by the identity of the heme, the nature of the protein ligand and associated amino acids, and the interactions of the protein with the porphyrin itself.

Although many other forms exist, the three most abundant forms of heme are heme *a*, heme *b*, and heme *c* (Figure 1.1). Other types of heme vary in more positions than the three shown in Figure 1.1. Heme *b* is the most widely used in nature, and is the cofactor used by the model system catalase-peroxidase that we will be studying further on. The differences between heme *a* and *b* occur at the R₁ and R₃ position. In both cases, the heme

Cofactor	Ligands	Ox. St.	Representative	Reactions
Fe	2His/1CO ₂	II	extradiol cleaving catechol dioxygenases	oxidative ring cleavage
			Reiske dioxygenases	arene hydroxylation
			α -ketoglutarate dependent enzymes	demethylation, hydroxylation, desaturation, ring reactions, epimerization
			pterin-dependent enzymes	monohydroxylation of aromatic amino acids
		II/III	sulfur oxygenase reductase	$S \longrightarrow SO_3^{2-} + HS^-$
			Hpp epoxidase	oxidative cyclization
	3His	II	cysteine dioxygenase	cysteine \longrightarrow cysteine sulfinic acid
	3His/1CO ₂	III	superoxide dismutase	$O_2^{\cdot-} \longrightarrow O_2 + H_2O_2$
Fe-Fe	2His/4CO ₂	II/II	hydroxylase	arene hydroxylation
Fe-Mn	2His/4CO ₂	II	class 1c ribonucleotide reductases	oxidation and electron transfer
2Fe2S	4Cys	II/III	ferredoxins	electron transfer
	2His/4Cys	II/III	Reiske proteins	electron transfer
4Fe4S	4Cys	II/III	ferredoxins	electron transfer
	3Cys	II/III	quinolate synthase	condensation
7FeMo9S	1His/1Cys	II/III	nitrogenase	$N_2 \longrightarrow NH_3$

Table 1.1: **Examples of Non-heme Iron Cofactors.**

a functional groups are more electron withdrawing than those on heme *b* (hydroxyfarnesyl is a long chain hydrocarbon), increasing the reduction potential of *a*-type hemes. Heme *c* differs from heme *b* by becoming covalently attached to the protein via two thioether linkages at the proximal carbons of the R₁ and R₂ vinyl groups. This covalent linkage is believed to primarily serve as structural support to the protein; however, given the same axial ligand set, heme *c* reduction potentials span a broader range than heme *b* [15, 16]. This may be due to the rigidity with which the heme is held affecting the interaction between the iron and proximal (typically histidine) ligand. Forcing the heme into specific positions or shapes would allow the protein to tune the reduction potential more specifically, which would be advantageous in the primary role of electron transfer in heme *c* containing proteins (cytochromes *c*).

Heme *b* is a prime example of how protein interactions affect the versatility of the cofactor, and also is the cofactor of the model enzyme KatG that this research is focused around. Heme *b*-containing proteins perform sensing or transport of O₂, NO, and CO, electron transport, heme transport, and a variety of metabolic and redox reactions. This is a direct result of the wide variety of protein folds (at least 20), heme anchoring residues, heme face interacting residues, heme ligands, and extended ligand environments [17]. For example, the propionate groups frequently form salt-bridges with arginines, but lysines, histidines, tyrosines, and even serines, threonines, and backbone amines can all be utilized to hold the heme propionate.

Even more influential on setting the reduction potential of the iron are the heme face interacting residues and the axial ligands. Figure 1.2 shows a sample of the various types of heme *b* ligand environments. The more anionic in nature the axial ligand is, the lower the reduction potential of the iron will be [16, 26, 27]. From most anionic to least would be the tyrosinate ligand in catalases, followed by the thiolates observed in the P450 cytochromes, then the histidine-aspartate couple in peroxidases, and finally the neutral histidine in the globin proteins [27]. The low reduction potential in catalases and peroxidases stabilizes higher oxidation states, which are used in their reactions with hydrogen peroxide. On the

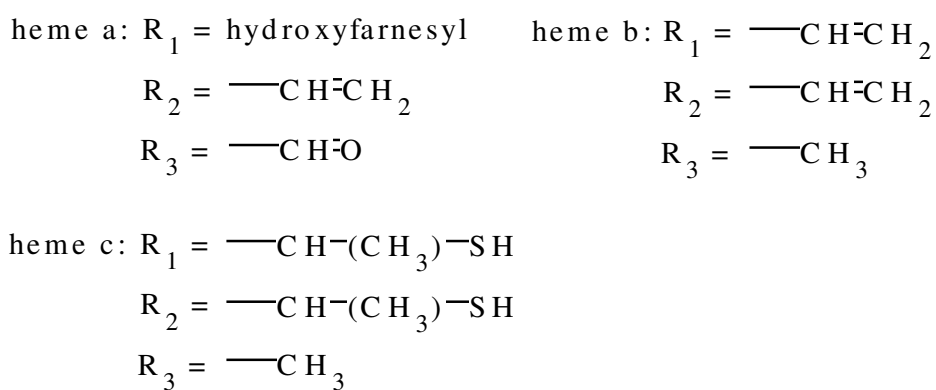
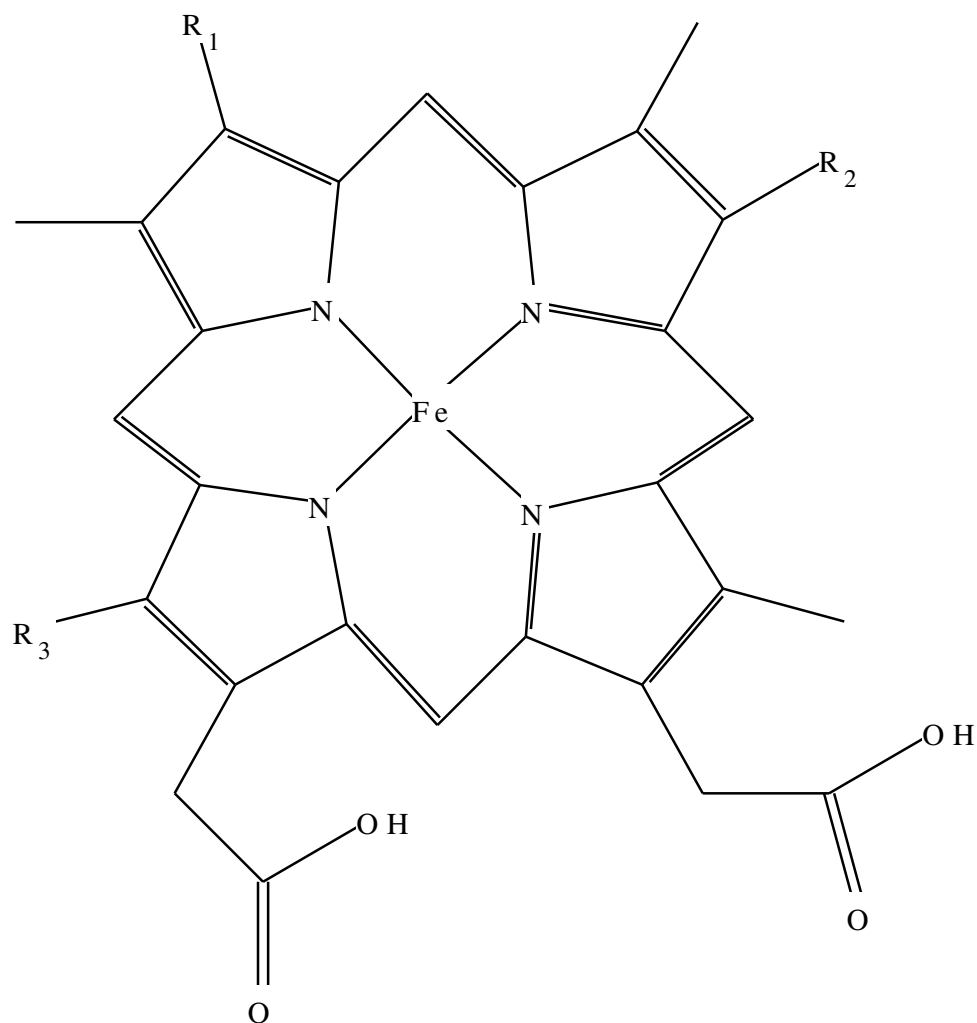


Figure 1.1: **Heme**. Structures were retrieved from the PubChem Public Chemical Database using the following CID numbers in the chemical search: heme a - 5288529, heme b - 4973, heme c - 25202875 [14].

other hand, the higher reduction potential in the globin proteins destabilizes the higher oxidation states and results in Fe^{II} as being the native state for hemoglobin and myoglobin and allows for the transport of dioxygen. Oxidation of the heme iron to Fe^{III} even converts hemoglobin to methemoglobin, increasing the dissociation constant for O_2 to the point that it is considered incapable of binding oxygen, thus interfering with its role of oxygen transport [28].

In spite of being able to identify relationships between the identity and ligand environment of cofactors with their chemical and electronic properties (as exemplified particularly by the hemoproteins), knowledge of an active site and cofactor is rarely sufficient to predict precisely the reaction catalyzed. Even the peroxidase family of proteins, which all undergo the same *type* of reaction and follow the same general reaction scheme, metabolize a wide variety of substrates that are often specific to individual members of the family. This is the limitation of analyzing active sites alone, and again reemphasizes the need to determine the roles of more distant enzyme features in catalysis.

Domains

Protein domains are discrete folding units of approximately 50 to 200 amino acids that are spatially distinct in the three-dimensional structure [29–32]. Many proteins are not large enough to have multiple domains, but others are so large that without multiple domains the folding time would become excessive. By having stretches of amino acids that fold spontaneously and independently of other sequences in the primary structure, a protein can fold much more rapidly.

Domains are often the functional units of a protein, like organelles are the functional units of the cell and organs are the functional units of a body [33]. Although being treated as functional units, domains are categorized based on structural similarities. Interestingly enough, not all similar domains share high sequence similarity, and not all those that share high sequence similarity have the same function. In light of these, analysis of protein domains is the source of many evolutionary studies [29, 31, 32].

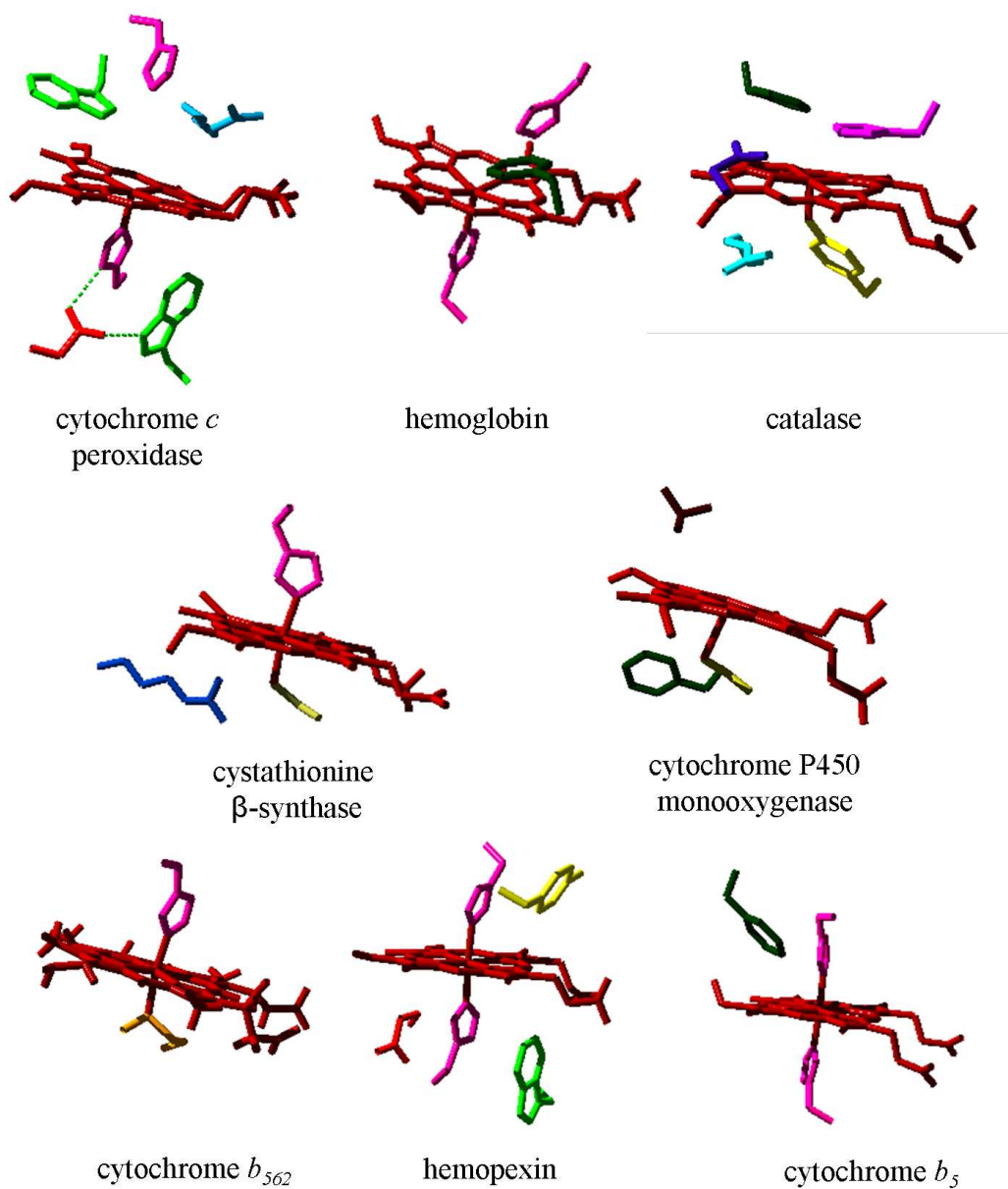


Figure 1.2: **Various Heme *b* Ligand Environments.** All structures have propionate groups oriented to the right. Amino acids are coded to the following color scheme: H - pink, R - light blue, W - light green, D/E - red, F - dark green, Y - yellow, N - dark blue, C - tan, T - brown, M - orange. Structures were taken from the following PDB accession numbers: cytochrome *c* peroxidase - 2CYP [18], hemoglobin - 1A3N [19], catalase - 7CAT [20], cystathionine β -synthase - 1JBQ [21], cytochrome P450 monooxygenase - 2BVJ [22], cytochrome *b*₅₆₂ - 1QPU [23], hemopexin - 1QHU [24], cytochrome *b*₅ - 1EUE [25].

Some domains are well-characterized. Most notably are those that appear with high frequency such as the zinc finger domains responsible for binding DNA [32, 34], or domains observed in well-characterized metabolic pathways such as the TIM-barrel in triosephosphate isomerase in the glycolytic pathway.

The zinc finger domain is the most prevalent domain in eukaryotes. The domain sequence is only about 30 amino acids in length, and being so small, the role of nearly all of the amino acids is known. It is an example of a domain where both sequence and structure are highly conserved in spite of such wide species distribution. The structure contains two anti-parallel β -strands followed by an α -helix, with a hydrophobic and an aromatic residue working concomitantly with the zinc-binding to stabilize the fold. The zinc is coordinated by four residues, most commonly two cysteines and two histidines, with the alternative having the C-terminal histidine replaced by a cysteine. Zinc finger proteins have multiple repeats of the zinc finger domain, and, when in complex with DNA, the α -helices fit into the major groove. The identity of the amino acids on the α -helices determine what sequence of DNA will be recognized [34]. The understanding of zinc fingers has progressed to the point that it has been proposed that by choosing the order of zinc fingers in a protein, one can engineer proteins to recognize desired DNA sequences [34, 35]. The structure of zinc fingers appear to be ideal for DNA interactions and it is unsurprising that these domains are commonly associated with transcription regulators. More recently, however, efforts are being made to better characterize the protein-protein interactions of zinc finger domains, such as the zinc finger protein FOG1 (Friend Of GATA1) that uses four of its nine fingers to interact with the GATA1 transcription factor [36, 37].

The TIM-barrel domain is named for the enzyme in which it was first characterized (triosephosphate isomerase). Consisting of eight α -helices and eight parallel β -strands, it is the most common domain in all living organisms, found in approximately 10% of all enzymes. The SCOP database (a structural database that will be addressed during the discussion of bioinformatics below) recognizes 33 different superfamilies that share this domain [38]. Eight of these are indicated to share a similar phosphate binding site, but

variations extend all the way to the Fe-S containing radical SAM enzymes, cobalamin requiring enzymes, copper homeostasis CutC protein, luciferases, and many others. Our current understanding of TIM-barrel proteins actually stems from the widespread utilization of the fold. Although there is very little sequence similarity among different superfamilies, the highest sequence conservation within a superfamily occurs in association with the β -strands. This is due to a clustering of the amino acid side chains stabilizing the core of the protein. The clustering locations are conserved in all TIM-barrel proteins, even though the sequence identity is not [39]. The loops connecting the ends of the β -strands to the helices typically carry conserved catalytic residues and form the active site [40–42].

The extent of our knowledge of the global features of zinc fingers and TIM-barrels is directly linked to the small size of the zinc fingers and the prevalence in nature of both domains. Zinc fingers are the smallest folding motifs that behave as actual domains. As the size increases, so does the complexity. Even with the widespread distribution of TIM-barrels, the α -helices have gone largely untouched in the literature - yet they compose the majority of the domain sequence. Most domains are large like the TIM-barrels, yet a scan of the SCOP database would reveal that most domains are unique to a single protein. In these cases, large-scale comparisons cannot be performed, such as those used to identify the clustering patterns in TIM-barrel proteins. The large sizes and limited comparable examples are what make studying the global features of domains so arduous and potentially unfruitful. Multidomain enzymes, however, can provide insight into global structure/function relationships.

Multidomain enzymes are believed to arise from the fusion of two or more enzyme precursors. These commonly appear to be the result of a gene duplication event, but this is not always the case. There are many known benefits to having multiple domains in an enzyme. One example of multidomain proteins has already been considered in the zinc finger proteins. Another benefit is that each domain could bind different substrates required for activity, such as the PEP-binding TIM-barrel domain and nucleotide binding domain of pyruvate kinase [43]. Pyruvate kinase also has a third domain that binds allosteric regulators

[44]. Multiple domains can also serve to protect reaction intermediates or bring catalytic sites into close proximity to prevent the release of product prior to its next metabolic step, such as seen in the enzyme TrifGART in purine synthesis in higher eukaryotes [45]. By being covalently linked through the primary sequence, multiple domains impart structural stability to each other and have the potential to alter each others structures from what they would have been isolated in solution [46]. By asking whether a specific task carried out by a multidomain enzyme could still be performed as efficiently if the domains were separated, and by analyzing the effects that the interdomain interfaces have on structure and function, one can make substantial strides in correlating global structure to function.

Post-translational Modifications

Post-translational modifications (PTMs) of proteins are not uncommon. Many modifications are seen regularly, such as the formation of disulfide bridges between cysteines or the addition of a lipid to an amino acid. The main categories of PTMs are the addition of a functional group (i.e.: methylation of a lysine or arginine, converting the carboxyl moiety at the C-terminus to an amide, attachment of heme *c*), changing the nature of an amino acid (i.e.: arginine to citrulline), and structural changes (i.e.: sulfide bridges, proteolysis) [47].

The difficulty PTMs pose to enzymology is that the genetic sequence cannot be used to predict PTMs, even though it is used frequently to predict the protein sequence. Since PTMs can only be found empirically, there will always be the possibility of encountering modifications that are not yet described; but setting out in search for a PTM would be wasteful in terms of time and resources. Instead, PTMs are usually discovered during regular protein analyses, however many approaches do have potential pitfalls requiring confirmation from an array of approaches. Some PTMs will affect the molecular weight of a protein through either the addition of a functional group or the removal of some part of the protein. These can be detected in any sort of size analysis such as (in increasing usefulness) some size-based chromatographic techniques, some electrophoretic techniques, or

bio-mass spectroscopy. Similarly, covalent modifications could affect the apparent molecular weight and would produce unexpected mass fragments in hard (molecule fragmenting) mass spectroscopy. Possibly the most straightforward method of detecting a PTM is through electron density mapping during X-ray crystallography. As this produces an actual image of the protein, PTMs can be observed directly. The pitfall of hard mass spectroscopy and X-ray crystallography is that they have the potential to induce covalent modification, reinforcing the need for corroboration from other techniques.

Once a PTM is observed, the next step is to deduce its role in the protein. Some PTMs are obvious and well-described, particularly those known to act as cell signalers to direct the protein to its location in the cell. Others may be more ambiguous, such as the role of the disulfide bridge. It may serve only a structural role, or the highly oxidized nature may play a role in catalysis or cofactor regeneration. Novel PTMs are even more difficult to assign a role as there is not always a good comparison in the existing literature. We will observe one such novel PTM in our model enzyme.

1.2.2 Analysis Techniques

Bioinformatics

Bioinformatics is a useful "first step" in enzymology. Essentially, it is the process of utilizing databases of information to compare a given enzyme under investigation to other studied enzymes in order to identify common and unique features, establish trends, make functional or structural predictions, or determine evolutionary relationships. We have already considered an example of the use of bioinformatics with the discovery of the side chain clustering in the β -strands of TIM-barrels. The clustering commonality was identified by applying graph theory algorithms to the structures of 36 TIM-barrel proteins that shared less than 10% sequence identity with any other protein in the data set [39]. Here we will survey some of the most common databases and applications including enzyme classification and nomenclature, structural classifications and databases, and sequence alignments.

The standard nomenclature system for enzymes is derived from the reaction which is catalyzed. Each enzyme is assigned a four-component Enzyme Commission (EC) number, the first component describing the main class of reaction catalyzed (Table 1.2). The second two components are the sub-class and the sub-sub-class, each specifying in more detail the reaction catalyzed. For example, the sub-class of oxidoreductases in most cases specifies the electron donor in the reaction and the sub-sub-class specifies the electron acceptor, with the exceptions being sub-classes 1.11.- (peroxide as acceptor) and 1.15.- (superoxide as acceptor).

While knowing the EC number of an enzyme is not all that valuable by itself, ExPASy (<http://www.expasy.ch/>) is a proteomics database where the EC number can be used to cross-reference many valuable tools. Using ENZYME database, for example, a user can access the list of all of the enzymes that share the same sub-sub-class for any comparison purpose. Basic information can be obtained about cofactors and substrates. Each enzyme has links to the UniProt database where sequences of that enzyme from specific organisms can be found, and links to the journal database PubMed to search the literature on the enzyme.

With the IUPAC nomenclature of enzymes being completely based on function, the EC number is the exclusive function-based classification system. Structural-based classifications are not as unified, resulting in two primary classification systems: Structural Classification of Proteins (SCOP) and Class Architecture Topology Homology (CATH). The main differences between the two classification systems are the treatment of domains containing both α -helices and β -sheets, and an extra layer of architectural classification in the CATH system. There are also other structural databases that can evaluate proteins and suggest structural neighbors, such as Families of Structurally Similar Proteins (FSSP) and Vector Alignment Search Tool (VAST). These rely on the protein databank (PDB) for their comparisons. PDB is a database where researchers can upload solved protein structures and other researchers can download the 3D structure for their own viewing and analysis. PDB entries include

EC number	Class	Reaction type
1.	Oxidoreductase	oxidation-reduction reactions
2.	Transferase	functional group transfers
3.	Hydrolase	hydrolysis reactions
4.	Lyase	double bond formations through functional group elimination
5.	Isomerase	isomerization reactions
6.	Ligase	bond formation requiring ATP hydrolysis

Table 1.2: **Enzyme Commission Classes.**

the downloadable structure, the techniques used in the structure determination along with associated publications, and both SCOP and CATH classifications.

The classic technique in bioinformatics in its application to enzymology is sequence alignment. Since the first protein sequence in 1955 [48] and the first complete DNA sequence of a bacteriophage in 1977 [49], sequencing of proteins and DNA is now commonplace, and massive databases exist that can be utilized for alignments. Aligning sequences of proteins or DNA can reveal conserved residues (and, if predicted from the sequence, conserved secondary structural elements) and establish evolutionary proximity. Two of the most common alignment tools are the Basic Local Alignment Search Tool (BLAST) and Clustal. With BLAST, a user may enter a nucleotide or amino acid sequence and have it compared to all existing sequences within the database of the users choosing. This provides the user with closest matches and is particularly useful for identifying evolutionary relationships. Clustal allows for the entry of multiple sequences to be uploaded and aligned. This is particularly useful for comparing enzymes from different species or closely related enzymes to identify their similarities and differences.

Instrumentation

Clearly, much can be learned from bioinformatic approaches to enzymology, but in order to fill the databases the data first must be accumulated. Also, the information gained from bioinformatics must be verified experimentally. For both reasons it is essential to have a belt full of tools for studying enzymes directly. There is such a wide array of instruments and techniques that can be used to study enzymes that an exhaustive review would be excessive. Instead, we will survey those most applicable to the research presented here, in particular the spectroscopic and kinetic approaches.

UV-visible spectroscopy has many applications in enzymology. A universal application is estimating protein concentration based on the absorbance of tryptophan, tyrosine, and cysteine near 280 nm [50]. In regards to heme-containing enzymes, such as catalase-peroxidases, it is particularly useful. There are a handful of electronic transitions available

within the porphyrin or from the porphyrin to the iron, all of which are very sensitive to the oxidation state of the iron and its ligand environment.

If we consider solitary Fe^{III} , the 5 d orbital electrons are degenerate and each orbital is occupied by a single electron. In the presence of ligands, however, the on-axis orbitals (those that lie on the axis between the metal and ligand) will be destabilized relative to those that are off-axis due to electron repulsion. Ligands that destabilize the on-axis orbitals to such a degree that the electron pairing energy is less than the energy required to place an electron in a destabilized orbital (or splitting energy) are called strong-field ligands. Ligands that do not split the energy levels so severely are called weak-field ligands. In the presence of a weak field ligand, Fe^{III} has a 5/2 spin, or high spin. In the presence of strong field ligands, it will be 1/2 spin, or low spin (Figure 1.3). In heme proteins, two sets of degenerate orbitals (on- and off-axis orbitals) do not sufficiently describe the system, as the porphyrin nitrogens are not equivalent to the axial (z -axis) ligands and are usually closer, destabilizing the $d_{x^2-y^2}$ orbital further. Also, the conjugation of the porphyrin slightly destabilizes the d_{π} (d_{xz} and d_{yz}) orbitals relative to the d_{xy} orbital.

In UV-visible absorption, an electron is excited by a photon from a ground energy state (E_0) to an excited energy state (E_1). The most basic example would be an electron in the π (bonding) molecular orbital of ethene ($\text{H}_2\text{C}=\text{CH}_2$) excited to the π^* (anti-bonding) molecular orbital. This transition requires energy equivalent to a photon with a wavelength near 170 nm. This amount of energy is generally too high for practical purposes; but the more conjugated a system is, the lower the energy requirement and absorption will occur at higher wavelengths. The porphyrin of heme is highly conjugated, and the available transitions in peroxidases can be seen in Figure 1.4. The Soret (γ) absorption band requires the most energy (thus being observed at the lowest wavelengths) and is the most intense signal in a heme spectrum. The Soret absorption band of free heme occurs at 380 nm. When incorporated in a protein, the absorption will occur at higher wavelengths. The charge transfer (CT) bands are observed when a porphyrin electron is excited into one of the e_g orbitals of the iron. These are not expected to be observed in low-spin systems

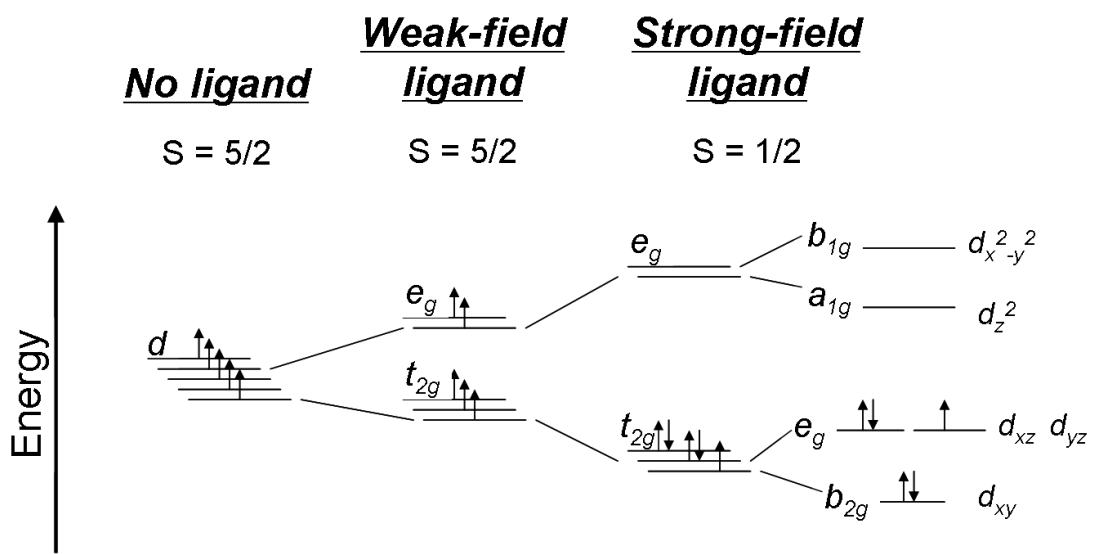


Figure 1.3: Effects of Ligands on Fe^{III} d -electrons.

and are usually too weak to see when the iron is in the ferrous state. The characteristic absorption bands for KatG in its resting state occur at 408 nm (Soret), 502 nm (CT2), and 629 nm (CT1) [51].

The main advantage of UV-visible spectroscopy is how quickly data can be obtained. Furthermore, the protein environment (such as buffer identity, pH, and temperature) can be varied or set at the investigators choosing. In regards to heme proteins, general conclusions about the oxidation and spin state of the heme iron can be arrived at quickly without consuming a large amount of protein. UV-visible spectroscopy can be utilized for kinetic measurements as well. If the substrate or product of catalysis is an absorbing species, it can be monitored to measure the velocity of the reaction directly. Also, by monitoring formation of heme intermediates, individual rate constants can be measured.

The primary disadvantage of UV-visible spectroscopy is the lack of detailed information that can be extracted from a heme spectrum. If the heme iron is high-spin, is the sixth coordination site open or is it occupied by a weak-field ligand? If it is low-spin, what is the identity of the axial ligand? The charge transfer bands and α and β bands are weak and can be easily obscured by light scattering. The heme absorption bands are broad enough that the presence of multiple species in solution are difficult to distinguish from each other, if possible at all.

One way to address some of these shortcomings is by using a spectroscopic technique called electron paramagnetic resonance (EPR). The basic premise behind EPR is that when a paramagnet (such as an unpaired electron) is placed in a magnetic field, the magnetic moment of the electron can be either aligned with the magnetic field ($m_s = +1/2$) or against the magnetic field ($m_s = -1/2$). This results in an energy difference between the two possible states for that electron and can be defined in terms of magnetic field strength:

$$\Delta E = g\beta\mathbf{B} \tag{1.1}$$

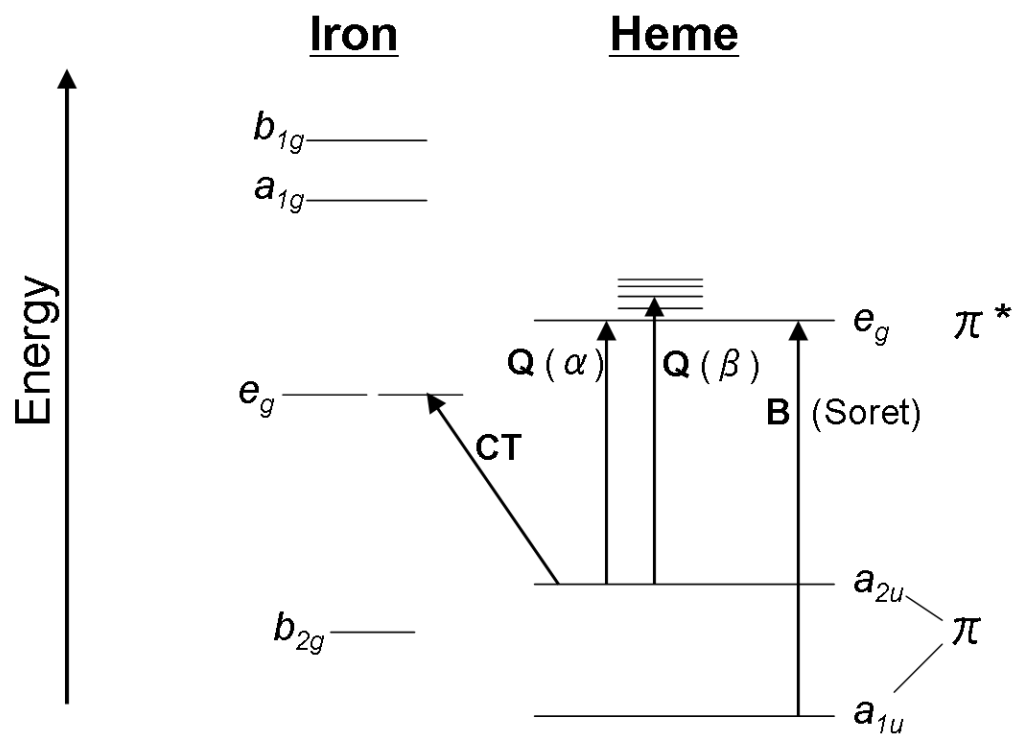


Figure 1.4: **Electronic Transitions Observed in Heme Peroxidases.**

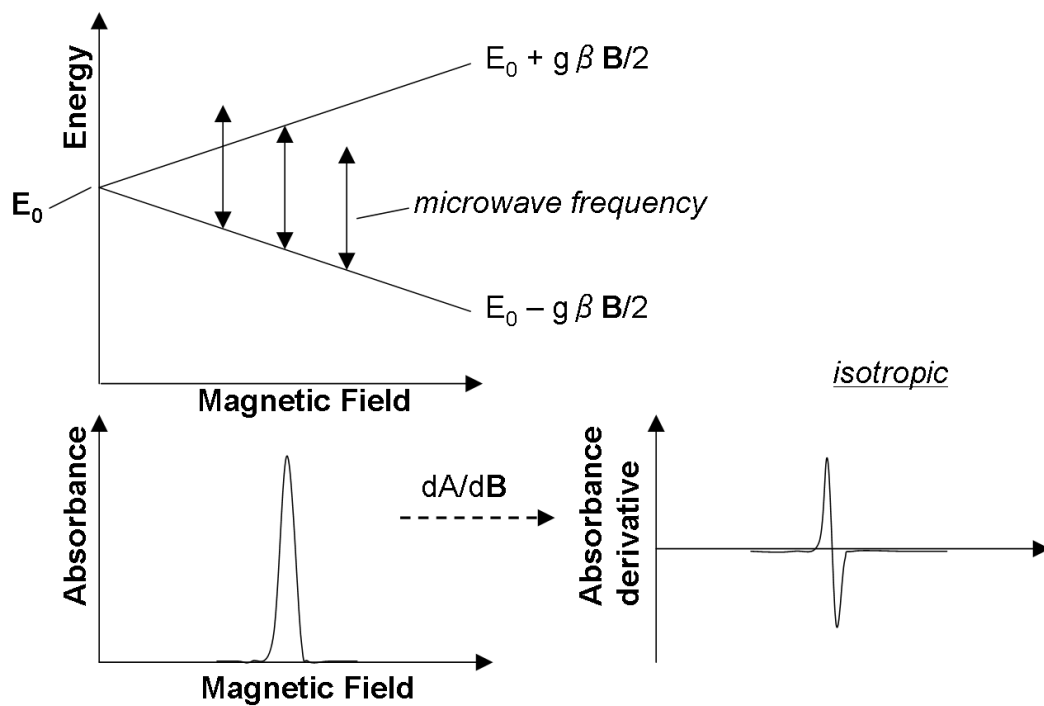


Figure 1.5: **Electronic Paramagnetic Absorption.**

where β is the Bohr magneton, \mathbf{B} is the magnetic field strength, and g is the splitting factor. Unlike UV-visible absorption where the energy used to excite the electron is varied by changing the wavelength of light, in EPR the resonance energy is held at a constant microwave frequency and the magnetic field is swept (Figure 1.5). Absorption occurs when the energy described in equation 1.1 is equivalent to that supplied by the microwave source.

The nature of absorption in EPR spectra make them more easily interpretable by observing the absorption derivative. This is due to the fact that the g -factor is influenced by changes in the environment around the paramagnet. When the g -factor is identical in all directions, the magnetic moment is not influenced by its orientation in relation to the magnetic field and absorption occurs at a single field strength. This is called an isotropic signal. Anisotropic signals occur when the local magnetic field around the electron is not uniform. Anisotropic signals can be either axial or rhombic (Figure 1.6). As the system can be oriented in any direction during the spectrum accumulation, this leads to a continuum of absorption between the three g -values. The g -values can be determined from the derivative spectrum by finding the zero crossing point of an isotropic signal, the peak (or trough) and zero crossing point of an axial signal, or the peak, zero crossing point, and trough of a rhombic signal.

A significant portion of EPR spectra analysis is empirical, particularly in bio-EPR. A metal center and certain properties can usually be rapidly identified from a spectrum. In the case of heme proteins, high-spin hexacoordinate (axial) and high-spin pentacoordinate (rhombic) species are easily distinguishable from both each other and low-spin species. Resolution of these species using UV-visible spectroscopy is nearly impossible. Furthermore, by taking the double integral of the absorption derivatives of the individual components, it is possible to quantify the relative amounts of each species. If a standard is available, concentrations can even be determined.

Although EPR can give high resolution and quantitative information concerning the metal center environment, it does have certain drawbacks. The most apparent is that the species must be a paramagnet. This limits detectable mono-iron or mono-heme species

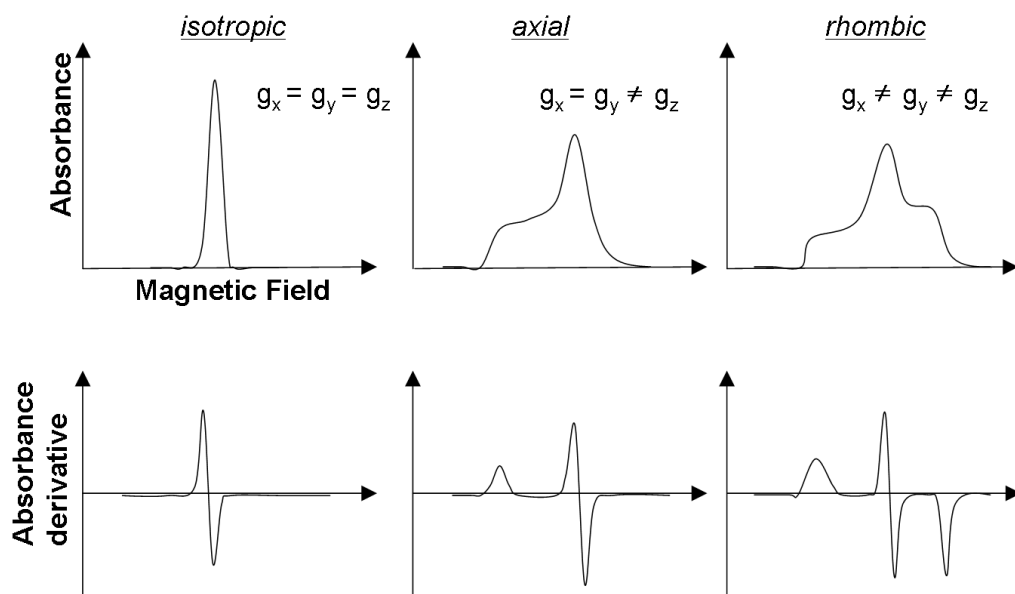


Figure 1.6: EPR Absorption Derivatives.

to Fe^{III}. Another limitation is the temperature sensitivity. For the purposes of the work here, spectra were recorded at 10K. Higher temperatures result in depopulation of the $|m_s = \pm 1/2\rangle$ doublet which has the largest signal intensity [52]. Although samples are frozen rapidly in liquid nitrogen, there is no guarantee that they are preserved in their native state without precipitation or protein damage. Also, the helium required to operate at such low temperatures is becoming more difficult to acquire as demand and prices increase [53]. Plus, instrument preparation time (vacuum pumping and cooling) and sample storage (in liquid nitrogen) add to the relative inconvenience when compared to other spectroscopic techniques.

A compromise between the easy-to-use but low resolution UV-visible and the complicated but high resolution EPR is magnetic circular dichroism (MCD). Circular dichroism (CD) spectroscopy measures the absorption difference between left and right circularly polarized light. This is an inherent property of chiral molecules. As such, CD itself has many practical biological applications, including determination of DNA conformation, protein-DNA complexes, and secondary structure content of proteins [54]. MCD is the measurement of a CD spectrum in the presence of a magnetic field. MCD absorption is a property of the magnetic field interacting with the electronic orbitals, not chirality, making MCD signals independent of CD signals. As a result, a raw spectrum is composed of both MCD and CD absorbance, and the CD component must be subtracted to obtain the MCD spectrum.

There are three types of MCD signals, each one based on different ways the magnetic field might interact with the molecular orbitals. The most straightforward of the three is called an A-term signal. In this case, the magnetic field splits the excited state S_1 such that excitation into one of the split orbitals requires the absorbance of left circularly polarized (lcp) light and the other requires right circularly polarized (rcp) light. At the wavelength where lcp light is absorbed, there will be a strong positive signal, and there will be a strong negative signal at the wavelength where rcp light is absorbed. This results in a signal that resembles the isotropic EPR absorbance derivative (Figure 1.7).

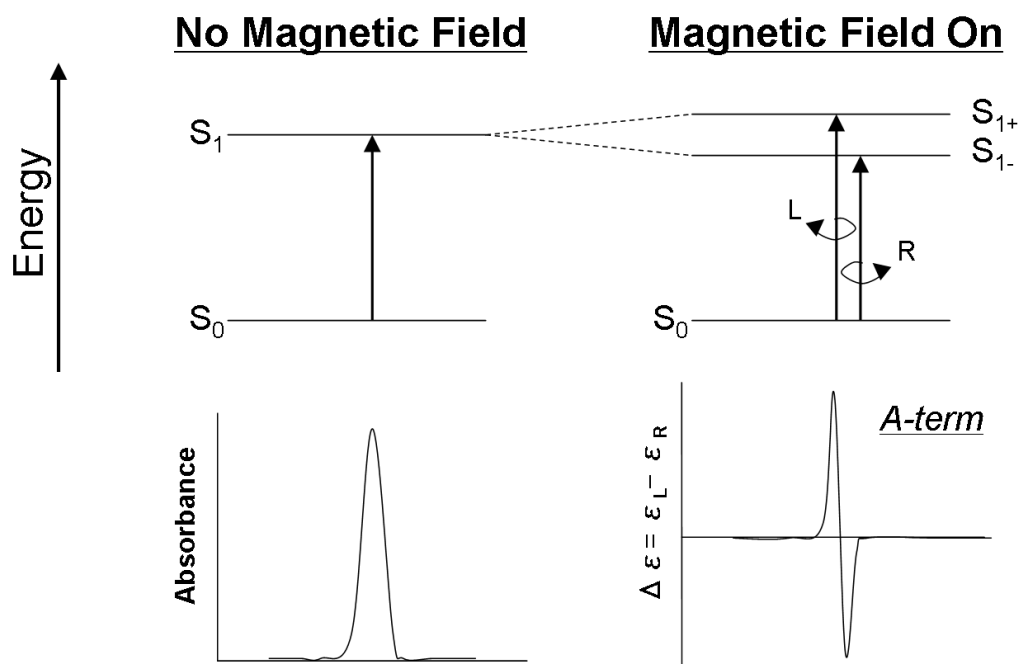


Figure 1.7: Origin of MCD Signals: A-term.

The C-term signal is very similar to the A-term in principal, but instead of the magnetic field splitting the excited state, the magnetic field splits the ground state. Again, excitation from one of the split states will absorb lcp light and the other rcp light, but C-term signals can be distinguished from A-term signals via temperature variations. At low temperatures, only the lower energy state will be populated and the resulting signal will appear like a simple absorbance band. At high enough temperatures, only the higher energy state will be populated and the signal will appear as an upside-down absorption band. At intermediate temperatures, more derivative-like signals will occur (Figure 1.8).

The origin of B-term signals is less straightforward. In a magnetic field, two transitions may experience a mixing of the electronic states such that one of the two transitions absorbs lcp light more strongly and the other absorbs rcp light equally more strongly. There is no splitting of degenerate orbitals such as with the A- and C-terms and therefore no temperature dependence is observed (Figure 1.9).

The easiest application of MCD to heme proteins is distinguishing between high- and low-spin ferrous heme. The transitions observed in ferrous heme MCD are due to the B-bands (γ) and Q-bands (α and β) (Figure 1.4). The low-spin ferrous heme Q-band produces a strong A-term signal centered near 550 nm. High-spin ferrous heme is not featureless in this region, but the features are complicated and far less intense. The difference in intensity between low- and high-spin ferrous heme Q-band signals is substantial. Even a small portion of low-spin ferrous heme would be detectable in a predominantly high-spin population. Considering that both B-band and Q-band transitions involve exciting an electron into the same orbital, it stands to reason that the B-band signal is also A-term. This is correct, but at room temperature the signal is highly susceptible to linewidth broadening [55], and differences between low- and high-spin ferrous heme of different proteins cannot be established from the B-band signals without correlation with the Q-band region of the spectrum.

It is not quite as easy to distinguish between low- and high-spin ferric heme species as it is with ferrous, but it is still possible. The primary difference is how the CT bands affect

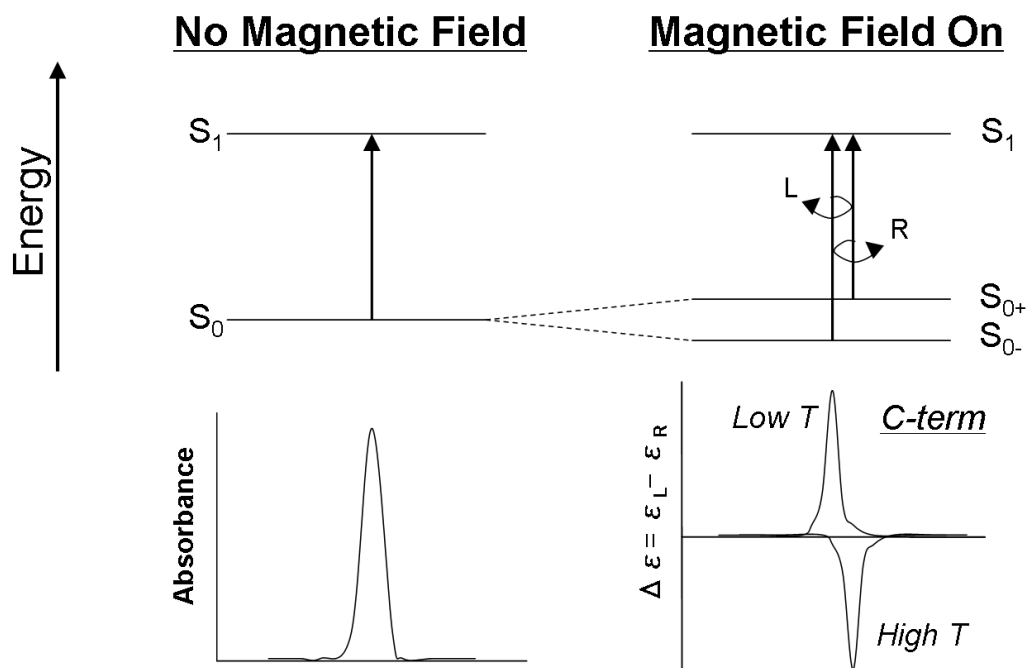


Figure 1.8: Origin of MCD Signals: C-term.

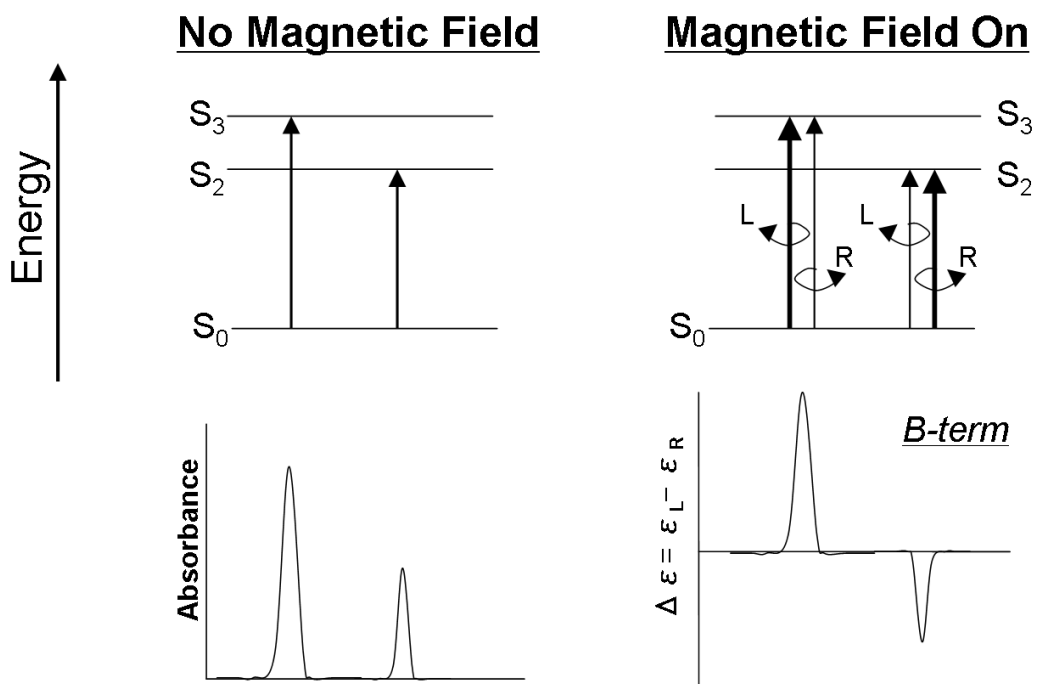


Figure 1.9: Origin of MCD Signals: B-term.

the spectra. Recall from Figure 1.4 that the CT bands arise from excitation of a heme π -electron into a d_π (e_g) orbital of the iron. As shown in Figure 1.3, in the presence of a strong field ligand (low-spin) the d_π orbitals are at a lower energy level, and CT occurs at very high wavelengths (> 900 nm). High-spin iron will have both higher energy d_π orbitals and more transitions available. This shifts the transitions into the B- and Q-band region, complicating the spectrum. Empirically, the B-band transition for low-spin is also more intense than that of high-spin ferric heme.

For MCD, sample preparation is as simple as with UV-visible spectroscopy, with the exception of possibly needing higher sample concentration. It still does not require as much sample as EPR, and adequate spectra can be acquired without freezing the sample. Also, the instrument itself only needs a 30 minute warm-up time - lengthier than UV-visible spectroscopy, but much shorter than the overnight required by EPR *after* liquid helium is obtained. The drawback is that it is most useful when the heme is in the Fe^{II} state, which requires reduction of the native state for many proteins such as peroxidases. Just like with freezing, there is no guarantee that reduction does not damage the sample or alter the structure of the active site or protein. The common reductant sodium dithionite, for example, in too high of concentration can acidify the solution which may cause protein to precipitate.

Overall, UV-visible spectroscopy serves as a good preliminary tool, providing basic information quickly and can be used for rapid concentration determination. MCD is a good intermediate tool. It does require more sample than UV-vis and data acquisition is on the order of hours rather than minutes, but it can more easily distinguish between high- and low-spin heme. EPR is an advanced technique that can not only easily distinguish between high- and low-spin ferric heme, but can also give information about the coordination sphere of the iron and relative concentrations of the different species in the population.

There are many other useful techniques that are not addressed here but are worth mentioning. Separation methods including gel electrophoresis, capillary electrophoresis, and liquid or gas chromatography have applications spanning from size determinations to

assay techniques. Many techniques directly probe the three-dimensional structure, such as x-ray crystallography, nuclear magnetic resonance (mainly for small or membrane-bound proteins), and x-ray absorption (for structural information just peripheral to the ligand sphere of a metal center). Other spectroscopic methods include mass spectroscopy, which was mentioned in relation to post-translation modification detection, raman spectroscopy to observe low-frequency or vibrational modes that give insight into the heme shape among other things, and fluorescence spectroscopy.

Kinetics

In order to determine the role of distant structural features in an enzyme, the two questions that need to be addressed are what is the impact on the active site structure, and what is the impact on catalysis. To this point, the only application considered for the instrumentation has been as spectroscopic probes of a metal center active site. The partner application is their role in kinetic evaluations.

The simplest enzymatic mechanism describes the association of enzyme with substrate followed by the release of product:



Named for the researchers who proposed this mechanism, the Michaelis-Menten equation identifies the minimum of four reaction compounds: S - substrate, P - product, E - free enzyme, and ES - the enzyme-substrate complex. Figure 1.10 is a basic representation of the relative concentrations of these compounds during the reaction progression.

Shortly after the reaction begins, ES reaches a steady state concentration, that is:

$$k_1[E][S] = (k_2 + k_{-1})[ES] \quad (1.3)$$

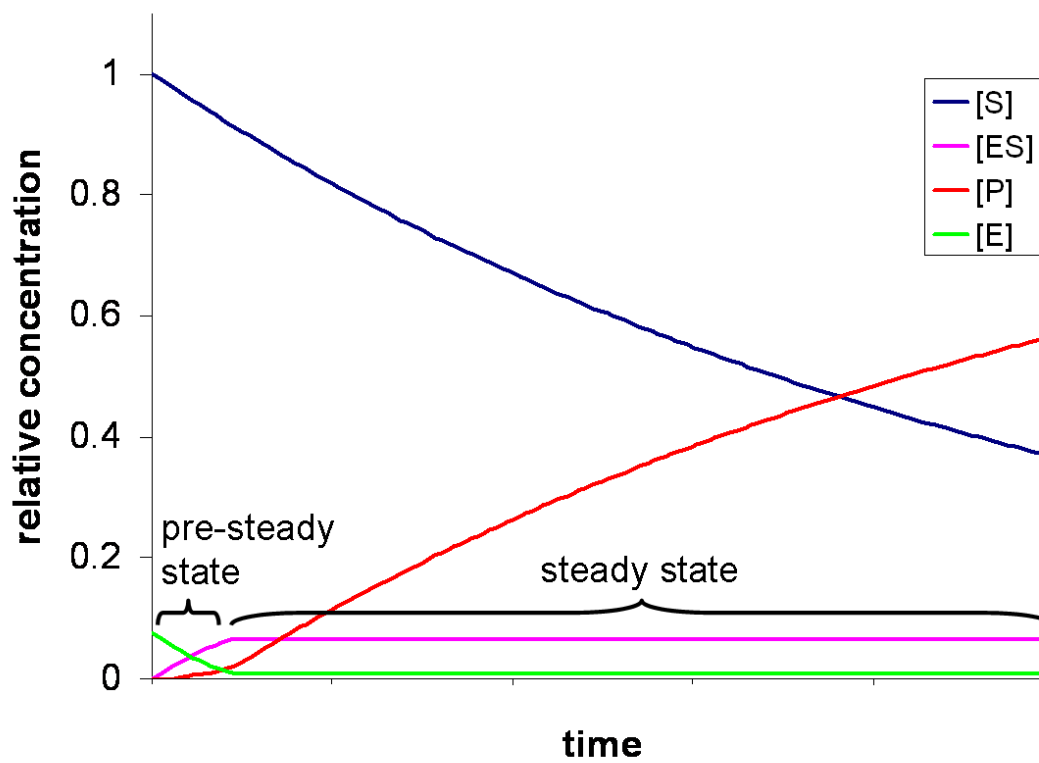


Figure 1.10: Relative Concentrations of S, P, E, and ES During Reaction Progression. Rate values are arbitrary.

If the reaction velocity is determined soon after steady state is reached, substituting equation 1.3 into $v = k_2[\text{ES}]$ gives

$$v = \frac{[\text{E}]_{\text{tot}}[\text{S}]k_2}{[\text{S}] + (k_2 + k_{-1})/k_1} \quad (1.4)$$

where $[\text{E}]_{\text{tot}}$ is the total enzyme concentration. This rearranges to the classic relationship,

$$\frac{v}{[\text{E}]_{\text{tot}}} = \frac{[\text{S}]k_{\text{cat}}}{K_M + [\text{S}]} \quad (1.5)$$

where k_{cat} is the maximum number of cycles that the active site can perform per unit time (the turnover number), and K_M is the concentration required to reach half the maximum reaction velocity (the Michaelis constant). The velocity at saturating substrate concentrations is k_{cat} . At low substrate concentration, the slope of $v/[\text{E}]_{\text{tot}}$ vs. $[\text{S}]$ approaches the apparent second-order rate constant k_{cat}/K_M , a measure of efficiency of the enzyme with a given substrate. Generally, k_{cat} reflects the reactivity of the ES complex, and k_{cat}/K_M reflects the reactivity of free enzyme and substrate [1].

Determining these values experimentally requires measuring the initial velocity at several different substrate concentrations above and below K_M . If either the substrate or product is a chromophore, this can be measured continuously using UV-visible absorption by monitoring its change in absorbance over time. Other continuous detection methods that might be useful include fluorescence spectroscopy or potentiometric detection. If it is not possible to monitor the evolution of the reaction directly (which is common with isomerization reactions, for example), an end-point assay can be used where the reaction proceeds for a fixed amount of time and then is quenched and analyzed.

Even in the simplest case, steady state kinetics can only be used to determine k_2 in the form of k_{cat} and the dissociation constant of the ES complex if k_{-1} is much greater than k_2 . Furthermore, since steady state kinetics rely on monitoring either the substrate consumption or product formation, multiple enzyme-based intermediates would go undetected. In order to get individual rate constants or detect multiple intermediates, pre-steady state or transient state kinetics must be used.

The main difficulty in analyzing pre-steady state kinetics is the time scale on which they occur. Mixing enzyme and substrate can require anywhere from a few seconds using inversion by hand to a few tenths of a second with a stir bar. The time it takes for the entire solution to be mixed is called the “dead time”. If any intermediates are formed within this dead time, rate constants cannot be determined without the use of rapid mixing techniques. To achieve this, instruments have been developed that use automated mixing devices that force solutions together using syringes. The mixed solution is forced through a tube past a detector, and the dead time is determined by the flow rate and the distance of the detector from the mixing chamber. The most common instrument that uses this principle is the stopped-flow. Enzyme and substrate are mixed together and forced past a detector when flow stops and the solution comes to rest. The dead time is determined by the time it takes flow to stop and can be less than one millisecond.

Due to the fact that the automated mixing apparatus requires space, detection methods must be compatible. Absorption and fluorescence detectors are example of compatible approaches. Electrodes or magnetic approaches are unlikely to be compatible. If the intermediates are not observable with compatible detectors, or the investigator wants to use other approaches to probe the intermediates, rapid quenching may be used. The same principle is used, but after mixing the enzyme and substrate, a set amount of aging time passes and the mixture is then combined with a quencher. A variation from chemical quenching was proposed in 1961 by using freeze quenching [56]. Its immediate and still most common application has been in Rapid Freeze Quench (RFQ) EPR. This is especially useful when reaction intermediates involve radical reactions that are difficult to observe with other techniques and too rapid to be detected with steady state approaches.

Parametric Effects

In the simplest mechanism (equation 1.5), the enzyme reacts with only one substrate and no external effectors are considered. Unsurprisingly, this is rarely the case. A glance at the EC classes (Table 1.2) should make it obvious that a number of enzymes must

require multiple substrates. Ligases require ATP plus a substrate, transferases need both a functional group donor and acceptor, and oxidoreductases very rarely use the same substrate for both oxidation and reduction. Ionizable groups on the enzyme can affect binding or catalysis, requiring consideration of pH and buffering. Temperature and ionic strength can also affect catalytic rates and folding properties. Even inhibitors introduced intentionally or not (such as inhibition by substrate, product, or buffer) can prove significant in developing a kinetic understanding of the enzyme. Here we will consider a few of these parameters not accounted for in the simplest Michaelis-Menten mechanism, particularly multiple substrates and pH effects.

There are only a few mechanisms by which multiple substrates bind. In the ping-pong mechanism, a substrate is bound and product is released resulting in a modified, stable active site to which another substrate can bind. Sequential mechanisms require the binding of all substrates before catalysis can occur. Some sequential mechanisms require binding to be in a specific order, in others it can be random. These mechanisms can be distinguished kinetically by varying all substrate concentrations simultaneously; but once the mechanism is determined, it is common to discontinue with such extensive protocols. Instead, it is common practice to transform the reactions into pseudo-first order kinetics by holding one substrate constant and treating the reaction as the simple Michaelis-Menten type mechanism [1]. This can be seen in the rate equations of the two types of mechanisms. The ping-pong mechanism rate equations is

$$\frac{v}{[E]_{\text{tot}}} = \frac{[A][B]k_{\text{cat}}}{K_A[B] + K_B[A] + [A][B]} \quad (1.6)$$

and the sequential mechanism rate equation is

$$\frac{v}{[E]_{\text{tot}}} = \frac{[A][B]k_{\text{cat}}}{K'_A K_B + K_A[B] + K_B[A] + [A][B]} \quad (1.7)$$

where A and B are the substrates and K_A and K_B are their respective Michaelis constants. By keeping one substrate at a constant concentration in great excess of its Michaelis constant, it is clear that these equations simplify to the form seen in equation 1.5.

Many enzymes have what is called a “pH profile”, indicating that at some pH a transition occurs that affects the rate of catalysis. This transition is often ascribed to an ionizable group that may play a part in acid-base catalysis. Other transitions could be macroscopic (the composition of multiple related changes or equilibria) or the result of protein unfolding or reorganization. Fortunately, mechanisms accounting for pH transitions can also be simplified to Michaelis-Menten type rate equations of the form

$$\frac{v}{[E]_{\text{tot}}} = \frac{[S]k_{\text{cat}}^{\text{obs}}}{K_M^{\text{obs}} + [S]} \quad (1.8)$$

where $k_{\text{cat}}^{\text{obs}}$ includes consideration of protonation of the ES complex and K_M^{obs} includes consideration of protonation of both the free enzyme and ES complex. Thorough derivations of two complex examples can be found in chapter 2 where rate equations are described that involve both pH dependence and multi-substrate reactions.

As seen in chapter 2, these examples of parametric kinetic analyses become more complicated when combined with each other or other considerations such as substrate or product inhibition. Only the simplest complications to the rate equations can be found in textbooks, leaving it up to the researcher to derive the appropriate rate equation in most cases. The model enzyme that we will be considering has the additional novel complication of being able to catalyze two reactions within the same active site. The implications of this for kinetics and parametric analysis will be discussed further on in this chapter and in chapter 3.

1.2.3 Therapeutics

Before proceeding on to consider the model enzyme that is the centerpiece of this research, it is notable to mention how catalase-peroxidases came into the spotlight. Studying

enzymes has many purposes beyond the sheer curiosity of understanding living organisms and how they operate. One of the most desired results is therapeutic applications.

Early advances in medicine came directly from biological studies, with the biochemical understanding coming later. Two of the most notable include insulin, a protein secreted by the pancreas involved in the regulation of blood glucose, and penicillin, a β -lactam antibiotic that acts by inhibiting the final step in peptidoglycan layer synthesis in gram-positive bacteria.

Insulin has been a hallmark of many biochemical advances, generating multiple Nobel prizes along the way. Not only was a Nobel Prize in Medicine awarded for its treatment of diabetes (1923), it was the first protein to have its sequence determined (Nobel Prize in Chemistry, 1958) [48], it was key in the development of x-ray crystallography technique of isomorphous crystals used in protein crystal structure determination, and was the motivation behind the development of the radioimmunoassay for detecting hormone levels (Nobel Prize in Medicine, 1977) [57].

Penicillin has also generated its share of Nobel Prizes and was involved in the isomorphous crystal technique, but the understanding of the biochemistry behind the action of penicillin is still in constant use today in designing new antibiotics. Penicillin-binding proteins (PBPs) catalyze the cross-linking of peptidoglycan in gram-positive bacterial cell walls. Penicillin is an analogue of the D-alanyl-D-alanine that is removed during the reaction. When PBPs act on penicillin, however, the penicillin irreversibly inactivates the PBP by forming a covalent bond to an active site serine. With this knowledge, a long list of penicillin derivatives have been developed with the goal of optimizing the binding of the derivative to the PBP by altering the β -lactam functional groups. Included in the list of these derivatives is ampicillin, which is widely used in molecular biology laboratories to select target strains that have intentionally had ampicillin resistance introduced.

This process of using biochemical knowledge as a foundation for drug discovery is now common practice. There are four primary cellular processes that antibiotics disrupt: DNA replication or RNA transcription, protein synthesis, metabolic processes, and cell

wall synthesis (Table 1.3) [58–60]. Each class of antibiotics targets a specific enzymatic process by interacting with either the enzyme or substrate, and as with the β -lactam class, the antibiotics are designed to optimize the interaction or prevent resistance to it. More recently, bactericidal antibiotics (those whose action kill the pathogen rather than halt its growth) have been shown to have the commonality of creating reactive oxygen species during their primary action, aiding in their bactericidal properties [60].

With drug resistance constantly arising, the search for new antibiotics is vigorous. Established targets (those that have been studied and are fairly well understood) require understanding of the mechanism of resistance so that new drugs can work around them. New targets (those whose disruption could be potentially harmful to the pathogen) need to be characterized for antibiotic development strategies. This is where catalase-peroxidases come in.

Mycobacterium tuberculosis is a pathogen responsible for the disease tuberculosis (TB). Tuberculosis is known to have affected humans since at least around 1500 BC (as verified by DNA analysis), and possibly much earlier [61]. According to WHO, around one-third of the world’s population is infected with TB [62]. In the 1950s, an organic compound called isoniazid (INH) was found to be anti-tubercular and was immediately implemented in sanitariums. Since then it has been one of two front-line drugs for TB treatment alongside rifampicin. Credited to improper treatment regimens, drug resistance has reached the point where TB strains resistant to both front-line drugs [63] and more than half of the second line drugs have emerged. It was not until 1992 that the antitubercular mechanisms began to be determined when isoniazid resistance was traced to mutations in the *katG* gene [64, 65].

Isoniazid is activated by the multi-functional enzyme KatG [64, 66, 67] by creating an isonicotinoyl radical that can form adducts with NAD^+ and NADP^+ . These adducts inhibit mycolic acid synthesis, a key ingredient in mycobacterial cell walls [68]. One specific adduct has also been shown to inhibit dihydrofolate reductase, a key enzyme in nucleotide production [68, 69]. Oxidation by KatG also produces NO^\cdot radicals that can interfere with respiratory enzymes [68].

Cellular process	Target	Antibiotic Class
DNA replication or RNA transcription	DNA gyrase or topoisomerase IV	quinolones
Protein synthesis	Peptidyl tRNA transferase	aminoglycosides macrolides amphenicols
	Transpeptidase	lincosamides
	Association of tRNA with mRNA-ribosome complex	tetracyclines
Metabolic processes	Tetrahydrofolate synthesis pathway (dihydropteroate synthase)	sulfonamides
Cell wall synthesis	PBP	β -lactams
	Peptidoglycan incorporation	glycopeptides

Table 1.3: **Antibiotic Classes.**

Mutant TB strains in most cases contain a modification to the *katG* gene that reduces INH binding in KatG. S315T KatG is the most prevalent example [65, 70, 71]. By preventing binding, INH cannot be activated and loses all antitubercular properties. As KatG is the only catalase (or hydroperoxidase) active enzyme in *Mtb* [72] and is crucial in the ability of *Mtb* to withstand the hosts oxidative burst [73], it is unfortunate that mutations such as the S315T only prevent INH binding but do not disrupt the ability of the enzyme to break down hydrogen peroxide [70, 71]. On the other hand, it is fascinating that non-active site mutations can selectively eliminate one activity from this multifunctional enzyme. As a result of the relation between isoniazid and KatG, a strong push has been made to better understand the enzyme itself in hopes of being able to design drugs that can still be activated by variants that cannot activate INH. Interest has continued to deepen as other periplasmic catalase peroxidases have been linked to the virulence of pathogens such as *Escherichia coli* O157:H7 (food poisoning) [74], *Legionella pneumophila* (Legionnaires disease) [75, 76], and *Yersinia pestis* (bubonic plague) [77, 78].

1.3 Catalase-peroxidases

KatG is commonly called catalase-peroxidase after its two most studied activities. It was mentioned in the previous section that KatG is the only catalase in *Mtb* and that makes it indispensable during the hosts oxidative burst defense mechanism. To expand on that, and to introduce the multi-functionality of KatG, we will first look at the products of the oxidative burst (reactive oxygen species) which serve as a substrate for KatG, and then consider the monofunctional catalases and monofunctional peroxidases to introduce possible mechanisms and roles for KatG and provide a basis for structural and kinetic comparisons.

1.3.1 Reactive Oxygen Species

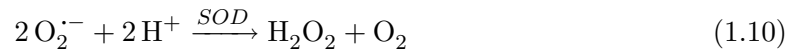
The reduction potential of O_2 to H_2O is around 0.8 V, indicating that molecular oxygen is a strong oxidant. As mentioned before, however, in its ground state it is not very reactive. Activating molecular oxygen allows access to its ability to oxidize and enables cells to harvest

the energy from its conversion to water, such as in the generation of ATP during respiration. Another application of activating oxygen is the generation of reactive oxygen species (ROS). ROS refers primarily to three compounds: superoxide ($\text{O}_2^{\cdot-}$), hydrogen peroxide (H_2O_2), and the hydroxyl radical (HO^\cdot). Superoxide and hydrogen peroxide are less reactive than the hydroxyl radical, which can react detrimentally with proteins, lipids, and DNA in the cell. Phagocytes attempt to overwhelm a pathogen's ability to neutralize ROS with what is called a respiratory or oxidative burst [79].

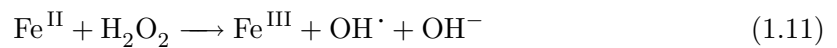
In mammals, the initial step in oxidative burst is the generation of extreme concentrations of superoxide by the multi-component enzyme NADPH oxidase:



The superoxide is disproportionated into hydrogen peroxide and molecular oxygen by the enzyme superoxide dismutase (SOD):



Hydrogen peroxide, being a neutral molecule, is more able to diffuse across the lipid membrane into the invading cell. Reaction of hydrogen peroxide with Fe^{II} (the Fenton reaction) within the cell generates the destructive hydroxyl radical:



The goal of the phagocyte is to generate as much H_2O_2 as possible to diffuse into the invading cell. The peroxide will damage metal-containing proteins, initiating a cascade of reactions such as heme degradation that results in the release of iron which can then initiate the Fenton reaction. Cells capable of breaking down H_2O_2 before or as it is able to diffuse into the cell have a significant advantage over our immune system. Disabling a cells ability

to deal with H_2O_2 is lethal to the cell, hence the significance of the KatG mutations that lead to INH resistance but not KatG inactivation.

ROS are generated on a much smaller scale during normal cell processes, as well, and cells are equipped to prevent the accumulation of these using catalase or peroxidase enzymes. Catalases disproportionate hydrogen peroxide into water and oxygen. Peroxidases use hydrogen peroxide to oxidize a wide variety of reactions. Although these enzymes both break down hydrogen peroxide, they are very different enzymes that serve different purposes.

1.3.2 Monofunctional Catalases

Function

The presence of catalase in living organisms was identified over a century ago by its ability to remove hydrogen peroxide from cells at very high rates. More recently other possible roles have been identified. Catalases were found to protect cells from UVB light that can directly damage DNA and other cellular molecules by absorbing the UVB energy to generate ROS that can be broken down by other anti-oxidant enzymes [80]. Catalase deficiency has also been linked to graying hair as hydrogen peroxide is able to accumulate and irreversibly inactivate the enzyme tyrosinase, leading to a decrease in the melanogenesis (pigmenting) pathway [81].

Active site

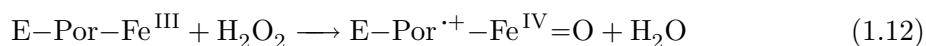
Out of the over 300 known catalases, more than 90% contain heme (mostly heme *b*), with the exceptions containing a dimanganese cluster [82]. The heme is coordinated to the enzyme via a tyrosinate ligand (Figure 1.2), which significantly lowers the reduction potential and stabilizes high oxidation states. The key active site residues are a histidine and an asparagine. The histidine is parallel to the heme surface, and is oriented above either pyrrole ring III (as in Figure 1.2) or pyrrole ring IV.

Global structure

Catalases crystalize as homotetramers. Each monomer has either four or five domains: N-terminal, β -barrel core (where the heme resides), α -helical, wrapping, and (in large subunit catalases) a C-terminal domain. The N-terminal extension of one domain is interweaved with the wrapping domain of an adjacent subunit, causing the tetramer to consist of two sets of tightly interlocked subunit pairs. The N-terminal domains in large subunit catalases are larger than the N-terminal domains in the small subunit catalases [83].

Activity and kinetics

Catalase breaks down peroxide via a ping-pong mechanism. The first step (equation 1.12) is a two-electron oxidation of the enzyme with one molecule of hydrogen peroxide to create a ferryl porphyrin cation radical intermediate known as Compound I (CpdI) and releasing water. CpdI is then reduced back to the resting state (equation 1.13) with another molecule of H_2O_2 releasing another molecule of water and a molecule of oxygen.



The second-order rate constant for catalases has been found to be as high as $6.6 \times 10^7 \text{ M}^{-1} \text{ s}^{-1}$ [84], approaching the diffusion limit for enzyme-substrate association ($10^9 \text{ M}^{-1} \text{ s}^{-1}$) [1]. Unbuffered studies also showed catalase to maintain maximal activity from pH 4.75 to 10.5 [84]. Kinetic determinations for catalases are complicated by peroxide dependent inactivation at high peroxide concentrations [82]. Large subunit catalases are more resistant to this inactivation [84].

1.3.3 Monofunctional Peroxidases

A peroxidase is any enzyme capable of catalyzing the following general reaction:



The electrons in equation 1.14 could be donated from a wide variety of donors, including organic compounds such as phenols, anilines, and azines or large molecules such as the protein cytochrome *c*. Some peroxidases have high substrate specificity such as the cytochrome *c* peroxidases [85–87], while others have very broad specificity such as chloroperoxidase [88].

Functions

In catalases, the function is obvious from the mechanism: eliminate hydrogen peroxide. With peroxidases, however, the function is not always as obvious. Still, the role of peroxidases is often ascribed as protection of the cell against oxidative damage [86, 87, 89, 90]. Other roles are not always as easy to detect, but have been identified.

First, variations of the peroxide substrate can give insight into alternative roles. For example, the selenium-containing glutathione peroxidases (Gpx) act on organic or lipid peroxides, but not hydrogen peroxide. Gpx-4 is membrane-associated and acts specifically on phospholipid peroxides, which also serve as activators of the lipoxygenase pathway. 5-lipoxygenase metabolizes arachidonic acid to leukotrienes. Improper Gpx-4 levels adversely affect the leukotriene balance, indicating that it has a role in 5-lipoxygenase regulation [90].

The other perspective is to consider the consequence of the oxidation of the electron donor. In fact, many peroxidases are named based on the identity of the reducing substrate. NADH peroxidase could easily be considered as having a role in the redox cycling of NADH and NAD⁺. Haloperoxidases (such as chloroperoxidase, myeloperoxidase, lactoperoxidase, and thyroperoxidase) are named such based on their ability to oxidize halogens into molecules that can halogenate organic compounds. These products have wide-ranging effects. Halogenated nucleic acids, for example, have anti-cancer and anti-viral activity as

they inhibit DNA synthesis [91]. Oxidation of thiocyanide and halogens by lactoperoxidase (found in milk) is bacteriostatic to gram-positive bacteria and potentially bacteriocidal to gram-negative bacteria, a feature crucial to infants during their immune system development [92]. Thyroperoxidase iodinates tyrosine residues in thyroglobulin (Tg) to synthesize the thyroid hormones T₃ and T₄ [93]. Manganese-dependent and lignin peroxidases depolymerize lignin in the biodegradation of wood by white rot fungus [94–97].

Active site

Like catalases, monofunctional peroxidase are found in nearly all organisms. Structures of monofunctional peroxidases, however, are not nearly as uniform as catalases [85, 86]. Substrates and mechanisms are equally diverse. As evident from equation 1.15, peroxidases are oxidoreductases and have nearly the entire EC subclass 1.11.x.x devoted to them. Being oxidoreductases, they need a redox active catalytic site. A few of the more uncharacteristic catalytic centers can be seen in glutathione peroxidases, NADH peroxidase, chloroperoxidase, class 1c ribonucleotide reductases, and some of the cytochrome *c* peroxidases. Five of the six glutathione peroxidases (enzymes that use glutathione as the electron donor) rely on a selenocysteine residue as the redox center [90, 98, 99]. The NADH peroxidase active site contains oxidized cysteine (cysteine-sulfenic acid) and the cofactor flavin adenine dinucleotide (FAD) [85, 100]. The chloroperoxidases are diverse in themselves, some having a vanadium metal center, some being metal-free and using the serine-histidine-aspartate catalytic triad, and some containing heme with glutamic acid as the peroxide cleaving catalytic base rather than the histidine seen in most heme-peroxidases [91]. Although not classified as peroxidases, class 1c ribonucleotide reductases demonstrate peroxidase activity at the Fe-Mn cofactor as a part of activation and maintenance of the metal center [4]. Cytochrome *c* peroxidases from *Pseudomonas aeruginosa*, *Pseudomonas nautica*, and *Nitrosomonas europaea* have all been shown to have di-heme centers with both hemes being *c*-type hemes with very different reduction potentials [86, 87, 101].

Yeast cytochrome *c* peroxidase (Ccp), on the other hand, only has one *b*-type heme, as do most other peroxidases. It is the heme *b* containing peroxidases that we will be focusing on, in particular the plant structural superfamily. The Ccp shown in Figure 1.2 is stereotypical for this family. All share the catalytic histidine and arginine on the distal side of the heme, as well as the triad aspartate-histidine-iron on the proximal side. The tryptophan shown is characteristic of the class that Ccp belongs to, but is a phenylalanine in the other classes.

Global structure

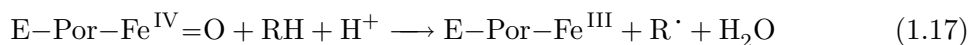
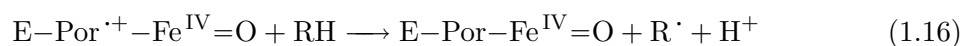
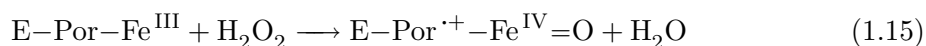
In 1992, Karen Welinder identified three classes within the plant peroxidase superfamily [86]. Class I is described as of prokaryotic origin and includes yeast Ccp and ascorbate peroxidase. Class II is the fungal peroxidases such as the manganese-dependent peroxidases, lignin peroxidases, and versatile peroxidases. Class III is the secretory plant peroxidases, encompassing the classical peroxidases such as horseradish peroxidase. Sequence similarity within a class can be as low as 32%, but all classes show consistent overall folding patterns. All have 10 helices, which are labeled A through J beginning at the N-terminus. The proximal histidine ligand is invariable and located on the F-helix. Catalytic residues are found on the B-helix.

Structural differences are primarily limited to the interhelical loop regions, but one major difference is the relationship each of the classes has with calcium ions. Class I peroxidases do not require any structural calcium. Crystal structures of class II and III peroxidases do indicate the presence of calcium ions [86, 97], but calcium depletion completely inactivates class II peroxidases while only decreasing class III peroxidase activity by around 50% [86, 94–97, 102]. The distal calcium ion is coordinated by residues and carbonyls on the loop connected to the active site histidine [97], and in lignin peroxidases the loss of calcium is concomitant with bis-histidine coordination of the heme as evidenced by low-spin iron features in the UV-vis, MCD, and EPR spectra [94, 96]. Calcium depleted

versatile peroxidase does still contain high-spin heme, but has a more flexible heme cavity that can become bis-histidine coordinated at certain pHs [102].

Activity and kinetics

The peroxidase catalytic cycle begins the same way as the catalase cycle with the peroxide oxidizing the heme center to create Compound I (equation 1.15). Instead of a two-electron reduction, peroxidases typically undergo two single-electron reduction steps. The first electron creates a second ferryl intermediate known as Compound II (equation 1.16), and the second electron reduction restores the enzyme to its native state and releases water (equation 1.17).



Some of the earliest work on the kinetics of horseradish peroxidase used the first version of the stopped-flow apparatus [103]. CpdI formation occurs with $k = 1 \times 10^7 \text{ M}^{-1} \text{ s}^{-1}$, which is not much slower than the apparent second-order rate constant for catalase activity ($6.6 \times 10^7 \text{ M}^{-1} \text{ s}^{-1}$). Oxidation of the substrates took place with a low turnover in the range of 5 s^{-1} , but with a second-order rate constant near $2 \times 10^7 \text{ M}^{-1} \text{ s}^{-1}$ [104]. These same experiments found that although peroxidases followed a ping-pong like mechanism, it still conformed to and confirmed the Michaelis-Menten and Briggs-Haldane theories [103, 104].

1.3.4 Catalase-peroxidases

In the 1970s, an enzyme from *Escherichia coli* was found to have both catalase and *o*-dianisidine peroxidase activity [105]. This was unique considering that known catalases

up to that point had been shown to be very poor peroxidases [85, 105]. Likewise, peroxidases were known to only have minimal catalase activity, a feature shared by many heme-containing enzymes partly due to the ability of heme to disproportionate peroxide non-enzymatically [85]. This enzyme, later to be named a catalase-peroxidase, has since been isolated from a number of other bacteria and fungi [51, 106–114].

Structural comparison of bifunctional catalase-peroxidase to monofunctional catalases and peroxidases

Sequence alignments placed catalase-peroxidases clearly within the plant peroxidase superfamily, specifically in class I [86, 115]. The prediction that catalase-peroxidase would contain the 10 helices in approximately the same positions as monofunctional peroxidases was confirmed by the crystal structure of catalase-peroxidase from *Haloarcula marismortui* [116]. Since this first crystal structure, others have been solved for *Burkholderia pseudomallei* [117], *Mycobacterium tuberculosis* [118], and *Synnechococcus* PCC 7942 [119], all signifying that the classification of catalase-peroxidase as a class I peroxidase within the plant superfamily was accurate. The active sites of catalase-peroxidases are identical to monofunctional class I peroxidases with all significant residues strictly conserved [115] (Figure 1.11). The bifunctional catalase-peroxidase shows no sequence or structural similarity to monofunctional catalases [122].

The superimposability of the active sites and structural similarities between catalase-peroxidases and monofunctional peroxidases makes the dual activity of catalase-peroxidases even more unexpected as non-active site features must somehow tune the active site for catalase activity without changing its structure. This has led to a search for and investigation of conserved structures of KatGs that are absent in monofunctional peroxidases [123–128]. The most obvious three structures were revealed through sequence alignment: two interhelical insertions and a C-terminal domain that is proposed to have originated from a gene duplication and fusion event [86, 115, 122, 129] (Figure 1.12).

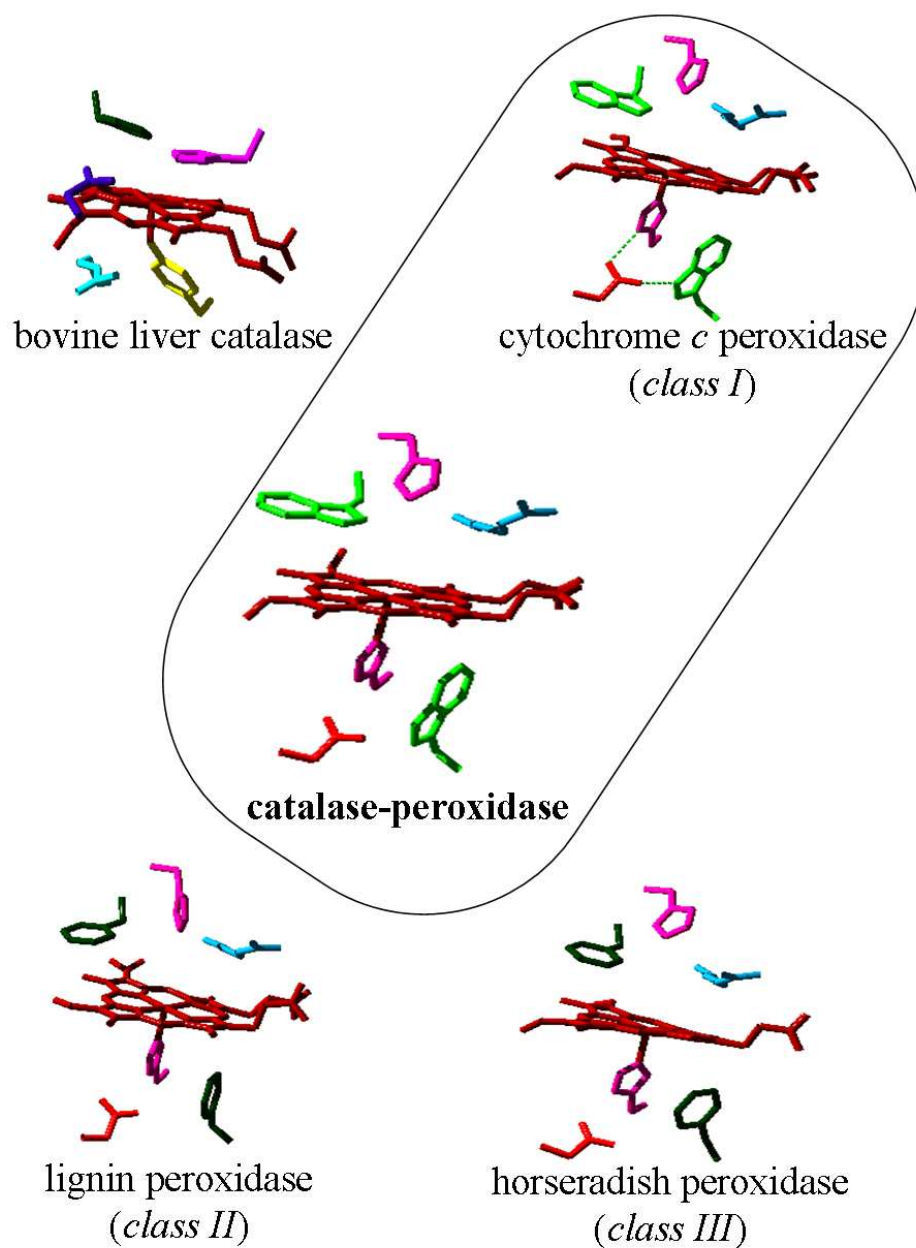


Figure 1.11: **Comparison of Catalase-peroxidase Active Site to Monofunctional Catalase and Peroxidases.** All structures have propionate groups oriented to the right. Amino acids are coded to the following color scheme: H - pink, R - light blue, N - dark blue, F - dark green, Y - yellow, D/E - red, W - light green. Structures were taken from the following PDB accession numbers: catalase-peroxidase - 1SJ2 [118], bovine liver catalase - 7CAT [20], cytochrome *c* peroxidase - 2CYP [18], lignin peroxidase [120], horseradish peroxidase [121].

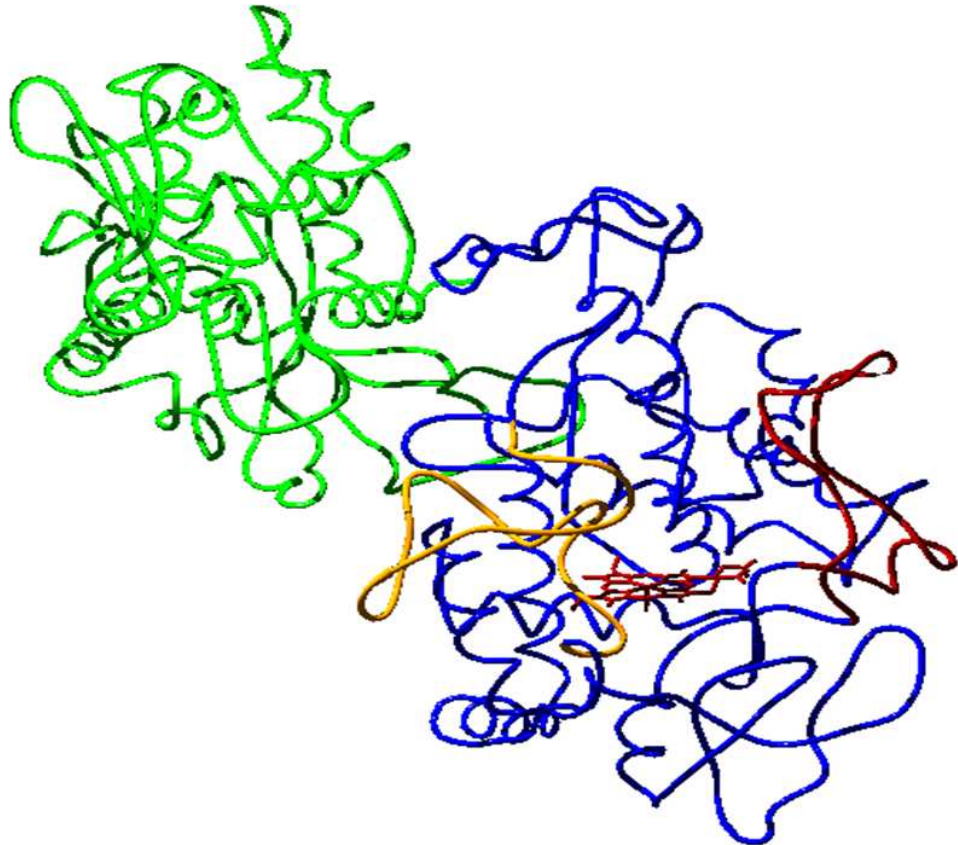


Figure 1.12: **Identification of Interhelical Insertions and C-terminal Domain in Catalase-peroxidase.** N-terminal domain shown in blue, C-terminal domain shown in green, DE insertion shown in yellow, FG insertion and heme shown in dark red. Structure is from *Mycobacterium tuberculosis* (accession number 1SJ2)[118].

If the C-terminal domain is a result of a gene duplication and fusion event, it has since lost the ability to bind heme and has no apparent catalytic capability. There is also no evidence of any substrate binding, allosteric control, or signaling purpose. Appearing to have no role, the C-terminal domain came to be considered “inactive”, a rare trait for protein domains considering their treatment as the functional units of proteins. Deletion mutagenesis, however, has elucidated possible roles for this “inactive” domain.

Deletion of the C-terminal domain results in enzyme preparation that is highly disturbed. The separately expressed N-terminal domain (KatG^N) expresses in inclusion bodies and has to be refolded. Once refolded, it still has no activity as the active site is collapsed and the catalytic distal histidine (106 by *Escherichia coli* numbering) coordinates the heme iron directly, reminiscent of calcium-depleted manganese-dependent and lignin peroxidases [130]. Introducing the separately expressed and purified C-terminal domain (KatG^C) reactivates the enzyme concomitant with removing the active site histidine from the coordination sphere of the heme iron [46]. The C-terminal domain thus has a significant structural role by supporting the integrity of the active site, and may also play a role in proper folding during expression. Chapters four and five will deal specifically with investigations of the residues at the interdomain interface.

The FG interhelical insertion in KatG begins near residue 270 and ends around residue 310 [115]. It has an ascending and descending arm with the base of each arm positioned between the active site and the solvent, and the apex protruding into a hydrophobic pocket in the C-terminal domain of the other subunit in the dimer. The insertion runs parallel to a catalase-essential hydrogen bonding network involving the catalytic His106 with Asp152 and Asn153 [123, 131, 132]. Deletion of the FG insertion results in enzyme that retains almost no catalase activity. The peroxidase turnover is half of that of the wild-type, but the apparent second order rate constant in respect to the reducing substrate ABTS is increased by an order of magnitude. It has been proposed that the increased apparent second order rate constant results from greater accessibility of the heme edge to reducing substrates [123].

The DE interhelical insertion begins near residue 195 and ends near residue 235 [115], and also constricts access to the active site [133]. This loop connects the proximal and distal catalytic halves of the N-terminal domain and has a stretch of highly conserved residues near the end of the insertion. The backbone nitrogen of Ile225 is within hydrogen bonding distance of the catalase-essential Asp152 [134]. Deletion of the DE insertion also eliminated catalase activity, but enhanced peroxidase activity [135]. The DE insertion deletion variant is susceptible to hydrogen peroxide inactivation, and in the absence of a reducing substrate readily forms an inactive intermediate known as Compound III. This is a heme dioxygen ($\text{Fe}^{\text{II}}-\text{O}_2 \longleftrightarrow \text{Fe}^{\text{III}}-\text{O}_2^-$) intermediate that is observed in monofunctional peroxidases when Compound II reacts with hydrogen peroxide [85]. It has also been observed in catalase-peroxidases, but only at high concentrations of hydrogen peroxide [66].

Another feature of the DE insertion revealed in the crystal structures is the presence of a covalent PTM involving the active site tryptophan (Trp105), a conserved tyrosine (Tyr226) on the DE insertion, and a conserved methionine (Met252) [116–119]. Mass spectroscopy and SDS-PAGE showed that the cross-link existed in solution and was required for catalase activity [136–138]. Disruption of the covalent adduct by creating variants of the participants also confirmed that the adduct is essential for catalase activity, but not peroxidase activity [124, 126, 139–141]. The exact nature of the role of this adduct is still contested with some proponents arguing that it may donate an electron to the heme initially forming a tryptophanyl radical that quickly transfers to the tyrosine [142, 143] whose radical is stabilized by an arginine residue [127]. Others argue that the tryptophanyl radical observed could not have been on the Trp106 as that radical is only stable during crosslink formation [144, 145]. Further possible incorporation of this adduct into the KatG mechanism will be dealt with in the discussion of chapter three.

Activity and kinetics

Considering that monofunctional catalases and monofunctional peroxidases share the same first step in catalysis (equations 1.12 and 1.15), directly combining the two results

in the classical representation of the KatG catalytic cycles schematically and textually and is the most common representation in literature (Figure 1.13) [51, 109–111, 123, 126, 127, 130, 145–147].

NADH can act as a reducing substrate in the peroxidase reaction, but KatG also has NADH oxidase activity. This activity is quite distinct from the peroxidase reaction in that it has a pH optimum of 8.5 and consumes oxygen while producing ROS [146]. KatG also has hydrazinolysis activity, which is part of the INH activation. These two activities appear to be synergistic based on studies involving an indicator radical that appears faster when both substrates are present than it does cumulatively with only one substrate present at a time. Manganese ion also accelerates radical production. KatG from *Mycobacterium tuberculosis* also is an efficient isonicotinoyl-NAD synthase, IN-NAD being the compound that interferes with mycolic acid synthesis. Binding sites for these substrates have yet to be determined, but the S315T variant in *Mtb*KatG inhibits the hydrazinolysis reaction by reducing INH binding. Only preliminary determinations of catalytic residues have been performed on residues known to be involved in the catalase and peroxidase activities.

Of the peroxide-dependent activities, catalase and peroxidase, the two most influential factors governing which activity is observed are pH and the availability of a reducing substrate. To date, the evaluation of pH-dependency has involved observing initial rates using single concentrations of substrates, typically at or near saturating conditions [51, 111, 146]. This method consistently identifies pH optima of 6.5–7.0 for catalase activity and 4.5–5.0 for peroxidase activity. Like many monofunctional peroxidases, KatGs are able to utilize a wide variety of electron donors to complete the peroxidase catalytic cycle [106, 107, 111, 126]. Chapter two covers a much more extensive analysis of the pH-dependency of these activities, and chapter three investigates the activity of the enzyme when both pathways are available.

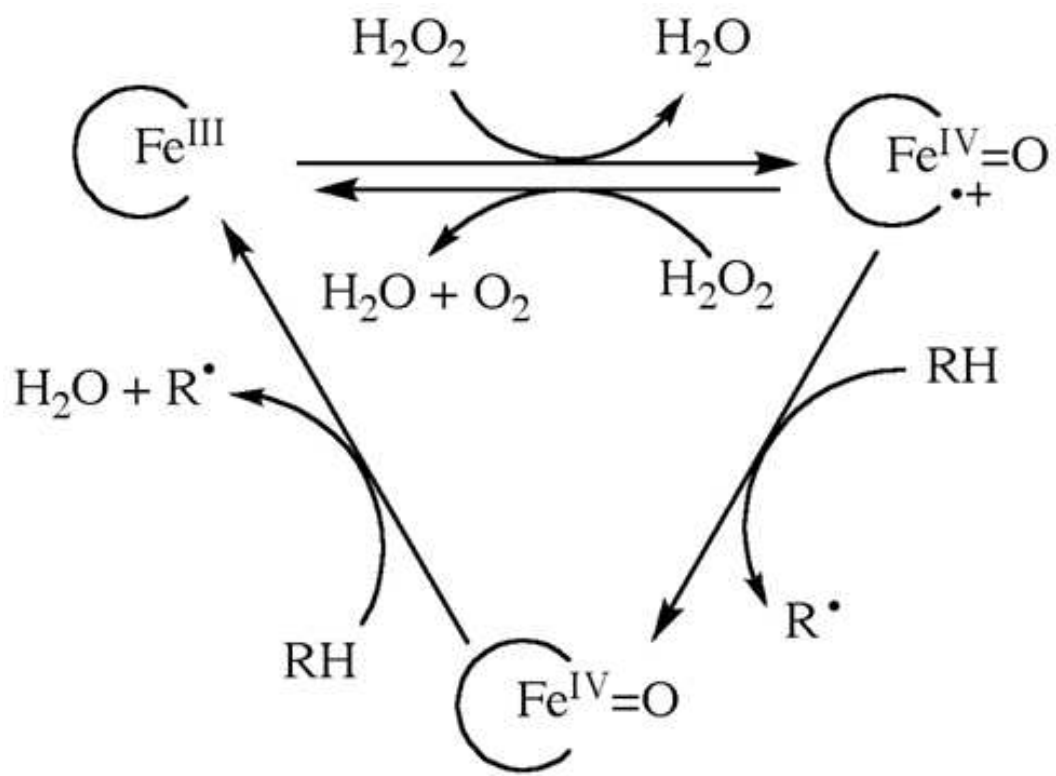


Figure 1.13: Classic Catalase-peroxidase Scheme.

CHAPTER 2

COMPLEXITY OF KATG KINETICS REVEALED BY pH ANALYSIS

2.1 Introduction

Many of the searches for catalase specific KatG features are based on the reasonable assumption that some structures will have a different configuration based on pH, considering that the dominant reaction catalyzed by KatG changes with pH. To be able to accurately relate the structure of the enzyme to function, a complete understanding of its kinetic behavior is necessary. This step has been primarily omitted, particularly in relation to pH. Steady-state parameters have been consistently determined only at the pH determined to be “optimal” based on velocities at expected saturating conditions.

In efforts to provide a basis for more thoroughly correlating structure and function and its dependence on pH, this chapter covers a full-scale kinetic evaluation to determine the kinetic parameters at pH intervals of 0.25 across the ranges of observed catalytic activity. For peroxidase kinetics measurements, one of the most common reducing substrates used *in vitro* 2,2'-azino-bis(3-ethylbenzthiazoline-6-sulfonic acid) (ABTS) was selected for the wealth of data to compare it to as well as the ease of measurements. Through this we discovered the first evidence of ABTS-dependent inhibition of peroxidase activity, most evident at pH values below 4.5. This subsequently revealed that while ABTS acts as the reducing substrate, the optimal pH for peroxidase activity is masked by the inhibition and is not, in fact, between 4.5 and 5.0. Also, we present results demonstrating that the lower pH limit for activity is due to an unfolding event.

These results have led to establishing the pH-dependent schemes for peroxidase cycle (Figure 2.1) and catalase cycle (Figure 2.2). Calculation of the catalase cycle pK_{as} for the various stages of catalysis for both the interactions between HCpdI and H_2O_2 and the

HCpdI-H₂O₂ complex (Figure 2.2) reveal that the catalase pH optimum of 6.5 is actually the intersection of the optimum for binding (the former) and the optimum for catalysis (the latter).

2.2 Materials and Methods

2.2.1 Materials

Hydrogen Peroxide (30%), imidazole, hemin, Sephacryl 300 HR, ampicillin, chloramphenicol, citric acid, phenylmethylsulfonyl fluoride (PMSF), 2,2'-azino-bis(3-ethylbenzthiazoline-6-sulfonic acid) (ABTS), pyrogallol, and 3,3'-dimethoxybenzidine (*o*-dianisidine) were purchased from Sigma (St. Louis, MO). Isopropyl- β -D-thiogalactopyranoside (IPTG), mono- and di-basic sodium phosphate, acetic acid, hydrochloric acid, and sodium acetate were obtained from Fisher (Pittsburgh, PA). Sodium tartrate was purchased from J.T. Baker Chemical Company (Phillipsburg, NJ). Bugbuster and benzonase were purchased from Novagen (Madison, WI). The *E. coli* strain BL-21 [DE3] pLysS was obtained from Stratagene (La Jolla, CA). Nickel-nitrilotriacetic acid (Ni-NTA) resin was purchased from Qiagen (Valencia, CA). All buffers and media were prepared using water purified through Millipore Q-PakII system (18.2 M Ω /cm resistivity).

2.2.2 Expression and Purification of wtKatG

Expression of wtKatG was done using plasmid that had been modified (pKatG1) to incorporate a six-histidine tag on the C-terminus of the protein. The pKatG1 plasmid carries the gene for ampicillin resistance. Expression was carried out in *E. coli* (BL-21 [DE3] pLysS) cells that are resistant to chloramphenicol. Cells were grown in 0.5 L of Luria-Bertani broth that had been supplemented with ampicillin and chloramphenicol at 37 °C with constant shaking. Expression was induced with IPTG once cells had grown to mid-log phase (OD₆₀₀ = 0.5) and monitored hourly to ensure growth. Cells were harvested by centrifugation 4 hours after induction and stored at -80 °C until purification.

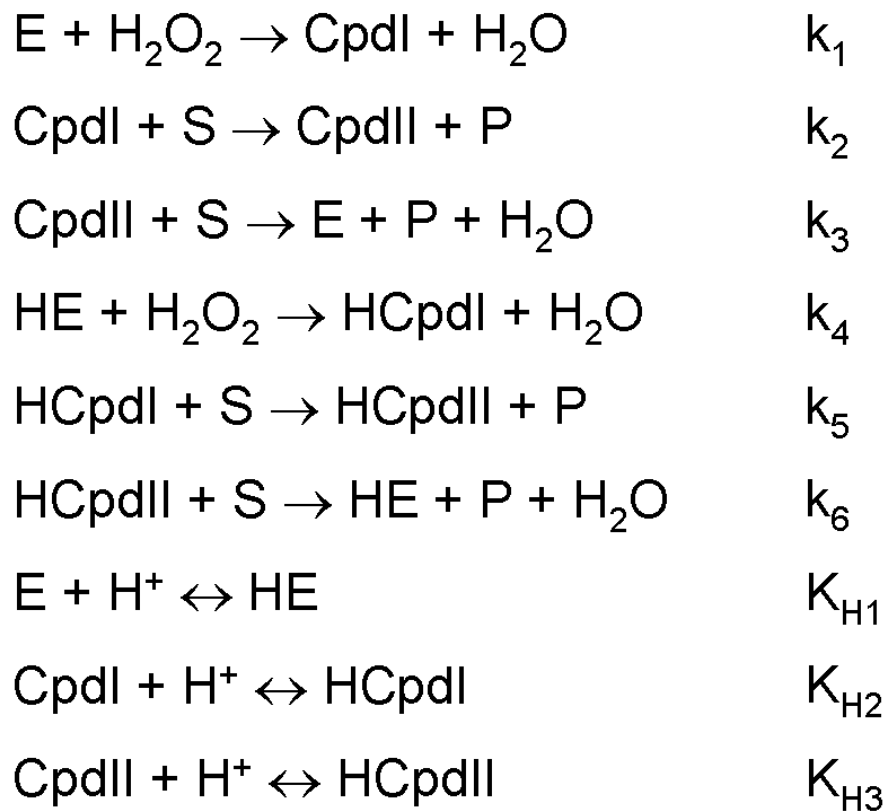


Figure 2.1: Peroxidase Cycle Scheme with pH Dependence.

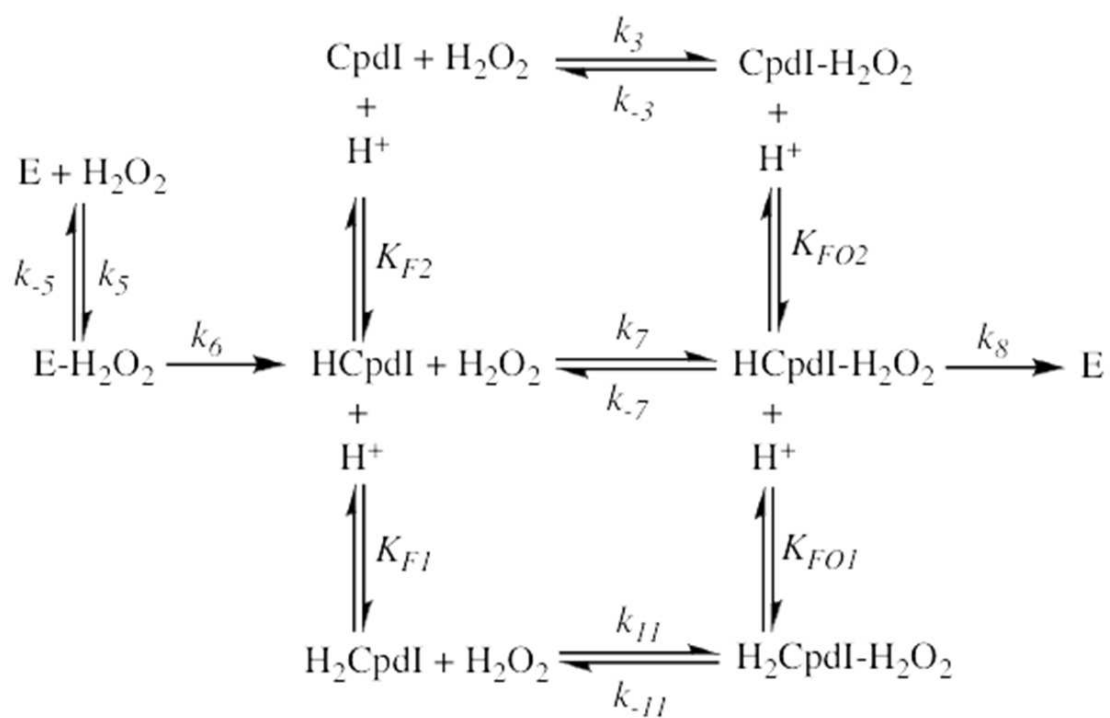


Figure 2.2: Catalase Cycle Scheme with pH Dependence.

Expression analysis was performed using the TCA precipitation technique. A quantity of cells sufficient to yield a 0.05 OD₆₀₀ reading (when diluted to 1 ml) was treated with an equal volume of 10% trichloroacetic acid (4 °C) followed by centrifugation. The pellet was washed with 1 ml acetone, then dried and resuspended in SDS-PAGE loading buffer, adjusting the pH as appropriate with trizma base. Samples were then separated by SDS-PAGE using a 7.6% acrylamide resolving gel.

Purification began by resuspending the cell pellets in Bugbuster reagent in the presence of PMSF (0.1 mM) and benzonase (250U). The cell lysate was centrifuged, and the supernatant loaded onto a Ni-NTA column by recirculating the solution with a flow rate of 1 mL/min through the column overnight. Once loaded, the column was washed with Tris buffer pH 8.0, followed by 50 mM phosphate buffer / 200 mM NaCl pH 7.0, then a repeat of the phosphate / NaCl buffer that also contained 2 mM imidazole. Protein was eluted using a gradient of the phosphate / NaCl buffer from 2 to 200 mM imidazole. Fractions were analyzed by SDS-PAGE, and those containing the purest target were combined and concentrated with an Amicon ultrafiltration concentrator. Excess imidazole was removed by gel filtration using a column packed with Sephacryl 300 HR. The elute was collected in 6 mL fractions and analyzed by SDS-PAGE. Protein-containing fractions were combined, concentrated, aliquotted, and stored at -80 °C.

Concentration of purified enzyme was estimated according to the method of Gill and von Hippel [50] ($\epsilon_{280} = 1.44 \times 10^5 \text{ M}^{-1} \text{ cm}^{-1}$). Even though no heme precursors had been added to the expression media, a small portion of the purified enzyme already had heme incorporated while inside the cells. Adding 0.9 to 0.95 heme equivalents directly to the enzyme solution was sufficient to introduce heme to the rest of the enzyme. Reconstituted enzyme solution sat for 72 hours to allow unincorporated heme to settle out of solution. The solution was then spun and removed from the precipitated heme. This was to ensure that free heme did not interfere with the accumulation of spectral or kinetic data. The concentration of the reconstituted enzyme was then determined using the Soret heme absorption band ($\epsilon_{408} = 120.7 \text{ mM}^{-1} \text{ cm}^{-1}$) [123].

2.2.3 Peroxidase Activity Assays

Peroxidase activity was evaluated by monitoring the production of ABTS radical ($\epsilon_{417} = 34.7 \text{ mM}^{-1} \text{ cm}^{-1}$), pyrogallol oxidation ($\epsilon_{430} = 2.47 \text{ mM}^{-1} \text{ cm}^{-1}$), or *o*-dianisidine oxidation ($\epsilon_{460} = 11.3 \text{ mM}^{-1} \text{ cm}^{-1}$) over time in the presence of 20 nM wtKatG; initial ABTS concentrations were also determined spectrophotometrically ($\epsilon_{340} = 3.66 \times 10^4 \text{ M}^{-1} \text{ cm}^{-1}$) [148]. All assays were carried out at room temperature on a Shimadzu UV-1601 spectrophotometer (Columbia, MD). Initial velocities were determined across a range of ABTS concentrations while keeping peroxide concentration constant, as well as a range of peroxide concentrations while keeping ABTS concentration constant. Enzyme inhibition (as evidenced by suppressed activity levels) was observed at hydrogen peroxide concentrations greater than 1.0 mM. It was therefore necessary to select a concentration below that of inhibition for performing assays for ABTS-dependent parameter determination; the peroxide concentration, however, was still slightly higher than twice the observed Michaelis constant for peroxide. For the substrates pyrogallol and *o*-dianisidine, initial velocities were determined across a range of reducing substrate concentrations at 0.4 mM H_2O_2 . The initial velocities (excluding those determined under inhibiting substrate conditions) were fit to the Michaelis equation using a non-linear regression analysis to determine apparent kinetic parameters. Peroxidase assays with ABTS were initially carried out in 50 mM acetate buffer, pH 3.50 to 6.00 in 0.25 pH increments. Recognizing that acetate has little buffering capacity at the extremes of this range, assays were also carried out in 50 mM tartate buffer, pH 3.50 and 3.75 and 100 mM phosphate buffer, pH 6.00. The data obtained using these buffers were the same as the data from assays performed in the acetate buffer. Peroxidase assays with pyrogallol and *o*-dianisidine were carried out in 50 mM acetate buffer, pH 4.00 to 6.00 in 0.5 pH increments.

2.2.4 Catalase Activity Assays

Catalase activity was evaluated by monitoring the decrease in H_2O_2 concentration over time at 240 nm ($\epsilon_{240} = 39.4 \text{ M}^{-1} \text{ cm}^{-1}$) [149] in the presence of 20 nM wtKatG. All

assays were carried out at room temperature on a Shimadzu UV-1601 spectrophotometer (Columbia, MD). Initial velocities were fit to the Michaelis equation using non-linear regression analysis to determine kinetic parameters. Accurate determination of catalase activity became increasingly difficult at $\text{pH} > 7$ due to the small Michaelis constant for hydrogen peroxide. Measurements carried out below the calculated K_M from preliminary data had initial absorbance below 0.1, and complete consumption of peroxide occurred within 30 seconds of initiation. To slow down the reaction (to obtain better initial velocities), enzyme concentration was reduced to 5 nM. Catalase assays were carried out in the following buffers: 50 mM acetate buffer, pH 5.0 to 6.0 in 0.25 pH increments; 100 mM phosphate buffer pH 6.0 to 8.0 in 0.25 pH increments.

2.2.5 Circular Dichroism Spectroscopy

All spectra were obtained using 5 μM enzyme in 5 mM citrate (pH 3.10, 3.30, 3.50, 3.60, 3.85) or acetate (pH 3.75, 4.05, 4.20, 4.60, and 4.90) buffer to minimize buffer interference below 200 nm. Acetate had little buffering capacity below pH 3.75, necessitating the overlap of the two buffers. Spectra were recorded at 23 °C in a quartz cell (0.5 mm path length) from 250 - 195 nm on a Jasco J-810 spectrophotometer (Tokyo, Japan). Baselineing and analysis were done using Jasco J-720 software.

2.2.6 pK_a Determination

The scheme in Figure 2.1 produced the equations (derived here) that gave the best fit to the peroxidase kinetic parameters across the pH ranges observed. The mechanism is a modification of the conventional mechanism [150] to account for pH effects and gives rise to the following equation:

$$\frac{v_0}{[\text{E}]_{\text{tot}}} = \frac{\alpha[\text{S}][\text{H}_2\text{O}_2]}{\beta_1[\text{S}] + \beta_2[\text{H}_2\text{O}_2]} \quad (2.1)$$

where α , β_1 and β_2 are as follows:

$$\alpha = 2k_4k_5k_6 + \frac{k_2k_4k_6K_{H2} + k_3k_4k_5K_{H3}}{[H^+]} \quad (2.2)$$

$$\beta_1 = k_5k_6 \left(1 + \frac{K_{H1}}{[H^+]} \right) \quad (2.3)$$

$$\beta_2 = k_4k_6 \left(1 + \frac{K_{H2}}{[H^+]} \right) + k_4k_5 \left(1 + \frac{K_{H3}}{[H^+]} \right) \quad (2.4)$$

Equation 2.1 can be rewritten as

$$\frac{v_0}{[E]_{\text{tot}}} = \frac{k_{\text{cat}}[S][H_2O_2]}{K_M^{H_2O_2}[S] + K_M^S[H_2O_2]} \quad (2.5)$$

Empirically, k_2 and k_3 (rates of product formation by the unprotonated intermediates) can be assumed to be very small (Figures 2.6 and 2.7), simplifying equation 2.2 to the following:

$$\alpha = 2k_4k_5k_6 \quad (2.6)$$

If we also assume that $k_5 \gg k_4$ and k_6 , then we can relate equation 2.5 to the classical Michaelis-Menten type kinetics by holding one substrate constant:

$$\frac{v_0}{[E]_{\text{tot}}} = \frac{k_{\text{cat}}^{\text{obs}}[S]}{[S] + K_M^{\text{obs}}} \quad (2.7)$$

where

$$k_{\text{cat}}^{\text{obs}} = \frac{k_{\text{cat}}[H_2O_2]}{K_M^{H_2O_2}} = \frac{\alpha}{\beta_1}[H_2O_2] = \frac{2k_4}{\frac{K_{H1}}{[H^+]} + 1}[H_2O_2] \quad (2.8)$$

$$K_M^{\text{obs}} = \frac{K_M^S[H_2O_2]}{K_M^{H_2O_2}} \quad (2.9)$$

$$\left(\frac{k_{\text{cat}}}{K_M} \right)_{\text{obs}} = \frac{k_{\text{cat}}}{K_M^S} = \frac{\alpha}{\beta_2} = \frac{2k_6}{\frac{K_{H3}}{[H^+]} + 1} \quad (2.10)$$

and similarly:

$$\frac{v_0}{[E]_{\text{tot}}} = \frac{k_{\text{cat}}^{\text{obs}} [\text{H}_2\text{O}_2]}{[\text{H}_2\text{O}_2] + K_M^{\text{obs}}} \quad (2.11)$$

where

$$k_{\text{cat}}^{\text{obs}} = \frac{k_{\text{cat}} [\text{S}]}{K_M^{\text{S}}} = \frac{\alpha}{\beta_2} [\text{S}] = \frac{2k_6}{\frac{K_{H3}}{[\text{H}^+]} + 1} [\text{S}] \quad (2.12)$$

$$K_M^{\text{obs}} = \frac{K_M^{\text{H}_2\text{O}_2} [\text{S}]}{K_M^{\text{S}}} \quad (2.13)$$

$$\left(\frac{k_{\text{cat}}}{K_M} \right)_{\text{obs}} = \frac{k_{\text{cat}}}{K_M^{\text{H}_2\text{O}_2}} = \frac{\alpha}{\beta_1} = \frac{2k_4}{\frac{K_{H1}}{[\text{H}^+]} + 1} \quad (2.14)$$

The relation between equations 2.8 and 2.14 and the relation between equations 2.10 and 2.12 are apparent and lead to the following equations that will be used to fit the peroxidase kinetic parameters:

$$\frac{k_{\text{cat}}^{\text{obs}}}{[\text{H}_2\text{O}_2]} = \left(\frac{k_{\text{cat}}}{K_M^{\text{H}_2\text{O}_2}} \right)^{\text{obs}} = \frac{2k_4}{\frac{10^{-pK_{H1}}}{10^{-pH}} + 1} \quad (2.15)$$

$$\frac{k_{\text{cat}}^{\text{obs}}}{[\text{S}]} = \left(\frac{k_{\text{cat}}}{K_M^{\text{S}}} \right)^{\text{obs}} = \frac{2k_6}{\frac{10^{-pK_{H3}}}{10^{-pH}} + 1} \quad (2.16)$$

These allow for the determination of pK_{H1} and pK_{H3} as well as k_4 and k_6 . Furthermore, given that k_{cat} (that is, α) is a constant, relative values for the two Michaelis constants can be assigned.

The kinetic evaluation of the catalase pathway can be done by treating it as a ping-pong bi-bi reaction. The general solution for such pathways is:

$$\frac{v_0}{[E]_{\text{tot}}} = \frac{\alpha[A][B]}{\beta_1[A] + \beta_2[B] + \beta_3[A][B]} \quad (2.17)$$

Since both substrates ‘A’ and ‘B’ are hydrogen peroxide, this simplifies further to:

$$\frac{v_0}{[E]_{\text{tot}}} = \frac{\alpha[\text{H}_2\text{O}_2]}{\beta_1 + \beta_2 + \beta_3[\text{H}_2\text{O}_2]} \quad (2.18)$$

or

$$\frac{v_0}{[E]_{\text{tot}}} = \frac{k_{\text{cat}}[\text{H}_2\text{O}_2]}{K_M + [\text{H}_2\text{O}_2]} \quad (2.19)$$

where according to the scheme in Figure 2.2, under the assumption that $k_6 \gg k_{-5}$, $k_8 \gg k_{-7}$, $k_8 \gg k_6$ [150–152], and that the $\text{p}K_a$ s for Compound I formation in peroxidases lie well outside the pH range used in current experiments [150],

$$\alpha = k_5 k_6 k_7 k_8 \quad (2.20)$$

$$\beta_1 = k_6 k_7 k_8 \quad (2.21)$$

$$\beta_2 = k_5 k_6 k_8 q_F \quad (2.22)$$

$$\beta_3 = k_5 k_7 (k_6 q_{FO} + k_8) \quad (2.23)$$

$$k_{\text{cat}} = \frac{\alpha}{\beta_3} = \frac{k_6 k_8}{k_6 q_{FO} + k_8} \quad (2.24)$$

$$K_M = \frac{\beta_1 + \beta_2}{\beta_3} \quad (2.25)$$

$$\frac{k_{\text{cat}}}{K_M} = \frac{\alpha}{\beta_1 + \beta_2} = \frac{k_5 k_7}{k_5 q_F + k_7} \quad (2.26)$$

and

$$q_F = \frac{K_{F2}}{[\text{H}^+]} + 1 + \frac{[\text{H}^+]}{K_{F1}} \quad (2.27)$$

$$q_{FO} = \frac{K_{FO2}}{[\text{H}^+]} + 1 + \frac{[\text{H}^+]}{K_{FO1}} \quad (2.28)$$

As the pH optimum is approached for maximum turnover and the apparent second-order rate constant, k_{cat} approaches k_6 and (k_{cat}/K_M) approaches k_5 . As pH varies from the optimum, the two values approach (k_8/q_{FO}) and (k_7/q_F) respectively. This can be used

to make approximations of k_5 and k_6 , however estimations of k_7 and k_8 are more inaccurate considering that q values vary logarithmically with pH. The pK_a values can be estimated by fitting the data to a simple 2- pK_a model:

$$k_{\text{cat}}^{\text{obs}} = \frac{k_{\text{cat}}}{\frac{10^{-pK_{FO2}}}{10^{-pH}} + 1 + \frac{10^{-pH}}{10^{-pK_{FO1}}} = \frac{k_6 k_8}{k_6 + k_8} \left(\frac{1}{q_{FO}} \right) \quad (2.29)$$

$$\left(\frac{k_{\text{cat}}}{K_M} \right)^{\text{obs}} = \frac{\frac{k_{\text{cat}}}{K_M}}{\frac{10^{-pK_{F2}}}{10^{-pH}} + 1 + \frac{10^{-pH}}{10^{-pK_{F1}}} = \frac{k_5 k_7}{k_5 + k_7} \left(\frac{1}{q_F} \right) \quad (2.30)$$

2.3 Results

2.3.1 Kinetic Parameters for Peroxidase Activity of KatG

Dramatic and differential effects of pH on the two most prominent activities of catalase-peroxidases have been widely observed [51, 127, 128, 146]. The standard approach for determining these pH profiles has been to vary pH, measuring activity at a single unvaried concentration of substrate(s) - often one approaching saturation. Using this approach, peroxidase activity has typically shown a maximum near pH 4.5. Indeed, in our hands KatG from *E. coli* shows precisely this behavior (Figure 2.3). Likewise, *E. coli* KatG and other catalase-peroxidases show maximal catalase activity at a substantially higher pH (~ 6.5).

Interestingly, a thorough kinetic evaluation of this phenomenon has not been undertaken, opening the possibility that mechanistic conclusions have been drawn based on an incomplete picture of pH effects on catalysis. In order to fill in some of the blanks, we measured the effect of pH on activity across a range of substrate concentrations in order to obtain apparent kinetic parameters for peroxidase activity with respect to H_2O_2 and reducing substrate concentration as well as for catalase activity. At first glance, effect of H_2O_2 concentration on peroxidase activity showed few surprises over pH ranging from 3.5 to 6.0. High concentrations of H_2O_2 (> 1.0 mM) resulted in inhibition of the enzyme

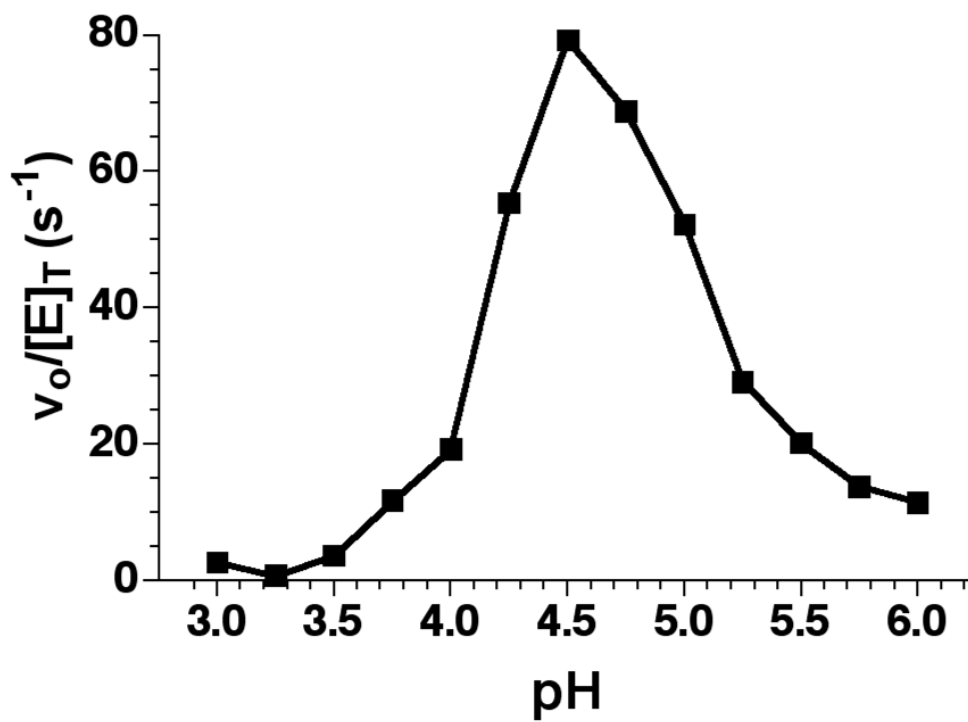


Figure 2.3: Initial Velocity of Peroxidase Activity Under Saturating Substrate Conditions. $[ABTS] = 1.2$ mM, $[H_2O_2] = 0.51$ mM.

which in peroxidase kinetics has been attributed to irreversible inactivation by formation of Compound III, a heme dioxygen ($\text{Fe}^{\text{II}}\text{-O}_2$) complex [26]. This complex results from the reaction of hydrogen peroxide with Compound II. It is unlikely that the inhibition is a result of competition by catalase activity since it was observed at all pH values. As a result of this inactivation, kinetic studies were carried out at concentrations below the inhibition threshold of hydrogen peroxide. The maximum catalytic output (as measured by k_{cat}) with respect to H_2O_2 concentration was observed at pH 4.5 (Figure 2.4). Likewise, optimum peroxidase efficiency (as estimated by apparent k_{cat}/K_M) was observed around pH 4.5.

Comparable experiments to evaluate the effect of pH on ABTS-dependent kinetic parameters showed that ABTS behaved not only as a substrate, but also as an inhibitor (Figure 2.5). Its abilities to act as a substrate and inhibitor were both dependent upon pH. A progressive decrease in pH led to more substantial inhibition by ABTS. Table 2.1 shows the lowest concentration of ABTS observed to result in inhibition under various pH conditions. No inhibitory effect was observed above pH 4.75, but at pH 3.75 as little as 0.1 mM ABTS resulted in appreciable inhibition of peroxidase activity.

In light of this phenomenon, the H_2O_2 -dependent kinetic parameters for peroxidase activity were reevaluated at the greatest concentration of ABTS that was never observed to inhibit peroxidase activity (0.05 mM). Under these conditions, the apparent k_{cat} and apparent k_{cat}/K_M for peroxidase activity with respect to H_2O_2 continued to increase as pH was lowered below 4.5. In terms of turnover number and efficiency, a maximum for both was now observed at pH 3.75, 175 s^{-1} and $1.2 \times 10^6 \text{ M}^{-1} \text{ s}^{-1}$ respectively (Figure 2.6). Below pH 3.75, an abrupt shift in kinetic parameters was observed consistent with a substantial loss of enzymatic activity.

Similar behavior in peroxidase activity was observed when the kinetic parameters with respect to reducing substrate (ABTS) were evaluated (Figure 2.7). A continuous increase in apparent k_{cat} was observed from pH 6.0 down to pH 3.75, reaching a peak value near 200 s^{-1} . As with H_2O_2 -dependent parameters, there was an abrupt decrease below pH 3.75. The increase in apparent k_{cat}/K_M between pH 6.0 and 3.75 was more dramatic, reaching

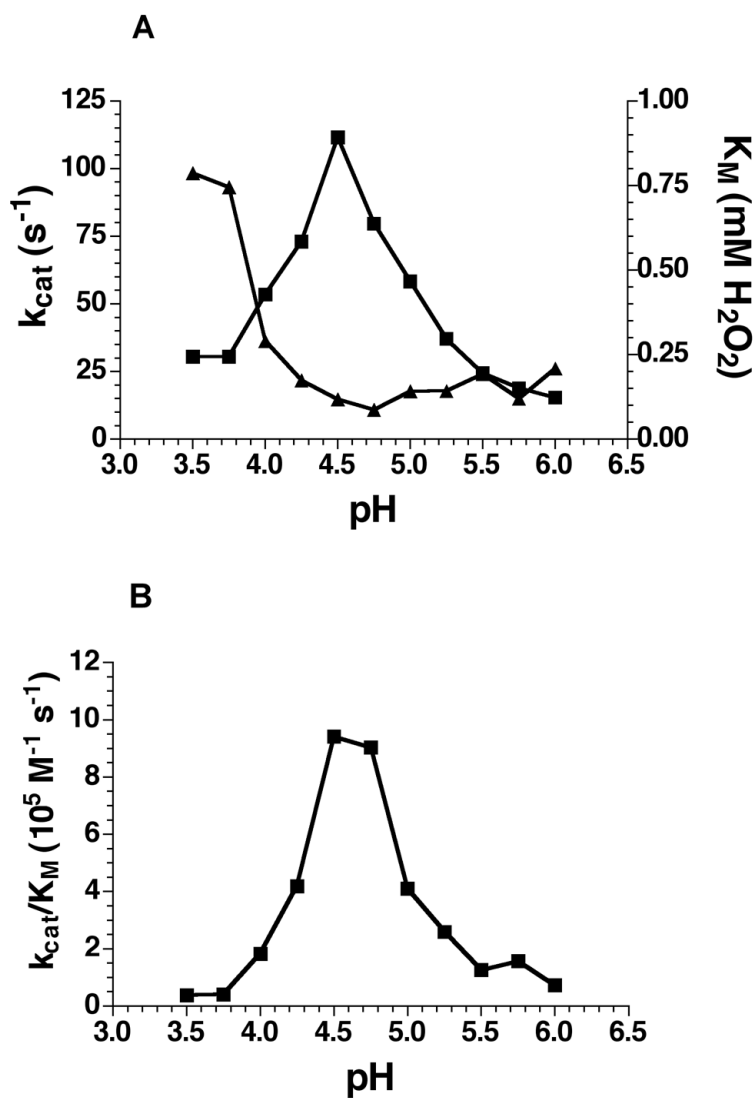


Figure 2.4: **Observed Peroxidase Kinetic Parameters Under Saturating ABTS Conditions.** (A) pH dependence of KatG peroxidase kinetic parameters k_{cat} (■) and K_M (▲) as determined by varying H_2O_2 concentration at 1 mM ABTS. (B) pH dependence of KatG peroxidase kinetic parameters k_{cat}/K_M as determined by varying H_2O_2 concentration at 1 mM ABTS.

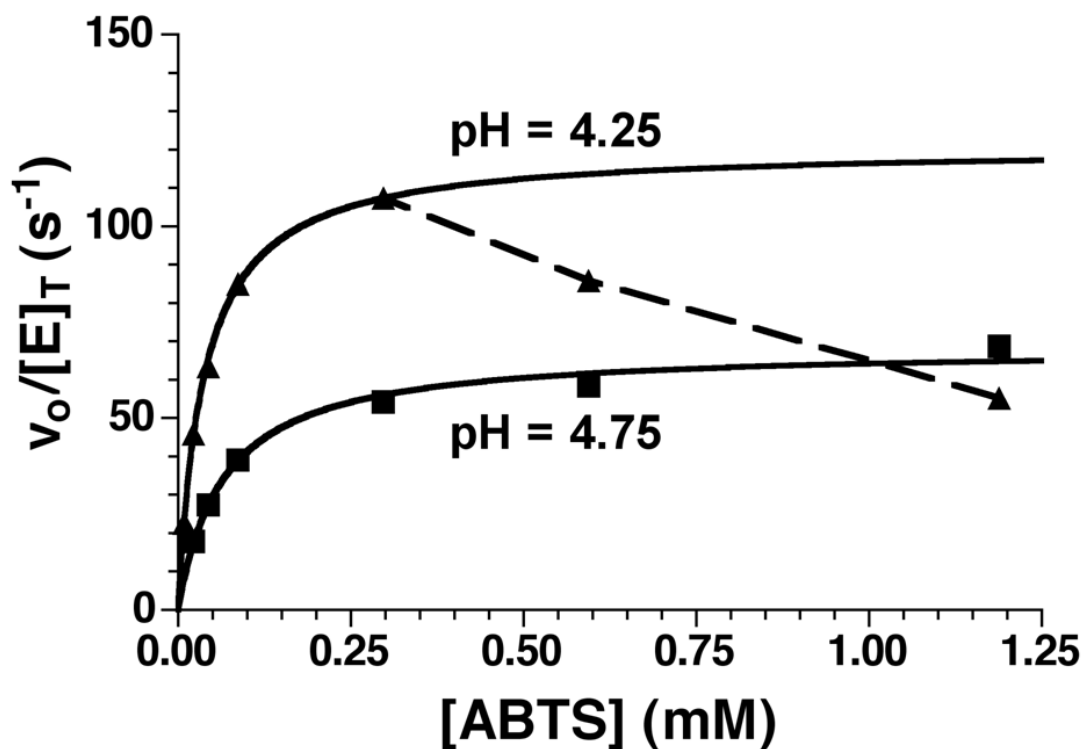


Figure 2.5: **Evidence of ABTS Inhibition.** Initial rates as a function of ABTS concentration at pH 4.75 (■) and 4.25 (▲). Dashed line demonstrates observed activity under inhibiting conditions.

pH	[ABTS]
4.5	1.2 mM
4.25	0.6 mM
4.0	0.3 mM
3.75	0.1 mM

Table 2.1: **Lowest Concentration of ABTS at Each pH Where Inhibition Was Observed.** As observed at 0.5 mM hydrogen peroxide in 50 mM acetate buffer.

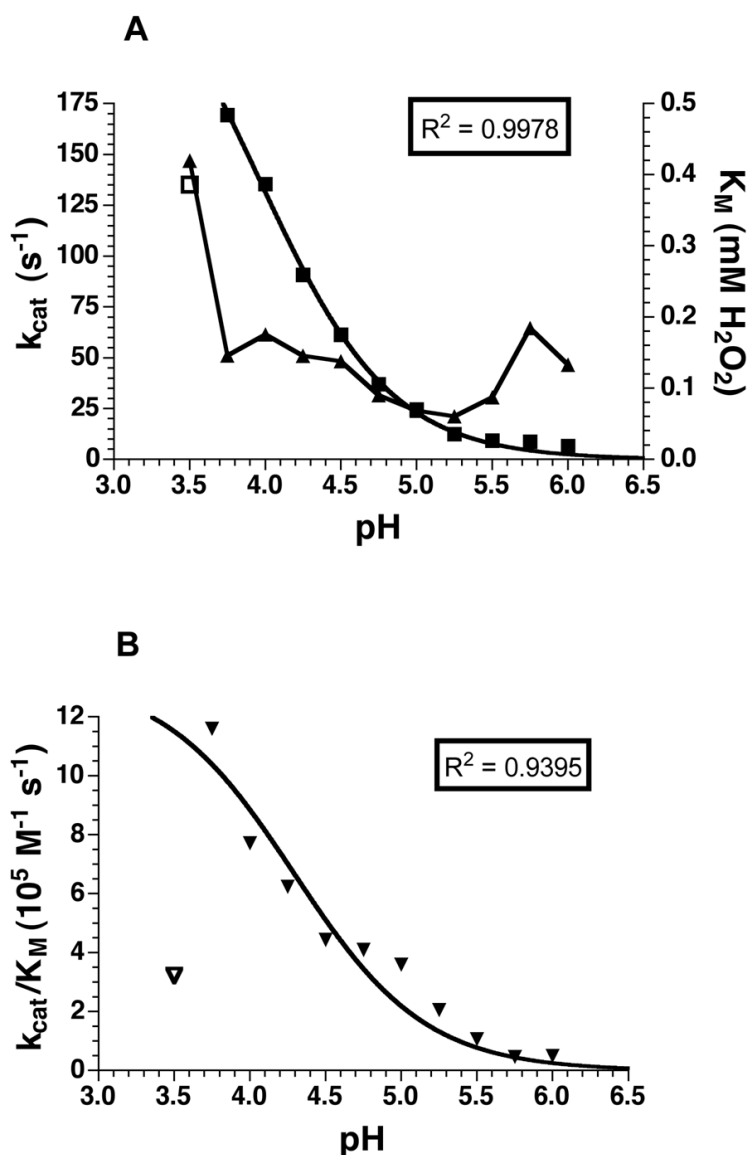


Figure 2.6: **Observed Peroxidase Kinetic Parameters Versus pH: Constant [ABTS]**. (A) Observed k_{cat} fit to equation 2.16 (■) and observed $K_M^{\text{H}_2\text{O}_2}$ (▲) of peroxidase when $[\text{ABTS}] = 0.05 \text{ mM}$. (B) Observed $k_{\text{cat}}/K_M^{\text{H}_2\text{O}_2}$ ($[\text{ABTS}] = 0.05 \text{ mM}$) fit to equation 2.15. Open symbols denote data not used in fitting.

a maximum at pH 3.75 of $9 \times 10^6 \text{ M}^{-1} \text{ s}^{-1}$. Although the exact values of the Michaelis constant towards ABTS and hydrogen peroxide cannot be determined from the data at hand, under the assumptions explained in the derivations, changes in k_{cat}/K_M should primarily be due to changes in K_M . This indicates that decreasing the pH is accompanied by a sharp decrease in K_M towards ABTS. This is consistent with increasing propensity of ABTS to act as an inhibitor of peroxidase activity at lower pH. Similar trends in observed K_M were seen with other reducing substrates (Table 2.2). The H_2O_2 - and ABTS-dependent kinetic parameters for the peroxidase activity of KatG indicated an abrupt shift in catalytic behavior below pH 3.75, indicating a substantial disruption of protein conformation. Far-UV CD spectra showed a dramatic loss of secondary structure with a mid-point for unfolding occurring at pH 3.6 (Figure 2.8). Spectra recorded between pH 5.0 and pH 3.75 were indistinguishable. Below 3.75, however, a dramatic change in the spectrum was detected, and below pH 3.5, the CD spectrum of KatG was relatively featureless. Furthermore, this is clearly not a buffer effect considering that both the folded and disrupted protein were observed in citrate buffer. A control assay at pH 3.5 containing heme and substrates but no enzyme had no significant activity. Therefore, any residual activity could be explained by a fraction of the protein remaining folded or partially folded.

2.3.2 Kinetic Parameters for Catalase Activity of KatG

The observed K_M for hydrogen peroxide determined at pH 7.0 was 3.8 mM, which is consistent with other KatGs (*Bp*KatG - 5.9 mM [70], *Syn*KatG - 4.2 mM [151], *Mtb*KatG - 2.5 mM [141]). The K_M s determined below pH 6.0, however, elevated to the point that saturating hydrogen peroxide concentrations could not be used due to inaccuracies inherent in absorbance values greater than 1. In those cases, the K_M should be treated as an estimate. The initial catalase velocity data points versus pH at hydrogen peroxide concentrations above the observed K_M s, (22 mM), below the K_M s (2.3 mM), and at an intermediate concentration (11 mM) did, in fact, follow typical activity trends (Figure 2.9A), that is, they indicate an enzymatic pH optimum at 6.50. This is true for all concentrations used

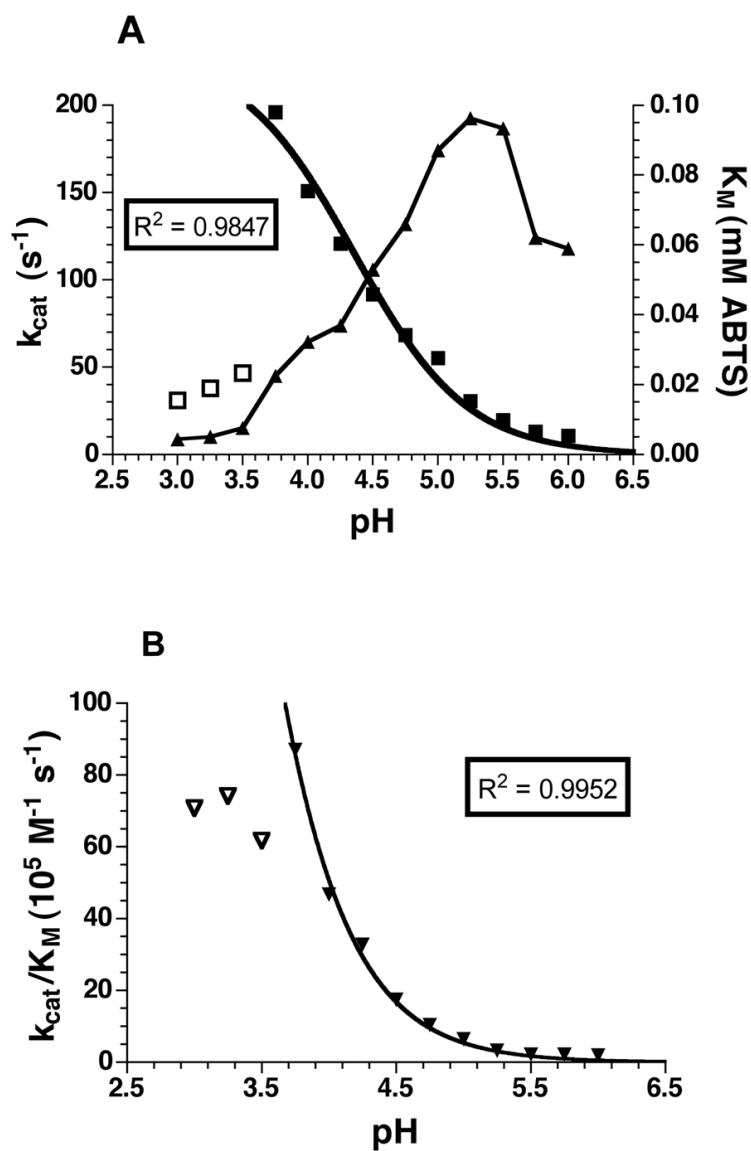


Figure 2.7: **Observed Peroxidase Kinetic Parameters Versus pH: Constant $[H_2O_2]$.** (A) Observed k_{cat} fit to equation 2.15 (■) and observed K_M^{ABTS} (▲) of peroxidase when $[H_2O_2] = 0.5$ mM. (B) Observed k_{cat}/K_M^{ABTS} ($[H_2O_2] = 0.5$ mM) fit to equation 2.16. Open symbols denote data not used in fitting.

pH	6.00	5.50	5.00	4.50	4.00
ABTS					
k_{cat} (s^{-1})	11 ± 1	20 ± 1	55 ± 1	92 ± 3	151 ± 6
K_M (mM)	0.06 ± 0.02	0.09 ± 0.03	0.09 ± 0.01	0.053 ± 0.006	0.032 ± 0.003
pyrogallol					
k_{cat} (s^{-1})	69 ± 2	64 ± 2	56 ± 1	44 ± 2	27 ± 1
K_M (mM)	1.6 ± 0.2	1.5 ± 0.2	1.3 ± 0.1	1.1 ± 0.2	1.1 ± 0.2
<i>o</i> -dianisidine					
k_{cat} (s^{-1})	71 ± 4	69 ± 6	58 ± 5	37 ± 5	24 ± 2
K_M (mM)	0.12 ± 0.02	0.11 ± 0.03	0.09 ± 0.02	0.05 ± 0.03	0.04 ± 0.01

Table 2.2: **Observed Kinetic Parameters for *E. coli* KatG Reducing Substrates.** Assays with ABTS contained 0.5 mM hydrogen peroxide. Assays with pyrogallol and *o*-dianisidine contained 0.4 mM hydrogen peroxide.

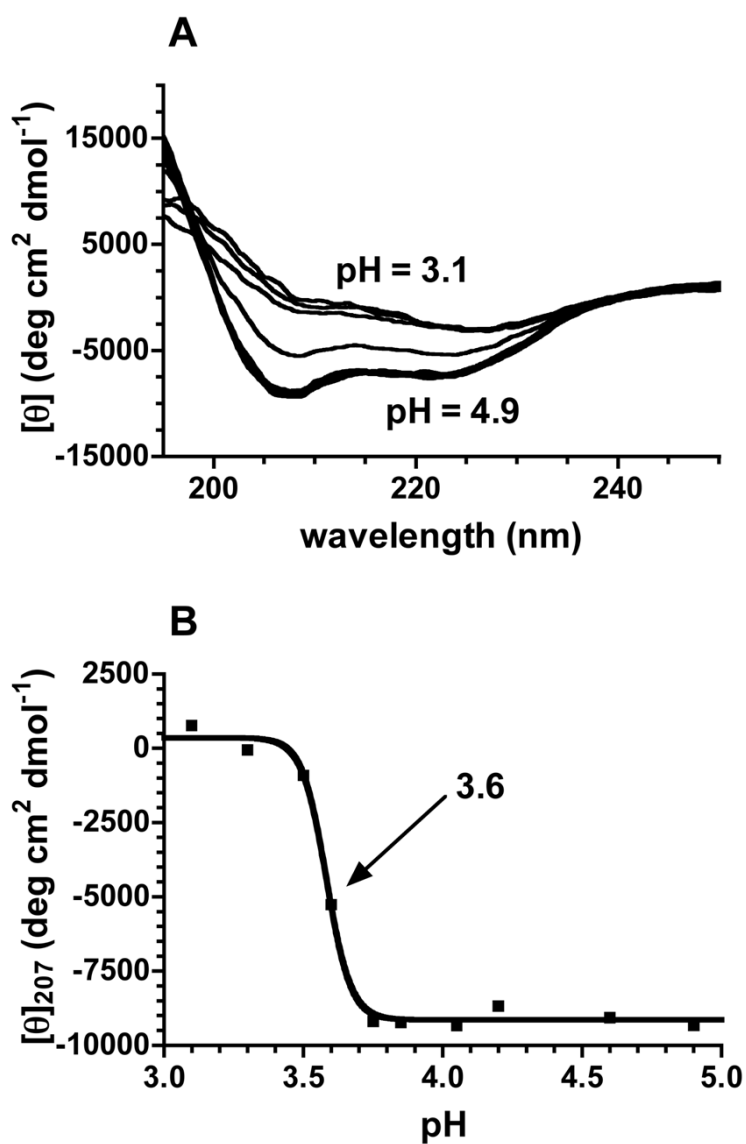


Figure 2.8: **Evidence of Protein Unfolding at Low pH.** (A) CD spectra obtained in 5 mM acetate buffer at pH 3.75, 4.05, 4.20, 4.60, and 4.90. CD spectra obtained in 5 mM citrate buffer at pH 3.10, 3.30, 3.50, 3.60, and 3.85. (B) CD signal at 207 nm as a function of pH.

in data collection, not just the three shown here. Curves generated from the catalase kinetic parameters, if they were to simulate the velocity curves, would have both exhibited optima at pH 6.5. Instead, the highest k_{cat} came at pH 5.75, while the greatest k_{cat}/K_M was observed at pH 7.00 (Figure 2.9B-C), indicating that understanding of a pH optimum is more complex than simply monitoring the velocity while varying the pH at saturating substrate conditions. A better understanding of the kinetic parameters is vital. Although the fitting of the kinetic parameter curves had surprisingly low R^2 values, the values obtained from the fitting were able to be used to generate the initial velocity curves with high accuracy in Figure 2.9A. This indicates that the pH optimum of 6.5 is an artifact of the balance between the optimum pH for reaction of the CpdI-H₂O₂ complex (5.75) and the optimum pH for the interaction of CpdI with H₂O₂ (7.00) (Figure 2.2).

2.3.3 Kinetic Parameters and p*K*_as

Not all kinetic constants could be determined from the steady-state approach taken here, however, the data do provide reasonable estimates of some of the slower rate constants. In the peroxidase cycle (Figure 2.1), HCpdI formation (k_4) and HCpdII reduction (k_6) can be determined from fitting the observed (k_{cat}/K_M) data for constant peroxide and constant ABTS to equations 1 and 2 respectively (Table 2.3). To eliminate protein-unfolding effects, data obtained at pH 3.5 and below were omitted in the analysis (Figures 2.6 and 2.7). The fit of the curves in Figures 2.6B and 2.7A (which were used for the determination of k_4) can both be seen to be less than ideal due to shoulders around pH 5.0. Alternative models (such as two p*K*_as with highest activity at lowest pH) were used to fit the data, but they did not improve the goodness of fit provided with a single p*K*_a model. As a result of loss of secondary structure, kinetic data could not be obtained below pH 3.75. This led to a degree of uncertainty in the peroxidase p*K*_as. It is clear from the data, however, that 4.5 can be established as an upper limit of the p*K*_as considering that the highest observed activity and efficiency were all at least twice the values of observed activity and efficiency at pH 4.5.

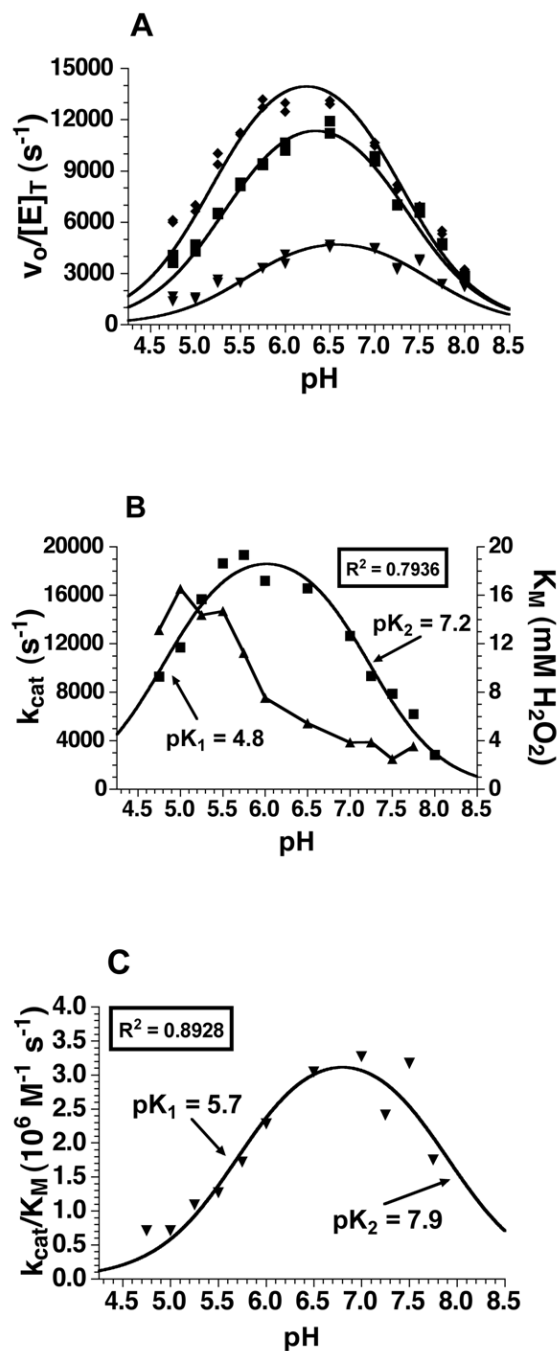


Figure 2.9: **Observed Catalase Kinetic Parameters Versus pH.** (A) Initial velocity as a function of pH at 22 mM H_2O_2 (\blacklozenge), 11 mM H_2O_2 (\blacksquare) and 2.3 mM H_2O_2 (\blacktriangledown). Fit lines are simulations of initial velocities given the above concentrations based on parameters determined by equations 2.29 and 2.30. (B) Observed k_{cat} fit to equation 2.29 (\blacksquare) and observed K_M (\blacktriangle) for catalase activity. (C) Observed k_{cat}/K_M for catalase activity fit to equation 2.30.

For catalase activity (Figure 2.2), the forward binding rate of peroxide to form E-H₂O₂ (k_5) and its subsequent reaction to form HCpdI (k_6) can be very nearly approximated from the fitting of the observed (k_{cat}) and observed (k_{cat}/K_M) data to equations 3 and 4 (Table 2.3). The data showed four $\text{p}K_a$ s for catalase activity - the HCpdI-H₂O₂ complex had a lower $\text{p}K_a$ of 4.8 and upper $\text{p}K_a$ of 7.2, whereas the HCpdI + H₂O₂ interactions had a lower $\text{p}K_a$ of 5.7 and upper $\text{p}K_a$ of 7.9. None of the catalase $\text{p}K_a$ s are close enough to possibly be attributed to the same residue, further emphasizing the separate pH optima for the HCpdI-H₂O₂ complex and the interactions between HCpdI and hydrogen peroxide. No effort is made here to assign $\text{p}K_a$ values to any specific residue. The rate constant data reported in Table 2.3, along with the $\text{p}K_a$ s reported here were used to calculate hypothetical initial velocities at the concentrations used in Figure 2.9A. The curves generated from these calculations are overlaid on the actual data, demonstrating a fit that validates the model and reported pH-independent constants.

2.4 Discussion

2.4.1 Optimal Peroxidase Activity and ABTS-dependent Inhibition

The kinetic behavior of KatG is not simple enough for a cursory evaluation. The multiple functions catalyzed by the same active site, the use of the same substrate to initiate two different catalytic cycles, inactivation of the enzyme by the presence of an excess of the oxidizing substrate peroxide, and an apparent control by pH as to which activity is dominant all lend to the kinetic complexity of KatG. The recognition that the catalytic pathway seemed to be directed by pH made it evident that optimal pH ought to be determined for each activity. To simplify the method of gaining this kinetic information, pH optima have been determined only by measuring initial velocities under highly saturating conditions across a wide range of pH values. This has consistently generated data that report catalase activity of KatG to be optimal at pH 6.5 and peroxidase activity of KatG to be optimal between pH 4.5 and 5.0.

Peroxidase	
k_4	$0.67 \times 10^6 \text{ M}^{-1} \text{ s}^{-1}$
k_6	$38.3 \times 10^6 \text{ M}^{-1} \text{ s}^{-1}$
Catalase	
k_5	$3.63 \times 10^6 \text{ M}^{-1} \text{ s}^{-1}$
k_6	$2.1 \times 10^4 \text{ s}^{-1}$

Table 2.3: **Approximated Rate Constants for *E. coli* KatG.**

A factor that has a profound influence on the activity of KatG that has not been considered is ABTS-dependent inhibition. Decreasing the pH below 4.5 correlates with a decreasing K_M for ABTS. This also correlates with an increasing effect of ABTS-dependent inhibition. In *E. coli* KatG lacking the large loop insertion between the F and G helices (or large loop 2), a low K_M for ABTS comparable to the K_M seen at low pH in the wild type KatG is observed for ABTS at pH 5.0, and with it strong evidence of ABTS-dependent inhibition [123]. The appearance of a smooth activity curve centered at pH 4.5 for peroxidase activity (as seen in Figures 2.3 & 2.4) can be explained by an apparent decrease in K_I for ABTS with decreasing pH. As long as ABTS concentration was held constant, the activity would be further inhibited. It should be noted that there have been instances where the optimal peroxidase activity of KatG has been reported below pH 4.5, but in those instances the optimal pH corresponds to the lowest pH at which the concentration of ABTS used does not inhibit (Table 2.1) [146].

By evaluating the kinetic parameters below the inhibition threshold, we saw that the pK_a s for the observable peroxidatic steps were below pH 4.5 with greater activity in the lower pH region, and that there was greater activity and efficiency at pH 3.75 than at any other pH or combination of substrate concentrations. Similarly, reduction rates for monofunctional peroxidases also increase as pH decreases for all substrates with the exception of substrates that are responsible for donation of both the proton and the electron for the formation of water. For these substrates, at sufficiently low pH, donation of a proton from solvent becomes competitive with substrate proton donation. ABTS is solely an electron donor, and proton transfer is required from the solvent [150]. This would suggest that the second-order rate constant and k_{cat} for reaction with ABTS should continue to increase as the pH decreases, contrary to a pH optimum centered at pH 4.5. In contrast, both pyrogallol and *o*-dianisidine are expected to transfer a proton [150, 153] leading to the anticipated decrease in activity as pH decreases (Table 2.2). As we have shown, maximum observed activity and catalytic efficiency do in fact increase and even accelerate as pH decreases to pH 3.75. Below pH 3.75, however, a sharp drop in activity was observed. Similar effects in

lignin peroxidase were ascribed to protein instability [154]. The loss of activity between pH 3.75 and 3.5 is concomitant with a significant loss of secondary structural content of KatG as shown by circular dichroism.

With the assumption that optimal peroxidase activity of KatG was in the range of pH 4.5 to 5.0, work has been done indicating a partial structural rearrangement of R426 in the *Bp*KatG sequence [128]. They report that at pH 4.5 R426(411 *E. coli*) is predominately (90%) oriented towards R492(479), R497(484), and D495(482) (R configuration); at pH 8.5 R426 is predominately (95%) oriented towards Y238(226) (Y configuration); and at pH 6.5 the orientation is approximately 50:50 R:Y. Ultimately, it is suggested that the optimal activities of peroxidase (4.5), catalase (6.5), and NADH-oxidase (8.75) may result from how the position of R426 affects the movement of electrons around the active site. In light of the data presented here, the structure / mechanism conclusions based on pH behavior may need to be explored further. Due to the structural disruption and loss of activity, the true optimum of peroxidase activity could not be observed, and we can only place an upper limit on the apparent pK_{as} (4.5). Although this does not negate the explanation given by Carpena *et al* [128], it does indicate that the orientation of the R426 may be only one of multiple pH-dependent features that optimize peroxidase activity. We will revisit this arginine movement in chapter 5 within the context of the roles of interdomain interface residues R479 and D482.

Our data show that pH control over which mechanistic pathway is utilized by KatG may be just as related to changes in substrate binding as it is to turnover mechanisms. Significant in the capacity of the enzyme to catalyze the peroxidase reaction is the decrease in K_M for ABTS simultaneous with the increase in apparent K_M for H_2O_2 in the catalase cycle as the pH is lowered. This would tend to favor a shift from catalase to peroxidase catalysis. Considering that peroxidase and catalase share the same initial oxidation step, this implies that binding of hydrogen peroxide to the ferryl-oxo form of the enzyme becomes less facile, disfavoring compound I reduction by H_2O_2 . As pH continues to drop, excess ABTS even interferes with activity itself. Although the binding site for ABTS is unknown,

it can be postulated that decreasing the pH below 4.5 results in a change in the binding site that allows for alternative inhibitory binding modes by ABTS. This would be facilitated with a more open and flexible binding site in this pH range - a flexibility that perhaps even foreshadows the secondary structural loss below pH 3.75. According to the CD data, however, any change in the ABTS binding site does not involve any observable change in secondary structural content of the protein. It is possible that increased affinity for ABTS is due to the negatively charged sulfonic acid groups being attracted to the more protonated enzyme at lower pHs, however, this would not explain the similar decrease in K_M of the neutral substrates pyrogallol and *o*-dianisidine (Table 2.2).

2.4.2 Different pH Optima for Binding and Activity in Catalase Cycle

With regards to catalase activity, it was expected that our data would simply be an addition to what was already known about catalase kinetics. It was surprising when our pH optima did not coincide with previously published results. This, however, resulted from the more exhaustive approach used to gather the data. Once it was realized that the data we had at any constant hydrogen peroxide concentration led to a pH profile comparable to those obtained by others, we were able to more fully accept the parameters as being as complex as they appeared. Different pH optima for binding and activity is certainly not uncommon. Recent spectral data lends support to this observation. Work done with *Syn*KatG, *Bp*KatG, and *Mtb*KatG show that catalase intermediates generated at pH 8.5 (and 7.0 for *Syn*KatG) have UV-visible spectral maxima at 418 and 520 nm, but intermediates generated at pH 5.6 have maxima at 415, 545, and 580 nm [151]. Our work with *E. coli* KatG indicates maximal catalase efficiency at pH 7.0, but maximal turnover number at pH 5.75. Furthermore, considering that saturating hydrogen peroxide concentrations were not feasible at the lower end of the pH range used, the k_{cat} values may be underestimated and the optimum pH for turnover would then be even lower than 5.75. Attempting to understand the structure-function relationship of catalase-peroxidases with the assumption of a pH optimum for catalase is 6.5 will yield unsatisfactory results if not coupled with the understanding that

this optimum results as the overlap of binding and activity pH curves. The multiple pK_a s of catalase activity give it a more complex appearance than peroxidase, which may have only one. The pH optimum for binding occurring where catalase turnover is not optimal (and vice-versa) provides a kinetic basis for what has primarily been a structural-based argument (concerning features such as the covalent cross-link and duplicated domain) that catalase activity was obtained by ancestral monofunctional peroxidases (possibly related to lignin peroxidases) and is not an activity that is indigenous to the enzyme.

CHAPTER 3
PRESENCE OF REDUCING SUBSTRATES BROADENS
CATALASE ACTIVITY PH RANGE

3.1 Introduction

Peroxidase kinetic characterizations have largely neglected the fact that some fraction of the enzyme population is going through the catalase cycle according to the classical scheme (Figure 1.13). This results in artificially lowering the peroxidase activity ascribed to KatG. In chapter 2, we saw that the pH optima of *Escherichia coli* KatG (*EcKatG*) for catalase and peroxidase were separated by nearly 3 pH units (3.75 for peroxidase, 6.5 for catalase), and from pH 4.5 to 5.5 the enzyme exhibited only a fraction (<50%) of either activity. To date, KatG kinetics have been performed by taking advantage of this large difference by performing them so that only the necessary substrates were present and at a pH appropriate to minimize the interference by the alternative catalytic cycle; but with the majority of published peroxidase data being acquired between pH 4.5 and 5.0, interference by catalase activity should not be considered negligible. Quantification of this interference would be beneficial in interpreting published kinetic data. Furthermore, understanding the kinetics of KatG while all catalytic pathways are available is much more biologically relevant than the classical assay.

We monitored the oxygen production attributed to catalase activity with and without a wide number of known or potential reducing substrates. We found that reducing substrates not only fail to inhibit catalase turnover around pH 5.0, but they actually enhance oxygen production rates. Evaluating the pH range over which this occurs suggests that this effect serves to broaden the pH range of optimal catalase activity. Finally, we suggest that the presence of the reducing substrate activates oxygen production by protecting the enzyme

from inactivation, corroborating recently published data and further supporting the concept that the classic portrayal of the KatG catalytic cycles is largely insufficient.

3.2 Materials and Methods

3.2.1 Materials

Hydrogen peroxide (30%), imidazole, hemin, Sephacryl 300 HR, ampicillin, chloramphenicol, sodium dithionite, phenylmethylsulfonyl fluoride (PMSF) 2,2'-azino-bis(3-ethylbenzthiazoline-6-sulfonic acid) (ABTS), L-tyrosine, phenazine, chlorpromazine (CPZ), 3,3'-dimethoxybenzidine hydrochloride (*o*-dianisidine), guaiacol, ferulic acid, L-ascorbic acid, and pyrogallol were purchased from Sigma (St. Louis, MO). Isopropyl- β -D-thiogalactopyranoside (IPTG), mono- and di-basic sodium phosphate, acetic acid, sodium acetate, ethanol, and sodium hydroxide were obtained from Fisher (Pittsburgh, PA). L-tryptophan was purchased from J.T. Baker Chemical Company (Phillipsburg, NJ). Bugbuster and benzonase were purchased from Novagen (Madison, WI). The *E. coli* strain BL-21 [DE3] pLysS was obtained from Stratagene (La Jolla, CA). Nickel-nitrilotriacetic acid (Ni-NTA) resin was purchased from Qiagen (Valencia, CA). All buffers and media were prepared using water purified through Millipore Q-PakII system (18.2 M Ω /cm resistivity).

3.2.2 Expression, Purification, and Reconstitution of *EcKatG*

Expression and purification of *EcKatG* was carried out as described in chapter 2. Heme reconstitution and holoenzyme concentration determination was also carried out as described in chapter 2.

3.2.3 Activity Assays

Data for the pH-dependent peroxidase and catalase assays come from chapter 2. To monitor the effects of peroxidatic substrate on catalase activity, assays were performed by

monitoring oxygen production with a Hansatech DW1 oxygen electrode chamber (Pentney, Norfolk, England) using accompanying Oxygraph Plus software. Reducing substrates ABTS, ascorbate, CPZ, ferulic acid, guaiacol, *o*-dianisidine, phenazine, pyrogallol, tryptophan, and tyrosine were each added to the assays to determine their effects on oxygen production. Ferulic acid and tyrosine stock solutions were prepared as 10 mM in 0.1 M NaOH. Guaiacol stock solution was prepared as 10 mM in 5% ethanol. Phenazine stock solution was prepared as 10 mM in 50% ethanol. All other stock solutions were prepared in water. Unless otherwise noted, assays were performed using 2.5 nM enzyme and appropriate volume of solvent (baseline) or stock solution in 50 mM acetate buffer and initiated with 10 μ L of the appropriate concentration of hydrogen peroxide (1 mL final reaction volume) at 21 °C. Effect of reducing substrate was represented using the following equation:

$$\text{effect} = \frac{\text{activity with substrate}}{\text{activity without substrate}} - 1 \quad (3.1)$$

A positive effect would indicate oxygen production enhancement, a negative number would indicate inhibition, and zero would indicate that the substrate had no effect on oxygen production. Due to the high concentration of ethanol required to dissolve phenazine, assays involving 1 mM phenazine could not be performed due to enzyme precipitation.

3.2.4 End-point Assays and UV-visible Spectra

End-point assays were used to determine which of the ten substrates listed above were serving as peroxidase substrates. Two samples were prepared for each substrate containing 2.5 nM enzyme and 0.1 mM substrate at pH 5.0. To one of the samples, 1.0 mM hydrogen peroxide was added. These reacted for 2 hours, and then their absorbance spectra were taken at room temperature using a Shimadzu UV-1601 spectrophotometer (Columbia, MD) with a cell pathlength of 1.0 cm. The difference between the two spectra was then

divided by the maximum absorbance to normalize the difference spectra of the various substrates to fraction-changed difference spectra. All other spectra were also recorded at room temperature on the Shimadzu UV-1601 spectrophotometer.

3.3 Results

3.3.1 Effect of Reducing Substrates on Oxygen Production

To evaluate what portion of the enzyme population was still contributing to catalase activity during peroxidase assays at pH 5.0, we measured catalase activity by oxygen production with and without ten different possible peroxidatic reducing substrates (Figure 3.1). Activity effects were determined at 0.1 and 1.0 mM reducing substrate and hydrogen peroxide. Of the ten, only the amino acids tyrosine and tryptophan did not have an effect on catalase activity. Of the remaining eight, only 1 mM *o*-dianisidine was actually observed to inhibit catalase activity, and it surprisingly served to enhance oxygen production at 0.1 mM, as did the remaining seven in all cases. Phenazine enhanced oxygen production by about 25%, and ferulic acid and guaiacol were only marginally more potent. ABTS, ascorbate, and pyrogallol, however, enhanced oxygen production by over 150% at certain concentrations of substrate and 1.0 mM hydrogen peroxide. The strongest activation was observed with the substrate CPZ where oxygen production was more than quadrupled at 1.0 mM hydrogen peroxide. In the absence of enzyme, reducing substrate and hydrogen peroxide did not generate molecular oxygen (data not shown).

A survey of the characterization of eight catalase-peroxidases from a variety of sources showed that *o*-dianisidine and pyrogallol have been shown to be a peroxidase substrate in nearly all cases [105–112]. ABTS has been reported as a substrate in many of those and is commonly used due to its high solubility in water and large absorption coefficient [106, 107, 111, 112]. No instances were found in which CPZ, ferulic acid, phenazine, or the amino acid tryptophan were tested, although all have been used as substrates for some monofunctional peroxidases [155–158]. Guaiacol was found to be a substrate for the

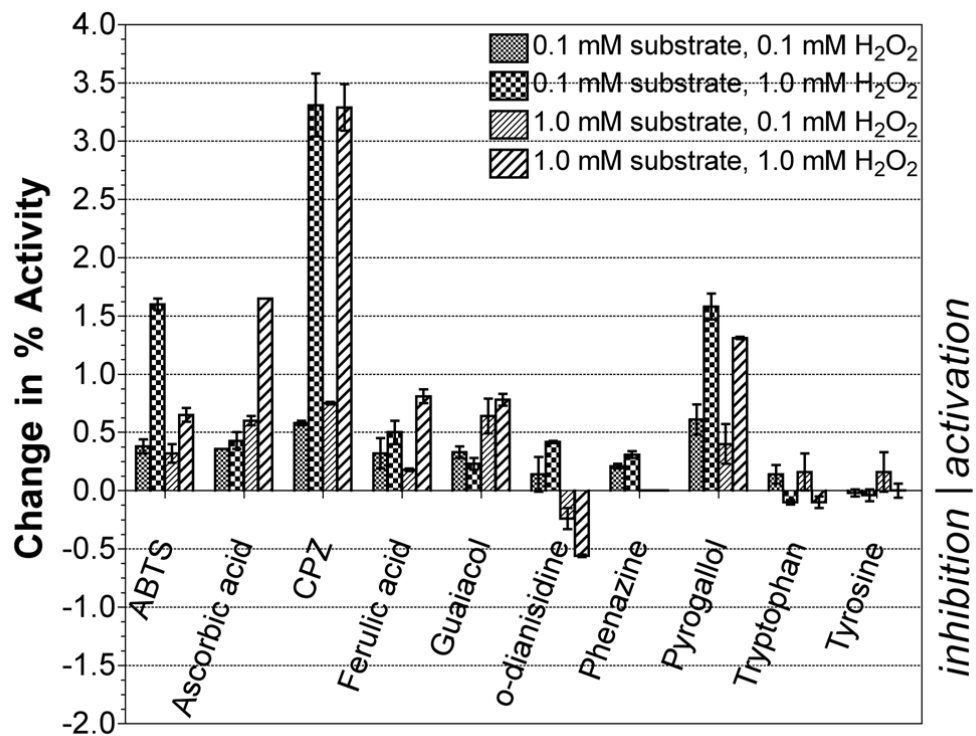


Figure 3.1: **Effects of Reducing Substrate on Catalase Activity at pH 5.0.** Change in % activity based on Equation 3.1

catalase-peroxidase isolated from *E. coli* [105], *Synechocystis* PCC 6803 [109], and *Penicillium simplicissimum* [107], but not from *Rhodopseudomonas capsulatus* [108] or *Burkholderia cenocepacia* [106]. Ascorbate was not found to be a peroxidase substrate for *Rhodopseudomonas capsulatus* [108] or *Synechocystis* PCC 6803 [109], but has been used as a peroxidatic electron donor along with tyrosine in the Y249F variant of *Synechocystis* PCC6803 KatG [126]. Using end-point assays to observe substrate consumption or oxidized product formation, we observed that ABTS, ascorbate, guaiacol, pyrogallol, and *o*-dianisidine all showed evidence of being peroxidase substrates with the predicted increase in absorbance at the wavelength corresponding to oxidized product: ABTS - 417 nm, guaiacol - 450 nm, *o*-dianisidine - 460 nm, pyrogallol - 430 nm (Figure 3.2). Oxidized ascorbate decomposes rapidly and could not be visualized, but a clear decrease in absorbance at 270 nm was observed. Small changes in the spectral features of CPZ and ferulic acid were also observed, but were too slight to be considered significant. Tyrosine and tryptophan showed no evidence of oxidation or consumption.

3.3.2 Evaluation of Role of pH on Activation Effects

It was important to establish whether this activation was isolated to the pH region where both peroxidase and catalase activities were diminished when measured independently, or if it also occurred close to their pH optima. ABTS was used to determine the effect of pH on the enhancement of oxygen production for the reasons listed above and the wealth of data already assembled for *Ec*KatG peroxidase activity with ABTS. At pH 4.0, ABTS does act as an inhibitor of catalase activity, but the most significant evidence of oxygen production enhancement occurs from pH 4.5 to 5.5 (Figure 3.3). This falls directly in the range where catalase and peroxidase activity fall below 50% of their individual optima.

It has been established that the increase in Michaelis constant (K_M) for hydrogen peroxide contributes significantly to the decrease in observed catalase activity as pH decreases [151, 159]. Determination of the K_M for hydrogen peroxide at pH 5.0 both with and without the presence of ABTS did reveal that having the electron donor present decreased the

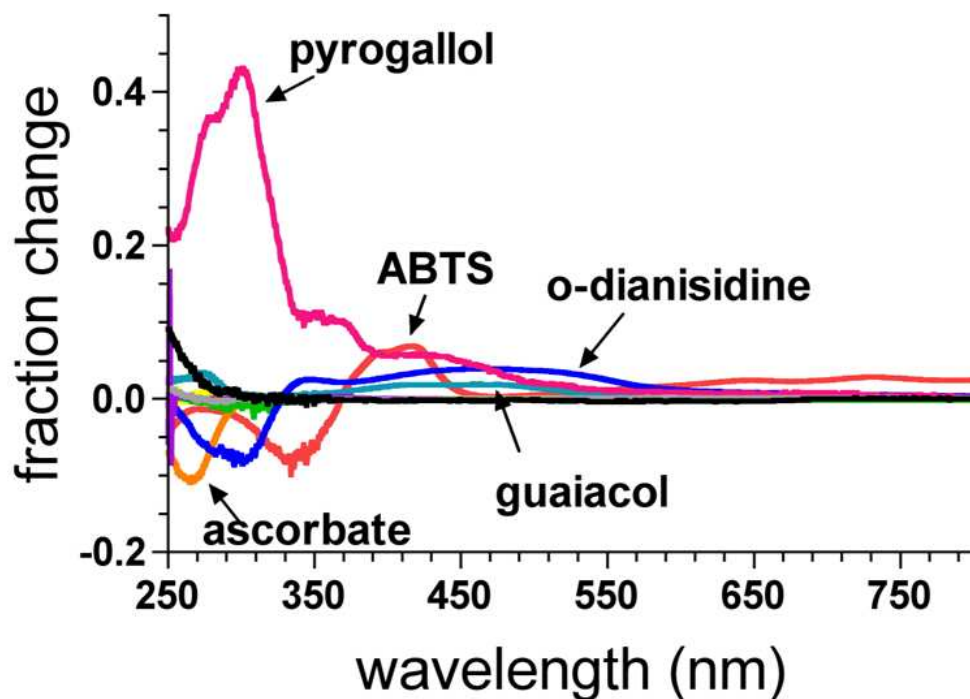


Figure 3.2: **Evidence of Peroxidatic Consumption of Reducing Substrates.** Each line is the difference spectrum of 0.1 mM substrate incubated with 2.5 nM *EcKatG* at pH 5.0 for 2 hrs with and without 1.0 mM H_2O_2 added normalized to the maximum absorbance for the respective species in that wavelength range. Those with most significant changes are noted. The ten substrates shown are ABTS (red), ascorbate (orange), CPZ (yellow), ferulic acid (green), guaiacol (cyan), *o*-dianisidine (blue), phenazine (purple), pyrogallol (pink), tryptophan (gray), and tyrosine (black).

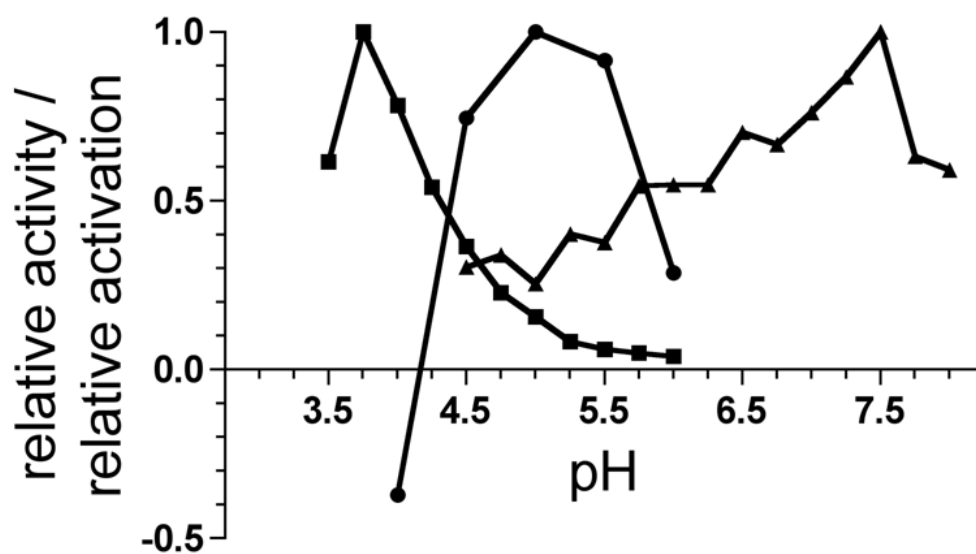


Figure 3.3: **pH-dependence of Activation with ABTS Compared to Catalase and Peroxidase Activities.** Peroxidase activity (■) determined with 0.06 mM ABTS, 1.0 mM H₂O₂. Maximum peroxidase activity observed was 145 s⁻¹ at pH 3.75. Catalase activity (▲) determined with 1.0 mM H₂O₂. Maximum catalase activity observed was 1200 s⁻¹ at pH 7.5. Oxygen activation (●) determined with 0.1 mM ABTS, 1.0 mM H₂O₂. Maximum activity (917 s⁻¹) observed with ABTS present was 2.6 times activity without ABTS (353 s⁻¹) at pH 5.0.

K_M (Figure 3.4). Although this would account for the activation at low hydrogen peroxide concentrations, it could not explain how all of the assays that evidenced activation had more linear traces than the slower baseline assays that did not contain the electron donor. Velocities are much more sensitive to changes in substrate concentration when it is present at sub K_M concentrations, and even peroxide consumption rates by KatG become more hyperbolic as the K_M increases relative to a given initial peroxide concentration [151]. Figure 3.5 shows an example of two assays with very similar rates, yet the more linear of the two includes the substrate ABTS and peroxide at sub K_M concentration, and the more hyperbolic trace has no reducing substrate and contains peroxide in excess of the K_M (ten times the concentration of peroxide in the ABTS-containing assay). Bearing in mind that the total peroxide consumption in these two assays is approximately 100 μM , reactant consumption should have a negligible effect on the oxygen production rate of the 10 mM peroxide assay and the assay would be expected to be more linear. Furthermore, with the products of catalase activity being water and molecular oxygen, it is equally unlikely that product inhibition could account for the hyperbolic nature of the trace. This leaves enzyme inactivation as the most likely suspect for the rate deceleration.

3.3.3 Effect of Reducing Substrate Presence on Reacted Enzyme Spectra

Assuming an inactive form of the enzyme would be produced in the presence of hydrogen peroxide, but would be prevented or rescued by the presence of reducing substrates, we took a series of absorption spectra to attempt to visualize any potential inactive intermediate (Figure 3.6). Spectrum **1** contained only *Ec*KatG at pH 5.0. Spectrum **2** was a control showing that the presence of ABTS and ascorbate did not affect the spectrum after a 60 second incubation. Ascorbate was included to prevent the accumulation of ABTS radical, a strong absorber in the heme Soret region. Spectrum **3** was taken following 60 seconds of reaction of *Ec*KatG with 1.0 mM hydrogen peroxide. A red-shift in the Soret band to 407.8 was observed, along with a loss of features at 516 and 543 and a blue-shift of the CT band at 633 to below 620. Also, an increase in light-scattering was observed which can

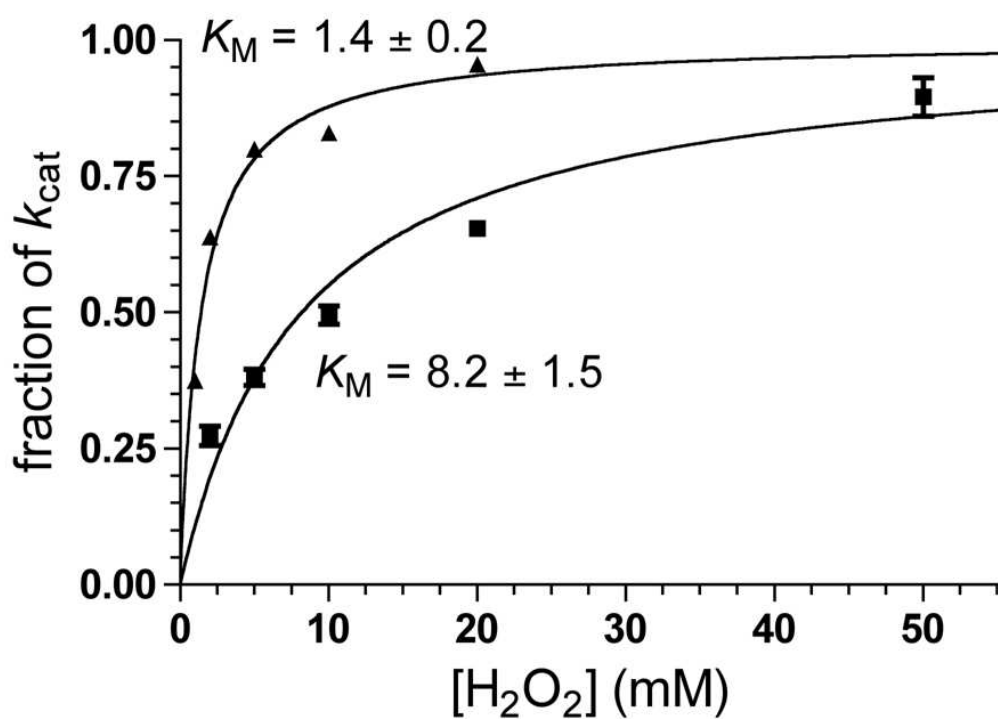


Figure 3.4: **Effect of ABTS on Apparent K_M for H_2O_2 at pH 5.0.** Activity assays with (▲) and without (■) ABTS fit to standard Michaelis-Menten curve.

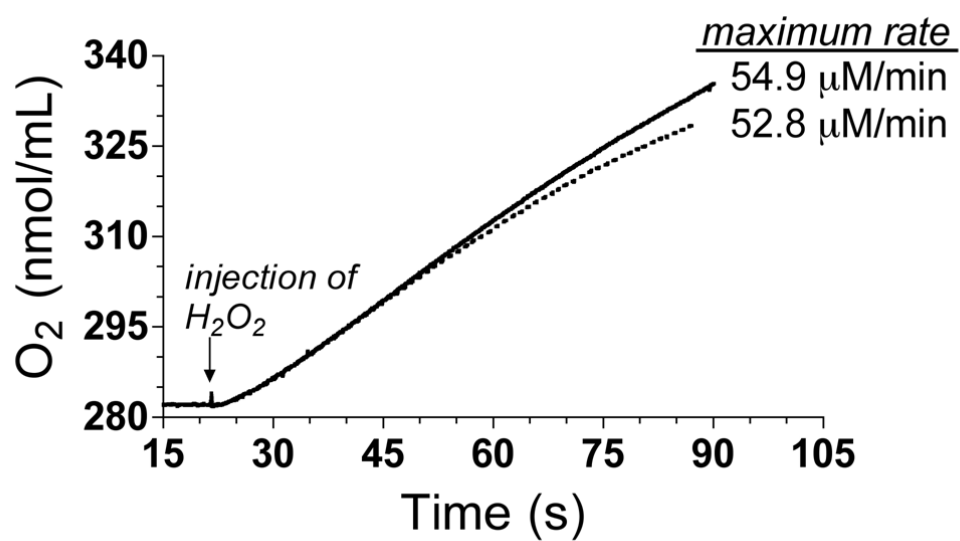


Figure 3.5: **Effect of ABTS on Linearity of Catalase Initial Rates.** Solid line is assay performed with 1.0 mM H₂O₂ and 0.1 mM ABTS. Dashed line is assay with 10 mM H₂O₂ without ABTS.

be characteristic of oxygen bubble production accompanying catalase turnover. With the high concentration of enzyme used, this was not unexpected. Spectrum 4 was also taken following 60 seconds of reaction with 1.0 mM hydrogen peroxide, but included ABTS and ascorbate in the reaction. The light scattering was even more evident, but the spectral features of the spectra 1 and 2 were retained, indicating a prevention of the accumulation of a non-resting state species. Assignment of the new spectral features to a species is not necessary for the purposes here and would be difficult due to low accumulation. However, further investigation into the identity of the accumulated species would provide more insight into the possible mechanism.

3.4 Discussion

The mechanism of differentiation between catalase and peroxidase activity in KatG is a process which is undergoing much discussion. Catalase-peroxidase isolated from *Archaeoglobus fulgidus* undergoes rapid inactivation in the presence of H₂O₂, but it has also been noted that ABTS has a “stabilizing effect” on the enzyme, increasing the half-life three-fold at pH 4.5 [111]. It was not suggested what this inactivation might be. Of the eight substrates expected to be good peroxidatic electron donors (this excludes tyrosine and tryptophan), all enhanced oxygen production rates with only one exception that will be discussed below. There is nothing in our data to suggest that this is anything other than a result of an increase in catalase turnover. The lack of oxygen production in the absence of enzyme eliminates the possibility of some non-enzymatic reaction as an explanation. Furthermore, considering that accumulation of oxidized substrate is not required to observe enhanced oxygen production rates, we can conclude that it is the reducing substrate itself, and not the oxidized counterpart, that activates the oxygen production (Figure 3.5).

The only substrate to demonstrate significant inhibition of oxygen production was *o*-dianisidine. This was also observed in *Escherichia coli* catalase peroxidase by Claiborne *et al* in the first characterization of a catalase-peroxidase [105]. They used the catalytic inhibition by *o*-dianisidine to monitor peroxidase activity without the interfering effects of

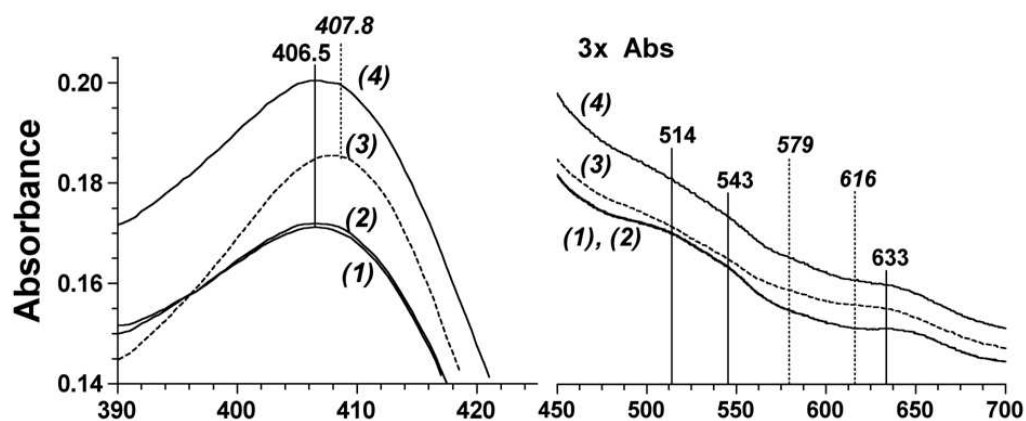


Figure 3.6: **“Dead-end” Species Does Not Accumulate When ABTS Is Present.** (1) $1.4 \mu\text{M}$ *EcKatG*. (2) $1.4 \mu\text{M}$ *EcKatG* incubated with 0.1 mM ABTS and 0.5 mM ascorbic acid for 60 seconds. (3) $1.4 \mu\text{M}$ *EcKatG* reacted with 1.0 mM H_2O_2 for 60 seconds. (4) $1.4 \mu\text{M}$ *EcKatG* reacted with 1.0 mM H_2O_2 for 60 seconds in the presence of 0.1 mM ABTS and 0.5 mM ascorbic acid. Italicized numbers indicate wavelengths of features more prominent in spectrum **3**; standard numbers indicate wavelengths of features diminished in spectrum **3**.

hydrogen peroxide consumption by catalase activity. Enzyme inactivation by 0.33 mM *o*-dianisidine was observed by monitoring peroxidase activity, but inactivation by numerous other electron donors (including guaiacol and pyrogallol) was not observed. Their results indicated that *o*-dianisidine at sufficiently high concentrations can irreversibly inactivate the enzyme. As such, inhibition by *o*-dianisidine can be treated as unique and occurs through a mechanism not yet described and unavailable to other electron donors.

At this point, two very surprising and significant facts become clear regarding both the enzyme mechanism and the ability of KatG to consume peroxide. First, differentiation between the catalase and peroxidase cycles must occur prior to interaction with the second substrate, a phenomenon not previously suggested for catalase-peroxidases and obviously unnecessary to suggest for monofunctional peroxidases. Secondly, nature has fine-tuned KatG to maintain high levels of catalytic hydrogen peroxide consumption across its entire range of pH, more similar to monofunctional catalases, in spite of its remarkable structural similarity to monofunctional peroxidases. We will discuss each of these individually.

If peroxidatic reducing substrates interacted with an intermediate involved in catalase turnover (such as the ferryl heme porphyrin cation radical), they also must act as competitive inhibitors of oxygen production. This is evidently not the case. If, however, differentiation between catalase and peroxidase turnover occurs following reaction with the first molecule of peroxide but prior to reaction of the second substrate, in the absence of a reducing substrate a fraction of the enzyme population would dedicate itself to a “dead-end” peroxidase pathway, progressively inactivating the population (Figure 3.7). The presence of an electron donor would, however, allow for the completion of the peroxidase cycle, opening a pathway back to the resting state, preventing inactivation and resulting in higher observed catalase rates. This is consistent with our results. The accumulation of a “dead-end” would explain the hyperbolicity seen in Figure 3.5 and spectral changes in Figure 3.6.

Coupled with research done on catalase intermediates found in the literature, our results have led us to propose the scheme found in Figure 3.7 as a possible mechanistic pathway. The inclusion of protein-based radicals in catalase-peroxidase mechanistic schemes has been

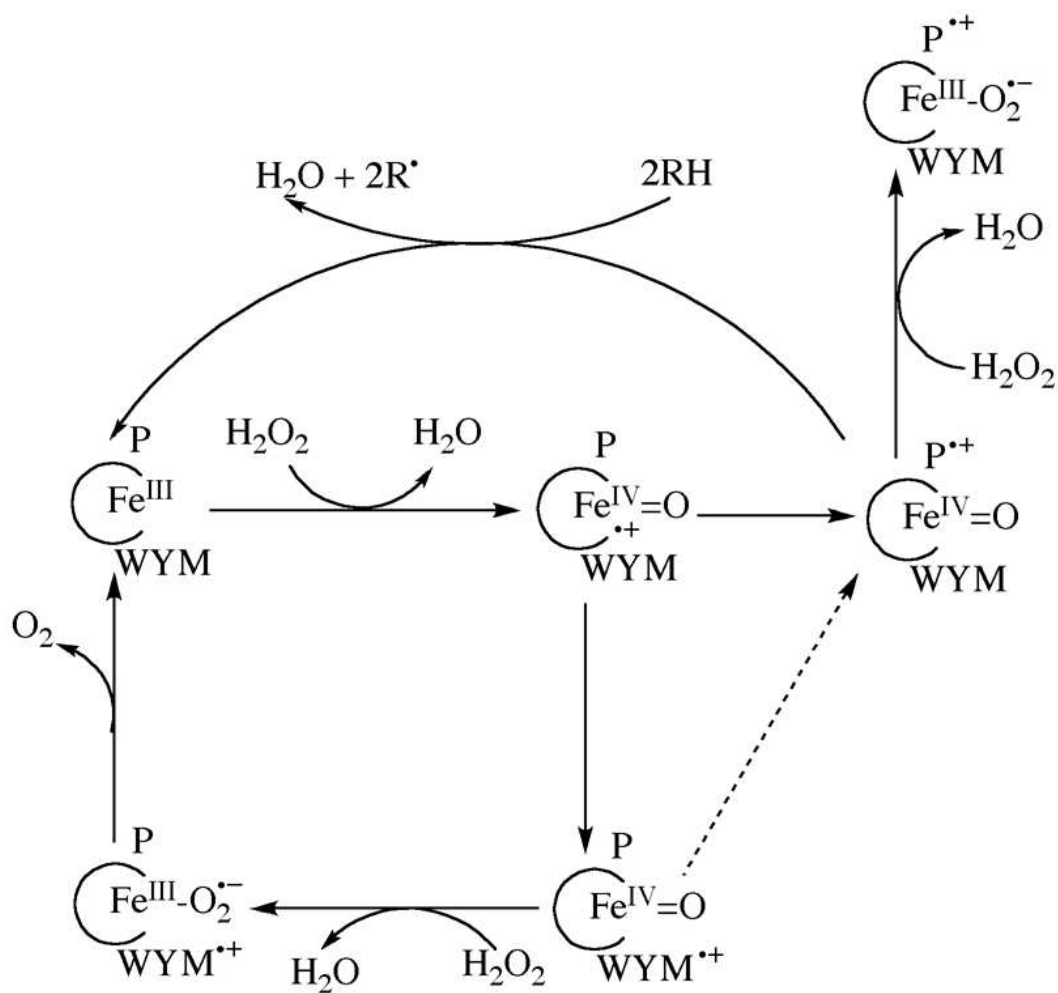


Figure 3.7: A Proposed Scheme Accounting for Differentiation Between Catalase and Peroxidase Prior to Substrate Interaction, and including possible dead-end pathway available when reducing substrate is not present.

discussed at length [124, 139–142, 144, 145, 160], particularly following the identification of the covalent adduct involving a methionine, tyrosine, and tryptophan. Heme-dioxygen intermediates in the catalase cycle have also been discussed more recently, and are the most recently proposed intermediates in the mechanism based on rapid freeze quench electron paramagnetic resonance studies of catalase intermediates [143]. Building on these recently published mechanisms, we propose that peroxidase activity also requires a rapid radical transfer prior to turnover completion. In variants incapable of forming the covalent adduct, rapid accumulation of a species with a Compound III-like spectrum in the presence of excess hydrogen peroxide has been observed in our lab (data not shown) and others [126, 139]. This supports the idea that rapid radical transfer occurs following reaction with the initial hydrogen peroxide. If the radical is transferred to the nearby covalent adduct, the heme-dioxygen intermediate formed upon further reaction with hydrogen peroxide can be rescued by the electron hole on the adduct. If the radical is transferred to some other (possibly external) site, reaction with peroxide would form an inactive heme-dioxygen species. Furthermore, an external site would explain the ability of large molecules like ABTS and CPZ to be such efficient electron donors in spite of the narrow access channel to the heme active site.

Prior to the observations made here, with catalase activity decreasing as pH dropped and peroxidase activity not being substantial until below the pK_a 4.5, there was a large apparent pH gap in activity, and thus a pH gap in peroxide consumption ability. A gap such as this would be detrimental to an organism's ability to deal with oxidative stress and would be expected to be disfavored by nature. At pH 5.0, we observed that *EcKatG* in the presence of 0.1 mM ABTS generates molecular oxygen at 250% of the rate of the enzyme with hydrogen peroxide alone (Figure 3.1). This also happens to be where catalase is around 30 - 40% of optimal activity (Figure 3.3), restoring oxygen production to 75 - 100% of optimal. ABTS only inhibited below the pK_a for peroxidase activity. Essentially, the presence of ABTS expanded the effective pH range of catalase activity all the way to the point where peroxidase turnover is most active, eliminating the gap in efficient hydrogen

peroxide consumption. This activity broadening mechanism would be particularly crucial for an organism such as *M. tuberculosis*, which does not have any other catalase active protein to deal with oxidative stress. Overall, it is striking to observe how nature has maximized this enzymes ability to decompose hydrogen peroxide using two mechanisms, utilized by the same active site, that work synergistically rather than competitively.

CHAPTER 4
GENERATION OF MIXED SPIN-STATE POPULATION
VIA Y111A SUBSTITUTION

4.1 Introduction

To this point, the focus has been on the parametrics affecting the kinetic properties of KatG. In these next two chapters, our attention will turn to the role of global structure in catalytic ability, particularly the interactions between the N- and C-terminal domains of KatG.

Just as the calcium in class II peroxidases interact with residues on the catalytic histidine bearing B helix and BC interhelical loop [94–97, 102], the C-terminal domain in KatG interacts with the N-terminal domain in the same region. Investigation of the interdomain interface reveals that the residues along the interface are highly conserved and create two hydrogen bonding networks between 25 and 30 Å away. The closer network involves interactions of Tyr111 and backbone carbonyls on the BC interhelical loop with Asp482 and Arg479 on the B'C' interhelical loop respectively. The other contact exists between Arg117 on the BC interhelical loop with Asp597 on the E' helix (Figure 4.1).

Elucidating the roles of the individual interdomain interactions is anticipated to help us in our understanding of how the C-terminal domain restructures the N-terminal active site and imparts activity to the enzyme. The interaction nearest the active site is the Y111-D482 pair. We chose to disrupt this interaction first by mutating only Y111 to an alanine (Y111A) since D482 is within hydrogen-bonding distance of R479 and may affect its positioning for interaction with the backbone carbonyls of the BC interhelical loop. We then observed the spectral and kinetic properties of Y111A. The spectral results demonstrated that preparations of this variant yielded a mixture of high- and low-spin heme states, thus creating the

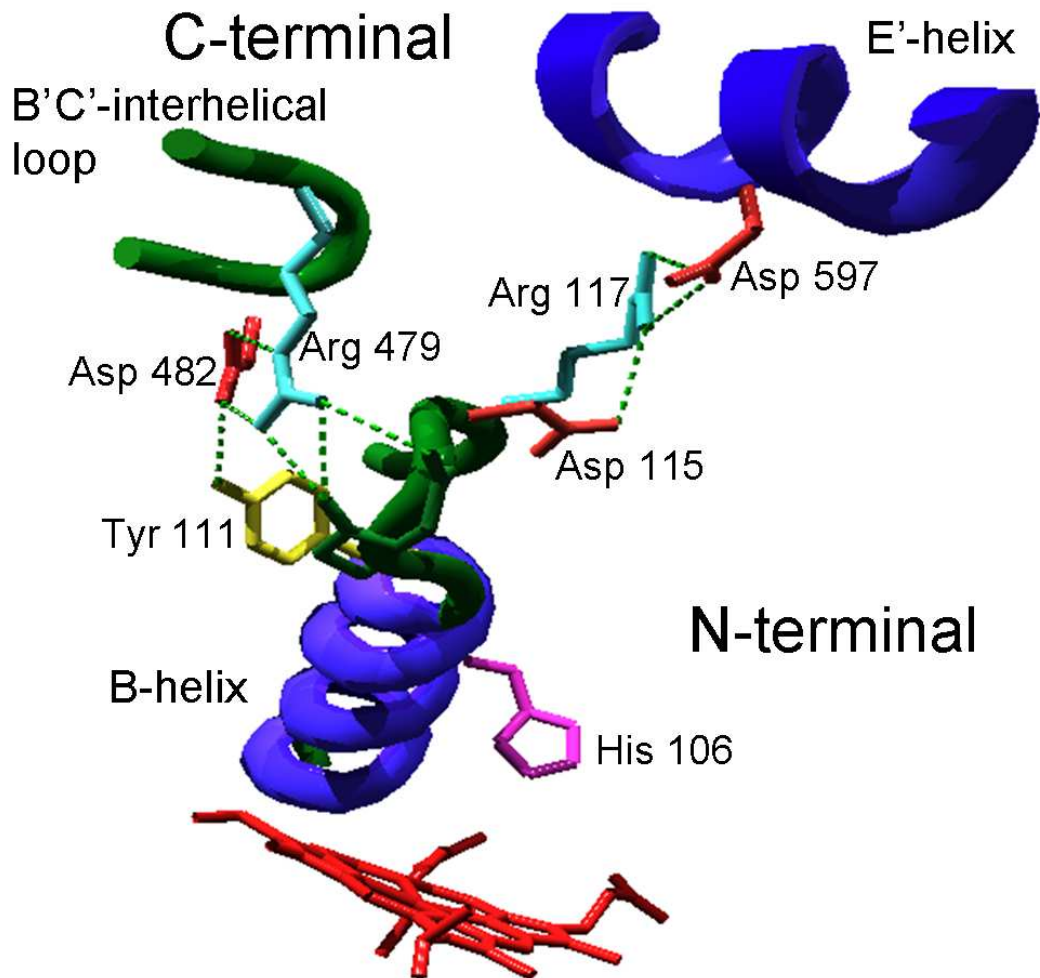


Figure 4.1: **Interactions Between the N-terminal BC Interhelical Loop and C-terminal Domain of KatG.** All C-terminal domain structures are labeled with primed letters (e.g., E'-helix), and all structures from the N-terminal domain are shown with unaccented letters (e.g., B-helix). Coordinates from the structure of *Burkholderia pseudomallei* KatG were used (PDB accession number 1MWV) [117]. Numbering reflects *Escherichia coli* KatG sequence.

appearance of a transition between wild type (high-spin) and C-terminal domain-lacking (low-spin) KatG (KatG^N). Concurrently there was a loss of activity, suggesting that the Y111-D482 does play a role in preventing His106 coordination. Furthermore, we showed that peroxidase activity becomes proportionally more favorable than catalase activity when compared to the wild type, insinuating that the Y111-D482 interaction is also involved in properly configuring the enzyme for bifunctionality.

4.2 Materials and Methods

4.2.1 Materials

Hydrogen peroxide (30%), imidazole, hemin, ampicillin, chloramphenicol, sodium dithionite, phenylmethylsulfonyl fluoride (PMSF), and 2,2'-azino-bis(3-ethylbenzthiazoline-6-sulfonic acid) (ABTS) were purchased from Sigma (St. Louis, MO). Isopropyl- β -D-thiogalactopyranoside (IPTG), urea, mono- and di-basic sodium phosphate, acetic acid, and sodium acetate were obtained from Fisher (Pittsburgh, PA). Bugbuster and benzonase were purchased from Novagen (Madison, WI). All restriction enzymes were purchased from New England Biolabs (Beverly, MA). All oligonucleotide primers were purchased from Invitrogen (Carlsbad, CA). All *E. coli* strains (BL-21 [DE3] pLysS and XL-1 Blue) and Pfu polymerase were obtained from Stratagene (La Jolla, CA). Nickel-nitrilotriacetic acid (Ni-NTA) resin was purchased from Qiagen (Valencia, CA). Desalting chromatography columns were purchased from Bio-Rad. All buffers and media were prepared using water purified through Millipore Q-PakII system (18.2 M Ω /cm resistivity).

4.2.2 Cloning

The plasmid pKatG(Y111A) was prepared using mutagenic primers [5'-GCG GGG ACT GCA CGT TCA ATC GAT GG-3' (coding) and 3'-CGC CCC TGA CGT GCA AGT TAG CTA CC-5' (non-coding)] for pKatG according to the QuikChange procedure (Stratagene, La Jolla, CA). Amplification products were used to transform *E. coli* XL-1 Blue by

electroporation (BIO-RAD MicroPulser, Hercules, CA). Plasmids from candidate colonies were evaluated by diagnostic restriction digest and DNA sequence analysis. Correctly mutated plasmid was used to transform *E. coli* (BL-21 [DE3] pLysS).

4.2.3 Expression and Purification

Expression and purification of Y111A KatG was carried out similar to wtKatG as described in chapter 2 with few exceptions. Prior to loading the cell lysate onto the Ni-NTA column, urea was added to a concentration of 2M to relax the protein for better column binding. Due to higher affinity of the protein for the Ni-NTA column than wild type, the protein did not require a gradient elution. Instead, the column was washed with 2, 20, and 200 mM imidazole in 50 mM phosphate buffer / 200 mM NaCl pH 7.0. The 20 and 200 mL washes were demonstrated to contain the target protein by SDS-PAGE and were combined. Also, due to such low levels of non-target protein contamination, the eluted protein only needed to be separated from the imidazole and urea using a desalting column. Protein fractions were combined and concentrated with Amicon ultrafiltration concentrator. Concentration of purified enzyme was estimated according to the method of Gill and von Hippel [50] ($\epsilon_{280} = 1.43 \times 10^5 \text{ M}^{-1} \text{ cm}^{-1}$).

4.2.4 Absorption Spectra and Activity Assays

Enzyme was reconstituted with 0.9 equivalents of hemin. Reconstituted enzyme solution incubated at 4 °C for 72 hours to allow unincorporated heme to settle out of solution. The solution was then centrifuged and the precipitated heme and other insoluble material discarded. Concentration of reconstituted enzyme was determined using the pyridine hemochrome assay [161]. Protein containing heme in the ferrous state was prepared by adding a small amount (<10 mg) of sodium dithionite to the native enzyme. All spectra were obtained at room temperature on a Shimadzu UV-1601 spectrophotometer (Columbia, MD) with a cell pathlength of 1.0 cm.

Catalase and peroxidase activity assays were performed as described in chapter 2. Initial velocities were fit to Michaelis-Menten equation by non-linear regression analysis to determine apparent kinetic parameters. If inhibition was evident, the fitting equation was modified to a general excess substrate-dependent inhibition model:

$$\frac{v_o}{[E]_{\text{tot}}} = \frac{k_{\text{cat}}[S]}{K_M + [S] + \frac{[S]^2}{K_N}} \quad (4.1)$$

where K_N is a macroscopic constant that reflects the ability of the substrate to act as an inhibitor.

4.2.5 Stopped-flow

Binding of CN^- by Y111A KatG was monitored using an SX.18 MV Stopped-flow Rapid Reaction Analyzer (Applied Photophysics, Surrey, UK) in single mixing mode. One syringe contained 5 μM Y111A KatG and the second contained KCN (20–400 μM). Spectra were recorded by diode array. Kinetic constants were determined from triplicate measurements of single wavelength data recorded at 414 nm. All reactions were carried out at 25 $^\circ\text{C}$ in 100 mM phosphate buffer, pH 8.0.

4.2.6 Magnetic Circular Dichroism

Y111A KatG, wtKatG, and KatG^N spectra were obtained using 15 μM enzyme in 50 mM phosphate 50 mM NaCl buffer, pH 7.0. Spectra were recorded at 23 $^\circ\text{C}$ in a quartz cell (5.0 mm path length) with 1.4 Tesla magnetic cell holder from 700–350 nm on a Jasco J-810 spectropolarimeter (Tokyo, Japan). Baseline and analysis were done using Jasco J-720 software. Y111A KatG containing ferrous heme was prepared by adding a small amount (<10 mg) of sodium dithionite to the native enzyme.

4.2.7 Electron Paramagnetic Resonance

Spectra were recorded using a Bruker EMX instrument equipped with an Oxford ESR 900 cryostat and ITC temperature controller. Additional sample concentration was performed using Amicon Ultra-4 centrifugal devices. The settings for the spectrometer were as follows: temperature, 10 K; microwave frequency, 9.38 GHz; microwave power, 0.1 mW; modulation amplitude, 10 G; modulation frequency, 100 kHz; time constant, 655.36 ms; conversion time, 655.36 ms; and receiver gain, 1.0×10^5 .

4.3 Results and Discussion

4.3.1 UV-visible Absorption

The heme absorption spectra for native (ferric) and reduced (ferrous) Y111A KatG were taken and compared with the spectra of the wild type KatG (Figure 4.2 and Table 4.1). The wild type ferric heme spectrum is consistent with a mixture dominated by penta- and hexa-coordinate high-spin heme iron [162]. The shift of the Y111A Soret band to 411 nm and the red shift of the charge transfer two (CT2) band into the beta region suggest a greater contribution from a low-spin species in the Y111A ferric heme spectrum. In fact, the band at 525 nm most likely has contributions from both CT2 and β -band absorption. These spectral features were not influenced by the identity of the buffer, the ionic strength of the solution, or by formation of the crosslink through reaction with 100 equivalents of hydrogen peroxide. Changes in pH also had no effect on the spectrum from 8.0 to 6.0. Between pH 6.0 and 4.5, however, the spectra indicated signs of increased protein aggregation as evidenced by light scattering and precipitation, but no change in the position of spectral features after centrifugation. At pH 4.0 removal of the precipitate through centrifugation resulted in a spectrum similar to wtKatG, indicating that the population of Y111A contributing low-spin heme was completely insoluble at this pH.

The ferrous Y111A Soret band appeared at 427 nm, consistent with a low-spin heme system, but also demonstrated a substantial shoulder near 440 nm where high spin ferrous

heme absorbs. In the alpha and beta region of the ferrous spectrum (520 nm - 600 nm), high-spin heme exhibits an absorption band near 560 nm and a shoulder between 580 and 590 nm, such as is observed with the wild type KatG. Low-spin ferrous heme exhibits absorption bands near 530 and 560 nm. Y111A absorbed at 560 nm with shoulders near 530 and 585 nm, also indicative of a mixture of both high and low-spin ferrous heme.

4.3.2 Cyanide Binding

Changes in the rates or mechanism by which a KatG variant binds cyanide compared to the wild type can provide insight into changes in accessibility of the active site. Y111A KatG, unlike the wild type [51, 130], demonstrated a two-phase binding process including a fast phase and a slow phase. Previous cyanide binding experiments with a novel periplasmic catalase-peroxidase, KatP, also showed a two-phase process. One phase was dependent on cyanide concentration, but the other was not [51]. In Y111A, however, both phases were linearly dependent on cyanide concentration (Figures 4.3A and B). The fast phase had an apparent rate constant (or on-rate - k_{on}) of $3.5 \times 10^5 \text{ M}^{-1} \text{ s}^{-1}$, which is comparable to the apparent rate constant of wtKatG - $5 \times 10^5 \text{ M}^{-1} \text{ s}^{-1}$ [51]. The slow phase had an apparent rate constant of only 4% of the fast phase - $1.7 \times 10^4 \text{ M}^{-1} \text{ s}^{-1}$. The amplitudes of the two phases were independent of cyanide concentration (Figure 4.3C), with 64.1% of the amplitude coming from the faster phase and the remaining 35.9% coming from the slower phase (determined from the average amplitude across all concentrations). When considered alongside the UV-Vis spectral data, it is reasonable to suggest that the two phases in the Y111A stopped-flow experiment are in fact two distinct species - each undergoing a single-phase binding step. The fast phase would correspond to a high-spin species, and the slow phase a low-spin species.

The dissociation rate of cyanide (k_{off}) is determined by the y-intercept of the k_{obs} vs. $[\text{CN}^-]$ plots (Figures 4.3 A and B), allowing for calculation of the dissociation constant (K_D) for cyanide from the k_{off}/k_{on} . The K_D corresponding to the first exponential was determined to be 11.1 μM . Within error, k_{off} for the slow phase was zero, suggesting that

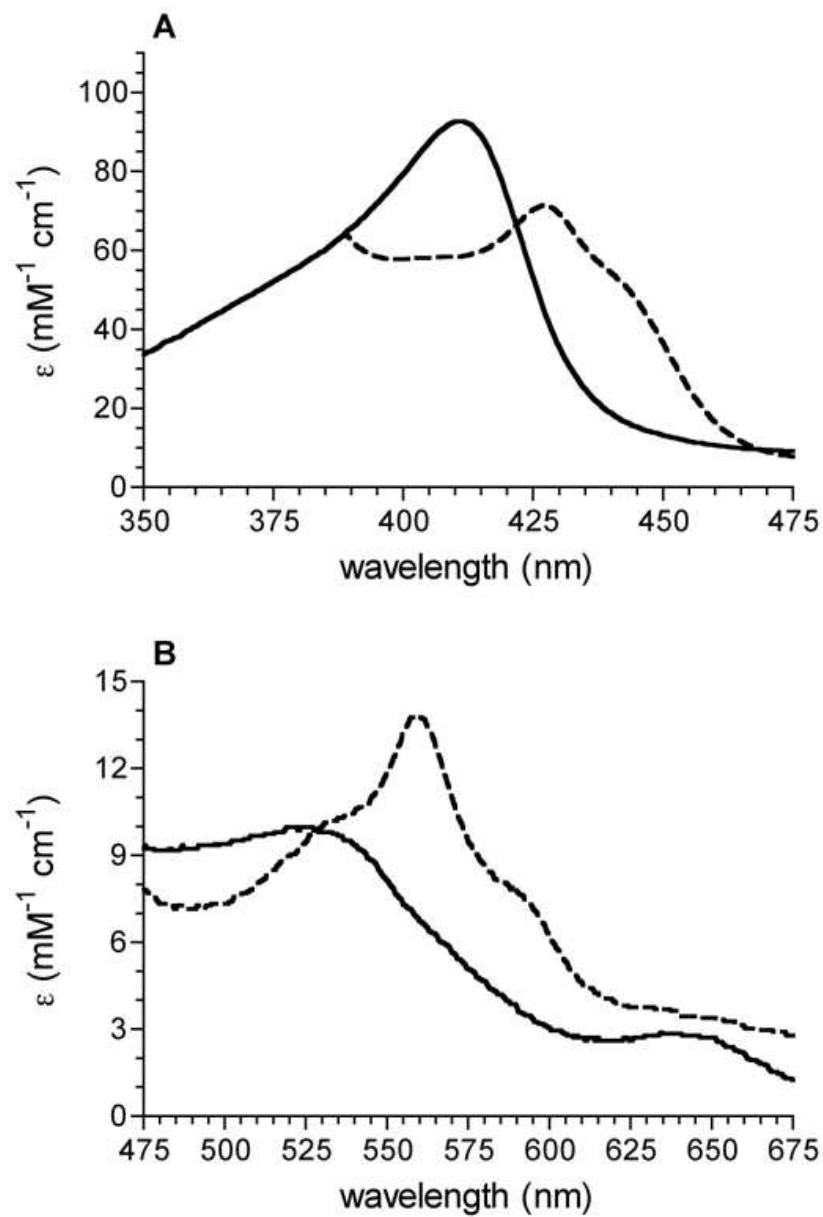


Figure 4.2: **UV-visible Absorption Spectra of Native and Reduced Y111A KatG.** Native Y111A (—) contains heme in the ferric state. Reduced Y111A (---) contains heme in the ferrous state. (A) Soret region of heme absorption spectrum. (B) α , β , and charge transfer region of heme absorption spectrum.

Heme state	protein	Absorption band maxima [nm (mM ⁻¹ cm ⁻¹)]				
		Soret(γ)	β	α	CT2	CT1
ferric	wtKatG	408 (120.7)	-	-	502 (17.5)	629 (9.7)
	Y111A	411 (92.7)	525 (9.98)	-	-	634.5 (2.91)
ferrous	wtKatG	439 (79.8)	565 (15.1)	581 (10.7)	-	-
	Y111A	427 (71.5)	535 (10.3)/ 559 (13.8)	586.5 (8.07)	-	-

Table 4.1: **Spectral Features of Ferric and Ferrous Wild Type and Y111A KatG.**

this CN^- binding event is irreversible. Performing an equilibrium titration with cyanide revealed only one K_D around $10 \mu\text{M}$, consistent with the stopped-flow data.

4.3.3 Magnetic Circular Dichroism

In order to more effectively differentiate the high and low-spin contributions to Y111A KatG spectra, we employed magnetic circular dichroism. As noted in chapter 1, this technique is preferable to UV-vis absorption in that the differences between ferrous high-spin and ferrous low-spin are significantly more pronounced. Empirically, low-spin ferrous heme is easily distinguished by a very strong A-term corresponding to the Q-band (i.e., the α -band). This signal is not present in high-spin ferrous heme. The B-bands (from Soret absorption) are also typically distinct for the high- and low-spin states. Examples of low- and high-spin ferrous heme spectra can be found in [163–166] as well as in reviews [55, 167].

The spectrum of the ferrous Y111A KatG (Figure 4.4) contained obvious low-spin features, but not exclusively. The A-term centered at 557 nm was clearly present, but it was accompanied by other features in the 575 to 625 nm range consistent with high-spin ferrous heme. Furthermore, the B-band more closely resembled that of high-spin ferrous heme than low-spin, albeit with less intensity. Similar to the UV-vis spectra, these features were unchanged after formation of the crosslink through reaction with 100 equivalents of hydrogen peroxide.

We were able to correlate this spectrum with the cyanide-binding data from our stopped-flow investigation by generating a simulated Y111A KatG MCD spectrum using ferrous wtKatG and ferrous KatG^{N} as endpoints on a continuum of spin-state populations observed in KatG, the wtKatG being dominated by high-spin species and KatG^{N} representing the exclusively hexacoordinate low-spin complex (Figure 4.4A). By calculating the weighted average of the two using the amplitude fractions from the stopped-flow data, a simulated spectrum was generated:

$$\text{calculated} = 0.64 \times (\text{wtKatG spectrum}) + 0.36 \times (\text{KatG}^{\text{N}} \text{ spectrum}) \quad (4.2)$$

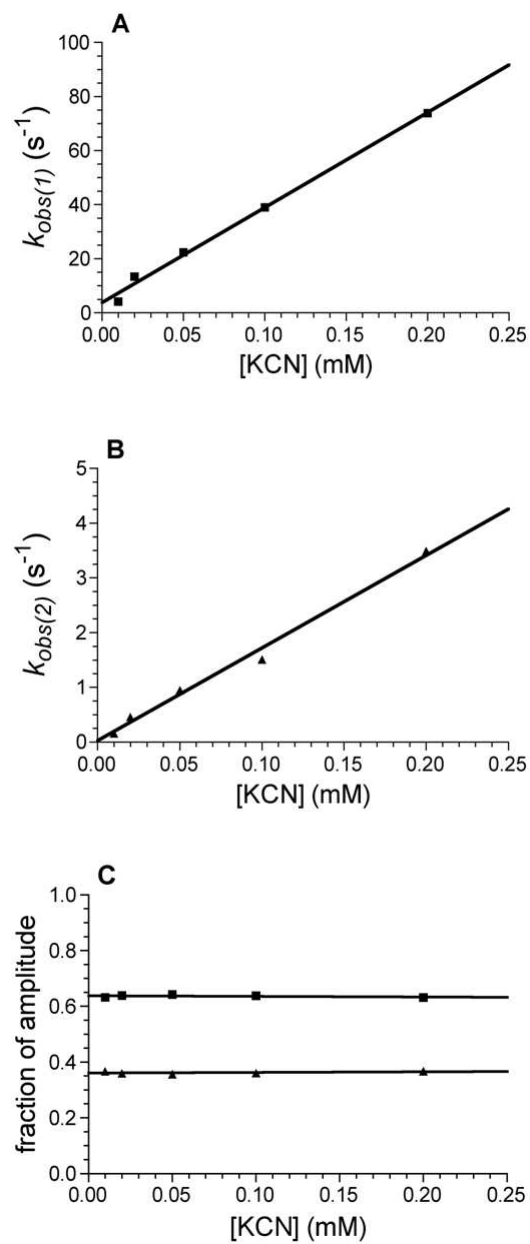


Figure 4.3: **Stopped-flow Cyanide Binding Shows Two Distinct Species in Y111A KatG.** (A) $k_{on} = 3.5 \times 10^5 M^{-1} s^{-1}$. (B) $k_{on} = 1.4 \times 10^4 M^{-1} s^{-1}$. (C) The fractions of amplitude of fast (■) and slow (▲) phases are independent of cyanide concentration. Fast phase: $64.1 \pm 0.7\%$. Slow phase: $35.9 \pm 0.7\%$.

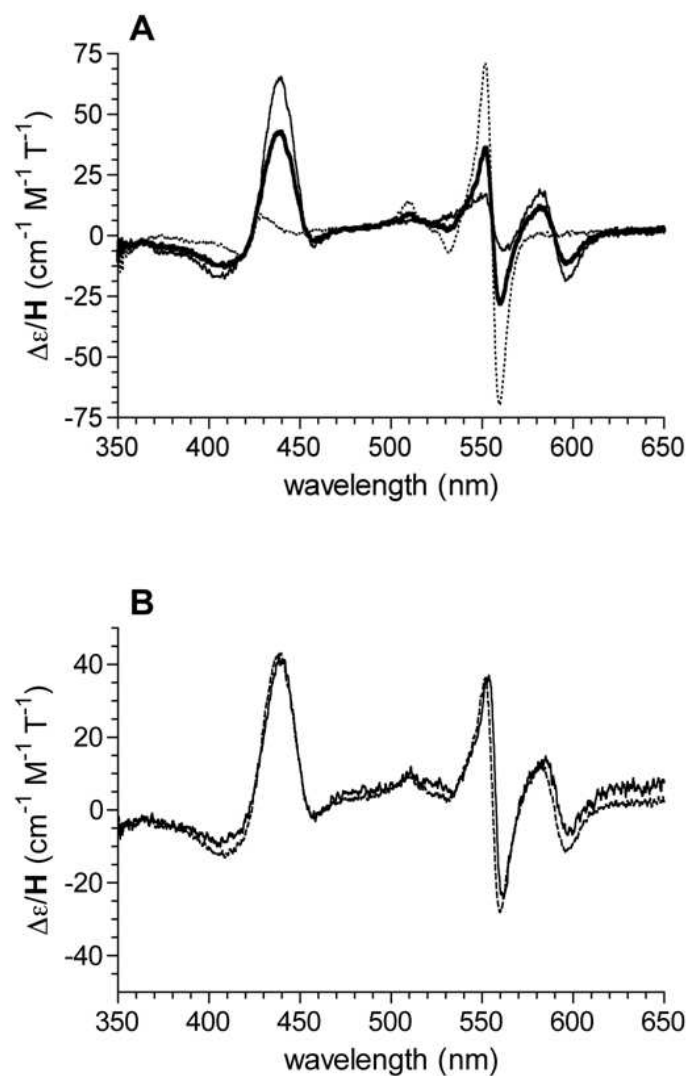


Figure 4.4: **Prediction of Y111A KatG Ferrous Heme MCD Spectrum.** (A) The calculated Y111A KatG spectrum (—) overlaid with the reduced wild type spectrum (---) and the reduced KatG^{N} spectrum (· · ·). (B) Actual Y111A KatG spectrum (—) overlaid with the calculated Y111A KatG Spectrum (— · —).

The actual MCD spectrum of ferrous Y111A KatG was virtually indistinguishable from the calculated (Figure 4.4B). In the absence of the C-terminal domain, His106 coordinates the heme iron [130]. Likewise, in Y111A the sixth ligand would most likely be that of histidine. Further, the ferrous low-spin A-term features of the Y111A and KatG^N variants are most similar to those of known bis-histidine coordinated heme systems such cytochrome b₅ [163] and an analogous ascorbate peroxidase variant [164].

4.3.4 Electron Paramagnetic Resonance

Although MCD verified the ratio of high-spin to low-spin species predicted by the stopped-flow, in order to obtain spectral evidence of both species in the native Fe^{III} state we employed EPR spectroscopy (Figure 4.5). The most prominent feature is the high-spin axial signal ($g_{\perp} = 5.97$, $g_{\parallel} = 1.99$) with rhombic contributions ($g_{x,z} = 6.65, 1.95$; g_y is obscured by the axial signal at 5.97). These features are nearly identical to wtKatG. In contrast to wtKatG, low-spin signals are also easily detectable ($g_{z,y,x} = 2.92, 2.27, 1.53$). This latter set of signals is indistinguishable from KatG^N [46].

4.3.5 Steady-state Kinetics

Substitution of Y111 affects catalase and peroxidase activity differently. We observed a five-fold reduction in the apparent k_{cat} for catalase activity and an eight-fold decrease in the apparent second-order rate constant (Figure 4.6 and Table 4.2). For peroxidase activity, the H₂O₂- and ABTS-dependent peroxidatic apparent k_{cat} were reduced by 66% and 40% percent respectively, however, this did not translate into any significant change in apparent second-order rate constant due to a reduction in apparent K_M for both substrates (Figure 4.7 and Table 4.3). The oxidation rate of ABTS is least likely to be affected by subtle changes in the active site, and therefore a 40% loss of activity is most likely a result of 36% of the Y111A protein containing low-spin heme. It is possible that the decrease in catalase activity is due to a decrease in the rate of compound I formation or a decrease in ability to form the Met-Tyr-Trp covalent cross-link necessary for catalase activity. A decrease in the

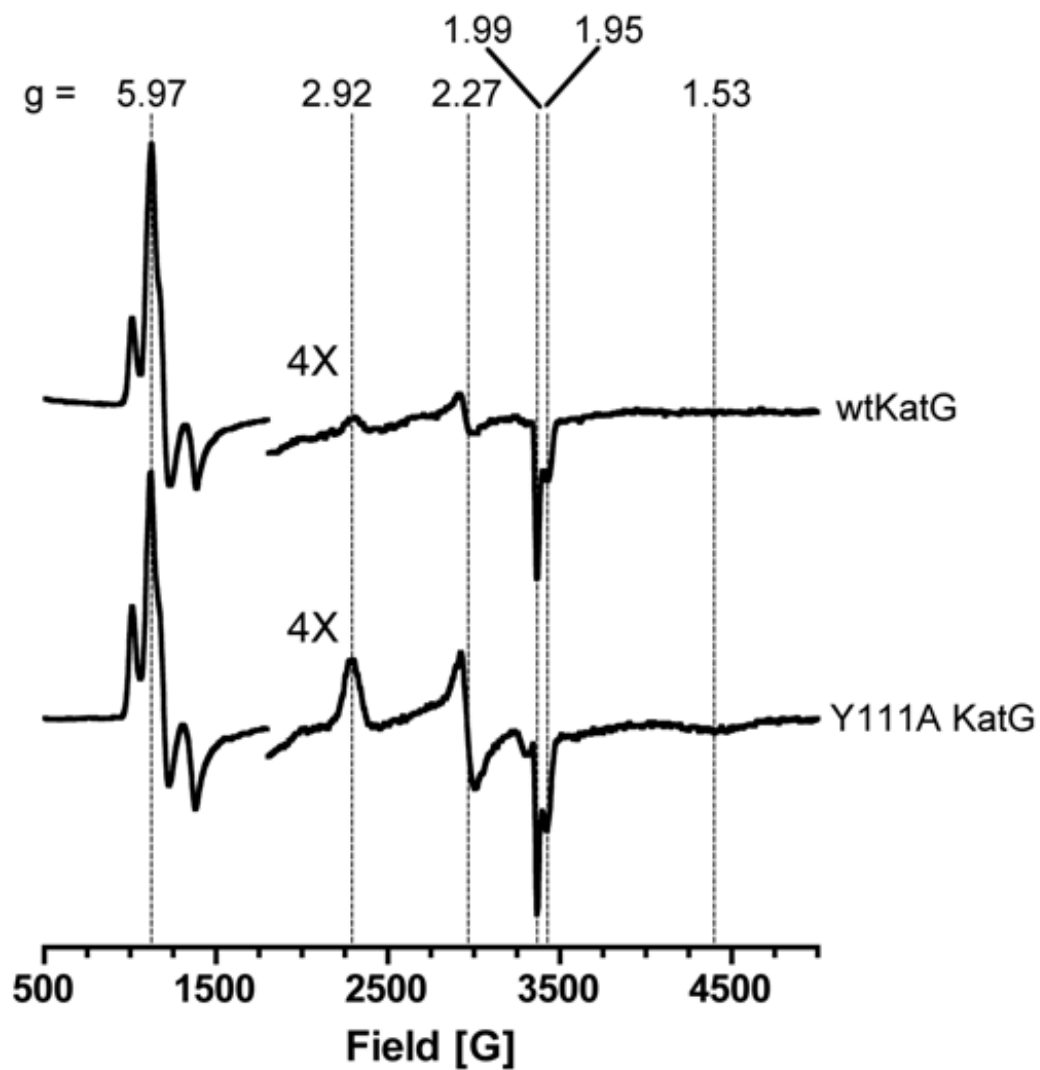


Figure 4.5: **EPR Spectrum of Y111A KatG Compared to wtKatG.** Relative intensity magnified by 4 at field strength greater than 1800 Gauss. g -values report Y111A KatG signals.

rate of compound I formation may or may not affect the peroxidase kinetics, but a lesser ability to form the covalent crosslink would have no effect as KatG is still peroxidase active even without the ability to form the covalent cross-link [126].

In chapter 2, we observed that ABTS can act as an inhibitor to the peroxidase reaction in wtKatG. ABTS affinity was assessed based on the apparent Michaelis constant and the lowest concentration of ABTS at which inhibition was evident. ABTS affinity was shown to increase with decreasing pH. ABTS inhibition was also observed in the Y111A variant (Figure 4.7B). The affinity of Y111A KatG for ABTS at pH 5.0, however, was most similar to that of wtKatG at pH 4.25 ($K_M = 0.06$, [ABTS] required for evidence of inhibition = 0.6 mM). It was also shown that wtKatG is much more active at pH 4.25 (and below) than it is at pH 5.0 - suggesting a shift in Y111A to a more peroxidase-like enzyme.

4.4 Discussion

Catalase-peroxidase lacking its C-terminal domain (KatG^N) contains a collapsed active site due to the energetically favorable coordination of histidine 106 to the heme iron [46, 130]. Upon introduction of the C-terminal domain as a separately expressed and isolated protein, however, the active site reorganizes into its functional form [46]. It is thus proposed that despite its distance from the active-site, the C-terminal domain serves to support an architectural framework necessary for proper active-site configuration by providing a series of interactions on the BC-loop that together are more favorable than the Fe-His coordination. Because of its strict conservation and its position near the interdomain interface, Y111 may have an important role in C-terminal domain-dependent support of the active site. Another consideration is that the C-terminal domain is not found in the monofunctional peroxidases and may have a role in imparting bifunctionality to KatG. The behavior of our Y111 variant supports both hypotheses.

Substitution of Y111 with an alanine resulted in enzyme preparations that contained a mixture of two heme spin states. All three spectroscopic techniques used (UV-visible absorption, MCD, and EPR spectroscopy) contained features seen in both wtKatG and KatG^N.

Protein	Catalase cycle parameters		
	k_{cat} (s^{-1})	K_M (mM H_2O_2)	k_{cat}/K_M ($\text{M}^{-1} \text{s}^{-1}$)
wtKatG	11000 ± 200	3.5 ± 0.2	3.2×10^6
Y111A	2140 ± 50	5.2 ± 0.3	4.1×10^5

Table 4.2: **Apparent Catalase Kinetic Parameters of Wild Type and Y111A KatG.** Assays included 20 nM wtKatG or 70 nM Y111A KatG, 100 mM phosphate buffer, pH 7.0, 23 °C

Protein	Peroxide-dependent parameters			
	k_{cat} (s^{-1})	K_M (mM H_2O_2)	k_{cat}/K_M ($\text{M}^{-1} \text{s}^{-1}$)	K_N (mM H_2O_2)
wtKatG	76 ± 9	0.22 ± 0.04	4.5×10^5	2.9 ± 1.1
Y111A	24.1 ± 0.8	0.081 ± 0.007	3.0×10^5	8.3 ± 2.2
Protein	ABTS-dependent parameters			
	k_{cat} (s^{-1})	K_M (mM ABTS)	k_{cat}/K_M ($\text{M}^{-1} \text{s}^{-1}$)	K_N (mM ABTS)
wtKatG	55.2 ± 1.3	0.087 ± 0.008	6.34×10^5	not detected
Y111A	33.3 ± 0.9	0.061 ± 0.004	5.46×10^5	1.6 ± 0.1

Table 4.3: **Apparent Peroxidase Kinetic Parameters of Wild Type and Y111A KatG.** Assays included 20 nM wtKatG or 70 nM Y111A KatG, 50 mM acetate buffer, pH 5.0, 23 °C

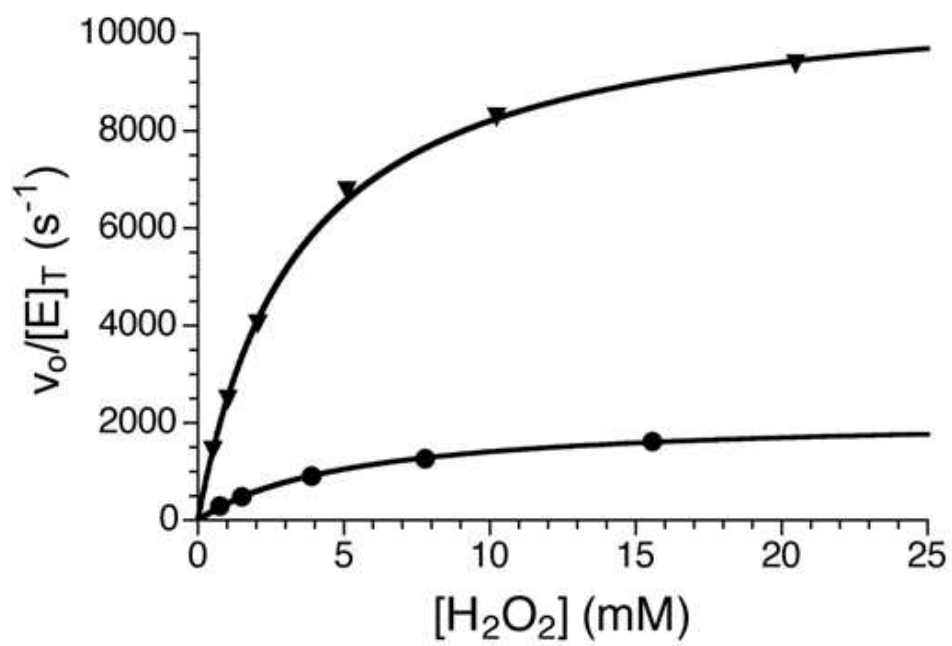


Figure 4.6: **Y111A KatG Catalase Activity.** Initial rates of catalase activity of wild type (▼) and Y111A (●) KatG as a function of H_2O_2 concentration.

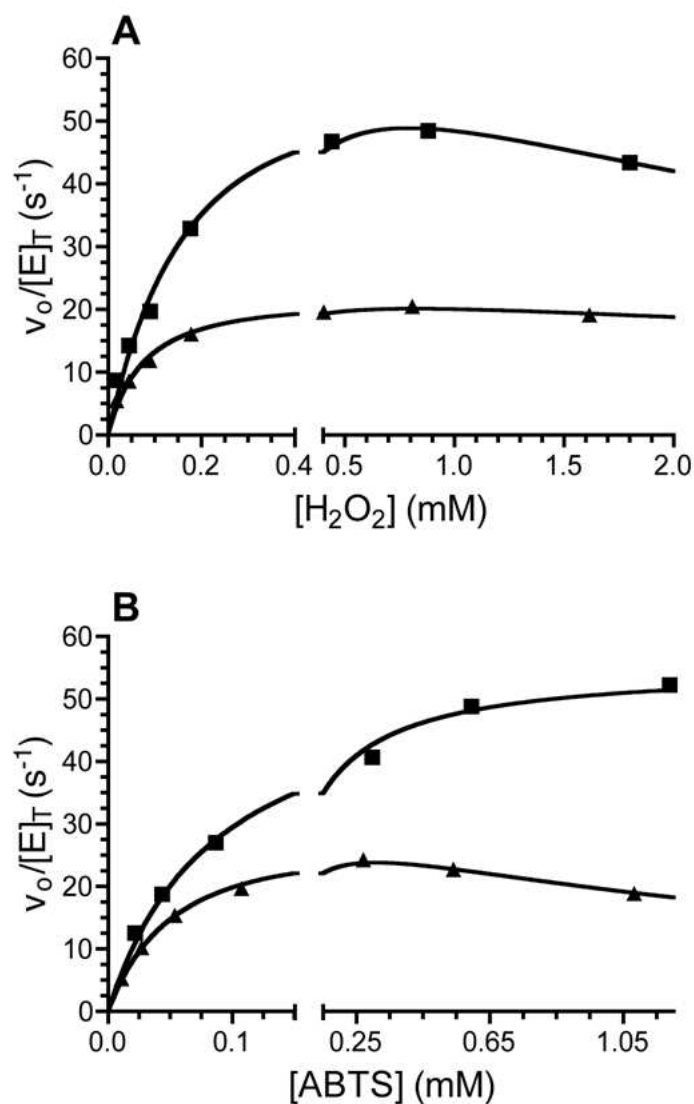


Figure 4.7: **Y111A KatG Peroxidase Activity.** (A) Initial rates of peroxidase activity of wild type (■) and Y111A (▲) KatG as a function of H_2O_2 concentration ($[ABTS] = 0.05$ mM). (B) Initial rates of peroxidase activity of wild type (■) and Y111A (▲) KatG as a function of $ABTS$ concentration ($[H_2O_2] = 0.5$ mM).

We established that the mixture was approximately 2:1 high-spin to low-spin using stopped-flow cyanide binding, and reduction (as demonstrated by MCD) did nothing to change that proportion. Furthermore, the accurate prediction of the MCD spectrum emphasizes that the high- and low-spin species present in the Y111A variant contain active-sites resembling wtKatG and KatG^N, respectively. The transition of one-third of the enzyme to a low-spin state indicates that Y111 is crucial in the interdomain interactions, and loss of this residue results in an increased tendency toward Fe-His coordination (KatG^N-type active site). Such a structural modification predicts diminished catalase and peroxidase activity, an effect we also observed. Indeed, the 40% decrease in ABTS-dependent peroxidase turnover reflects closely the mixture of the spin states. Catalase activity, however, was more substantially decreased than peroxidase activity, and the behavior of the variant towards the reducing substrate, ABTS, in regards to binding and inhibition at pH 5.0 was more akin to wtKatG at its more active pH 4.25 than wild-type at pH 5.0. Both suggest that Y111 and perhaps the interaction of the C-terminal domain with Y111 play at least an indirect role (such as through crosslink formation ability or some other mechanism) in tuning the enzyme for bifunctionality.

CHAPTER 5

COMPREHENSIVE ANALYSIS OF INTERDOMAIN INTERFACE SINGLE VARIANTS

5.1 Introduction

The results from chapter 4 provide a good framework for continuing on with variants of the other interdomain interface residues. The Y111A variant existed in a mixed population. The majority (64%) retained wild-type active site configuration, whereas the remaining resembled enzyme lacking the C-terminal domain (KatG^N). Also, catalase activity was affected to a degree that could not be explained simply by accounting for a population with only 64% active species. Although these results were substantial considering the distance of the variation from the active site, this variation did not entirely replicate the effects observed by deleting the C-terminal domain.

To follow up on this, we have additionally created alanine variants of the other four residues on the interdomain interface (R117A, R479A, D482A, and D597A) and evaluated all variants spectroscopically and kinetically for comparison to wild type KatG (wtKatG) and KatG^N. We will refer to sets of variants based on two criteria: the distance of the hydrogen bonding network from the active site (Y111A, R479A, and D482A are the near-network variants; R117A and D597A are the distant-network variants), or the domain on which the residue exists (Y111A and R117A are the N-terminal variants; R479A, D482A and D597A are the C-terminal variants). All single variants expressed as soluble proteins and all had catalase and peroxidase activity, distinguishing them immediately from KatG^N. The complexity of the hydrogen bonding networks is reflected in the observation that disrupting either side of the amino acid pairs (Y111-D482 and R117-D597) produces different results. While all variants exhibited some spectroscopic and kinetic disruption compared to wtKatG,

the effects of the near-network variants were more substantial and even comparable to certain active site variants.

5.2 Materials and Methods

5.2.1 Materials

Hydrogen peroxide (30%), imidazole, hemin, ampicillin, chloramphenicol, sodium dithionite, phenylmethylsulfonyl fluoride (PMSF) and 2,2'-azino-bis(3-ethylbenzthiazoline-6-sulfonic acid (ABTS) were purchased from Sigma (St. Louis, MO). Isopropyl- β -D-thiogalactopyranoside (IPTG), urea, mono- and di-basic sodium phosphate, acetic acid, and sodium acetate were obtained from Fisher (Pittsburgh, PA). Bugbuster and benzonase were purchased from Novagen (Madison, WI). All restriction enzymes were purchased from New England Biolabs (Beverly, MA). All oligonucleotide primers were purchased from Invitrogen (Carlsbad, CA). All *E. coli* strains (BL-21 [DE3] pLysS and XL-1 Blue), Pfu polymerase, and T4 DNA ligase were obtained from Stratagene (La Jolla, CA). Nickel-nitrilotriacetic acid (Ni-NTA) resin was purchased from Qiagen (Valencia, CA). Desalting chromatography columns were purchased from Bio-Rad (Hercules, CA). All buffers and media were prepared using water purified through Millipore QPakII system (18.2 M Ω /cm, resistivity).

5.2.2 Cloning of R117A, R479A, D482A, and D597A

The preparation of the plasmid pKatG(Y111A) was described in chapter 4. The plasmids pKatG(R117A) and pKatG(D597A) were prepared using mutagenic primers [5'-ACT GCT GAT CGC GAA AGC ACA GC-3' (R117A coding), 5'-GCT GTG CTT TCG CGA TCA GCA GT-3' (R117A non-coding), 5'-GTT CAA TCG ATG GCG CCG GTG GCG CGG G-3' (D597A coding), and 5'-CCC GCG CCA CCG GCG CCA TCG ATT GAA C-5' (D597A non-coding)] for pKatG according to the QuickChange procedure (Stratagene, La Jolla, CA). Amplification products were used to transform *E. coli* XL-1 Blue by electroporation (Bio-Rad Micropulser, Hercules, CA). The plasmids pKatG(R479A) and

pKatG(D482A) were prepared using mutagenic primers [5'-Phos-GCG GCG ACA AAC GCG GTG G-3' (R479A coding), 5'-Phos-CGG CGA AGG TAG AAG CAG ATG CCC-3' (R479A non-coding), 5'-Phos-CGC GGT GGT GCC AAC G-3' (D482A coding), and 5'-Phos-TTT GGC GCC ACC ACG GAA GGT AG (D482A non-coding)] for pKatG according to the 'Round-the-Horn procedure. 'Round-the-Horn differs from the QuickChange procedure in that the mutagenic primers are not complementary. Instead, if the 5' end of the forward primer is at position "x" in the sequence, the 5' end of the reverse primer is at position "x-1". As a result, the amplification products must undergo blunt-end ligation with T4 DNA ligase, after which they were used to transform *E. coli* XL-1 Blue by heat shock. Plasmids from candidate colonies were evaluated by diagnostic restriction digest and DNA sequence analysis (Davis Sequencing, Davis, CA). Correctly mutated plasmids were used to transform *E. coli* (BL-21 [DE3] pLysS) expression hosts.

5.2.3 Expression and Purification

Expression and purification of all variants was carried out identically to Y111A as described in chapter 4. Concentration of purified enzyme was estimated according to the method of Gill and von Hippel [50] [$\epsilon_{280}(\text{Y111A}) = 1.43 \times 10^5 \text{ M}^{-1} \text{ cm}^{-1}$, $\epsilon_{280}(\text{R117A}, \text{R479A}, \text{D482A}, \text{and D597A}) = 1.44 \times 10^5 \text{ M}^{-1} \text{ cm}^{-1}$].

5.2.4 UV-visible Absorption Spectra and Activity Assays

Enzyme was reconstituted with 0.9 equivalents of hemin. Reconstituted enzyme solution incubated at 4 °C for 72 h to allow unincorporated heme to settle out of solution. The solution was then centrifuged and the precipitated heme and other insoluble material discarded. Concentration of reconstituted enzyme was determined using the pyridine hemochrome assay [161]. Protein containing heme in the ferrous state was prepared by adding a small amount (<10 mg) of sodium dithionite to the native enzyme. All spectra were obtained at room temperature on a Shimadzu UV-1601 spectrophotometer (Columbia, MD) with a cell pathlength of 1.0 cm.

Catalase and peroxidase assays were performed as described in chapter 2. Initial velocity fitting was performed as described in chapter 4.

5.2.5 Circular and Magnetic Circular Dichroism

Circular dichroism spectra were obtained in 5 mM phosphate buffer, pH 7.0. Spectra were recorded at 23 °C in a quartz cell (0.5 mm path length) from 300-180 nm on a Jasco J-810 spectropolarimeter (Tokyo, Japan). Baselineing and analysis were done using Jasco J-720 software.

Magnetic circular dichroism spectra were obtained in 50 mM phosphate 50 mM NaCl buffer, pH 7.0. Spectra were recorded at 23 °C in a quartz cell (5.0 mm path length) with 1.4 Tesla magnetic cell holder from 700-350 nm on a Jasco J-810 spectropolarimeter. Baselineing and analysis were done using Jasco J-720 software. Enzyme containing ferrous heme was prepared by adding a small amount (<10 mg) of sodium dithionite to native enzyme.

5.2.6 Electron Paramagnetic Resonance Spectroscopy and Spin Quantification

Spectra were recorded using a Bruker EMX instrument equipped with an Oxford ESR 900 cryostat and ITC temperature controller. Additional sample concentration was performed using Amicon Ultra-4 centrifugal devices. The settings for the spectrometer were as follows: temperature, 10 K; microwave frequency, 9.38 GHz; microwave power, 0.1 mW; modulation amplitude, 10 G; modulation frequency, 100 kHz; time constant, 655.36 ms; conversion time, 655.36 ms; and receiver gain, 1.0×10^5 . Spin quantification was carried out using the Biomolecular EPR Spectroscopy Software package available online [168].

5.3 Results

5.3.1 Mutagenesis, Expression, and Purification of KatG Interdomain Variants

We successfully cloned single alanine variants of all five interdomain interface residues Y111, R117, R479, D482, and D597 as confirmed by sequencing of the plasmid isolates. Each

of the variants over-expressed in a soluble form and had detectable catalase and peroxidase activity. There was no observable change to secondary structural content based on the circular dichroism of the variants when compared to wild type (Figure 5.1).

5.3.2 UV-visible Spectroscopy

Spectra of the variants in the resting ferric state show only slight differences from the wild type enzyme (Figure 5.2). The red-shifting of the Soret and charge transfer 2 bands in the near-network variants suggest the presence of low-spin heme. R117A exhibited the largest shoulder at 380 nm consistent with a more penta-coordinate (5-c) heme environment. The signal at 380 nm is most concave in the D482A and D597A variants, suggesting a more hexa-coordinate (6-c) system in these variants.

Differences among the variants were more pronounced in the ferrous form (Figure 5.3). In wtKatG, the primary absorption bands are located at 439 nm (Soret), 559 nm (β), and 589 nm (α), characteristic of high-spin ferrous heme. KatG^N absorption bands occur at 427, 530 and near 560 nm, characteristic of low-spin ferrous heme. The near-network variants contained all features found in both wtKatG and KatG^N. The near-network variants all had blue-shifted Soret bands (relative to wtKatG) with shoulders at 439, indicative of a mixture of high spin (439 nm) and low spin (\sim 425 nm) species. Evidence of shoulders at both 530 and 589 also confirmed the presence of a mixed spin-state population in all near-network variants. Additionally, the R479A and D482A variants were less stable and prone to precipitation in the ferrous state, resulting in more light-scattering evident in the spectra and broadening of the signals. This can be particularly well seen in the less pronounced absorption bands in the R479A variant in relation to Y111A, for example. Centrifugation resulted in samples that produced purely high-spin spectra (data not shown). The distant-network variants more closely resembled the wild type, although the D597A Soret band was slightly blue-shifted and the spectrum was less concave around 535 nm.

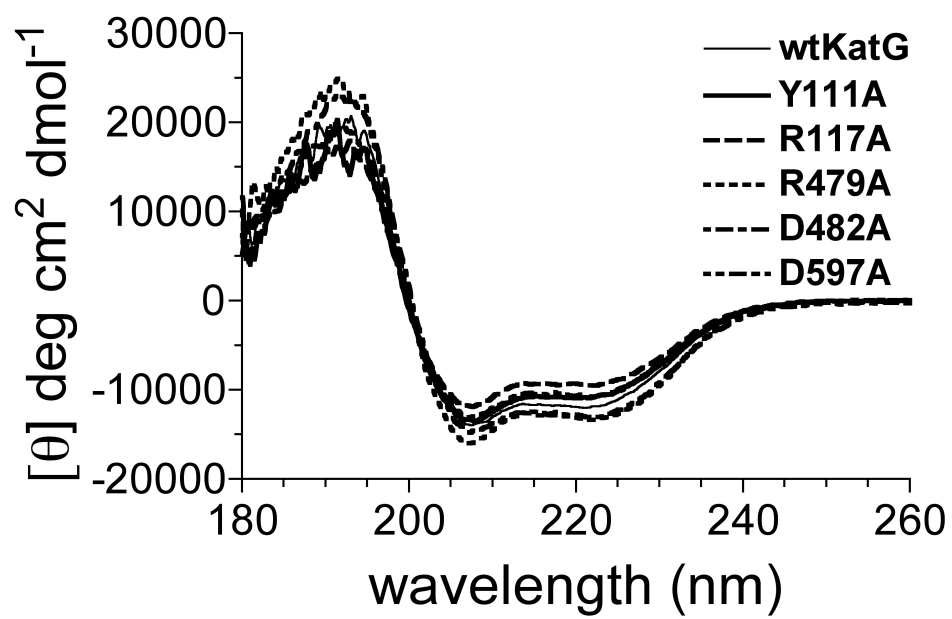


Figure 5.1: Far-UV Circular Dichroism of wtKatG and Interdomain Interface Variants.

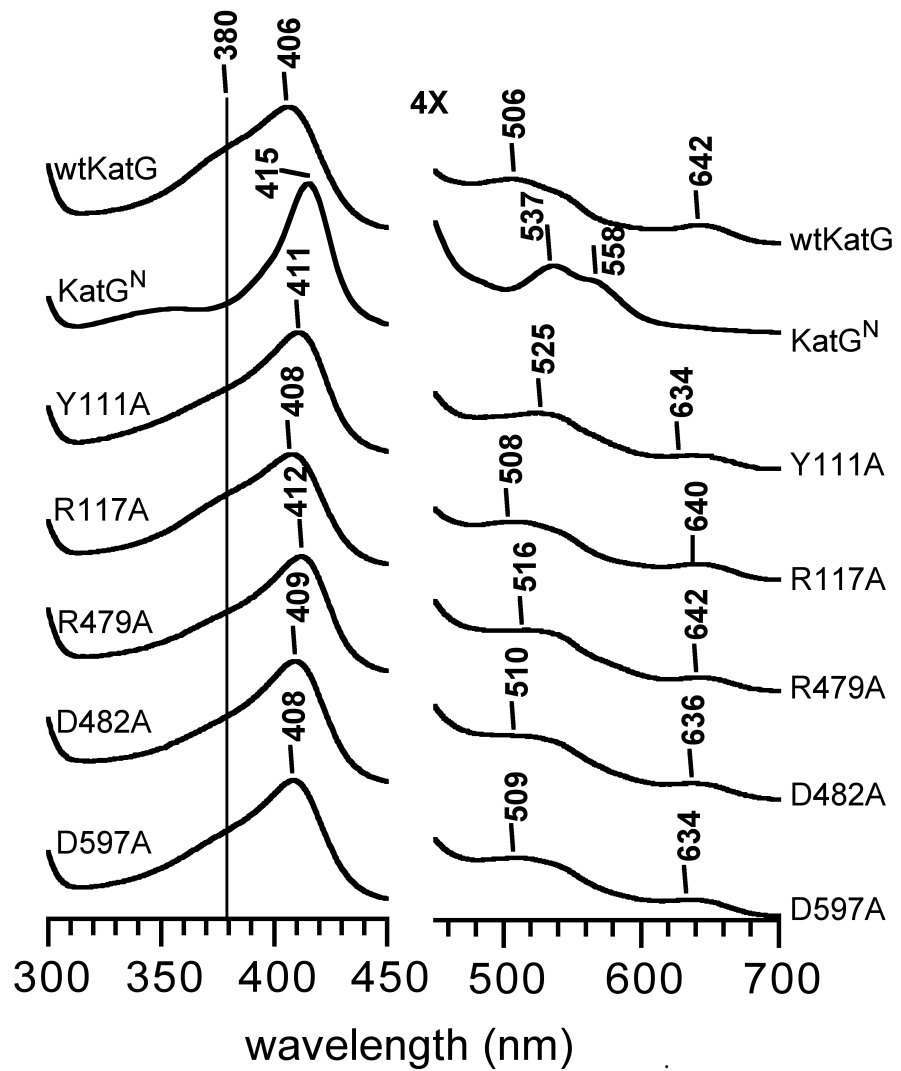


Figure 5.2: UV-vis Spectra of wtKatG, KatG^N, and Interdomain Interface Variants: Ferric Heme.

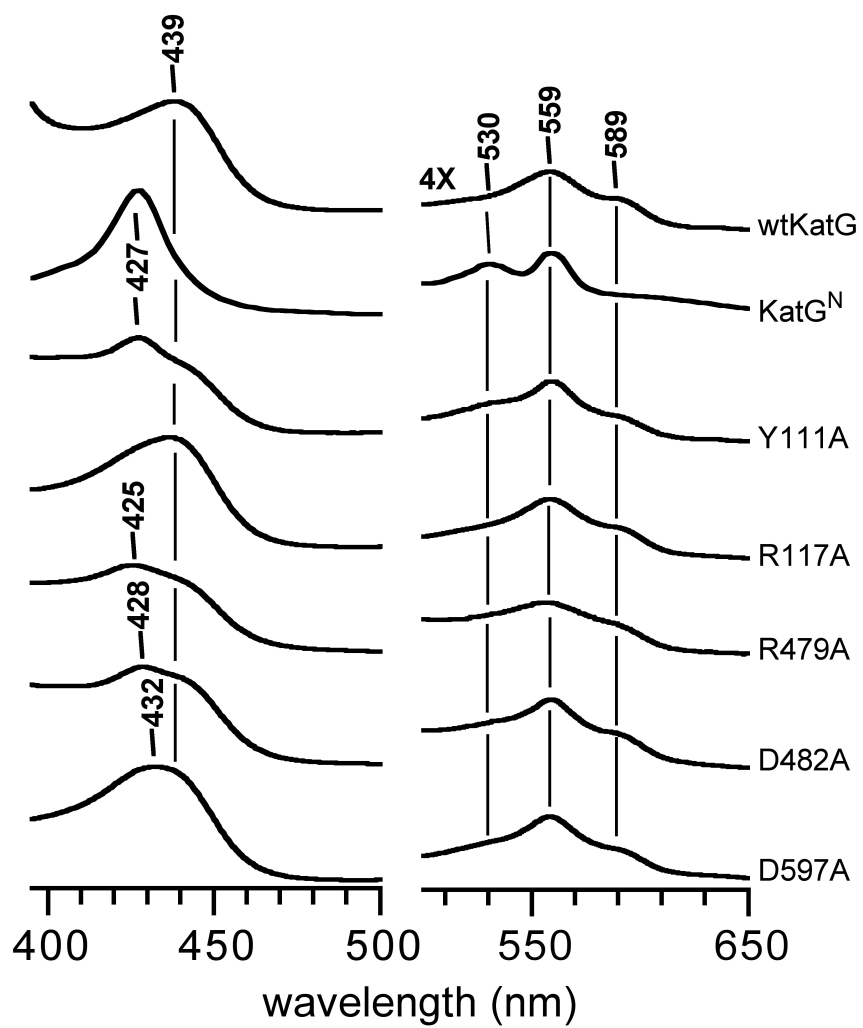


Figure 5.3: UV-vis Spectra of wtKatG, KatG^N, and Interdomain Interface Variants: Ferrous Heme.

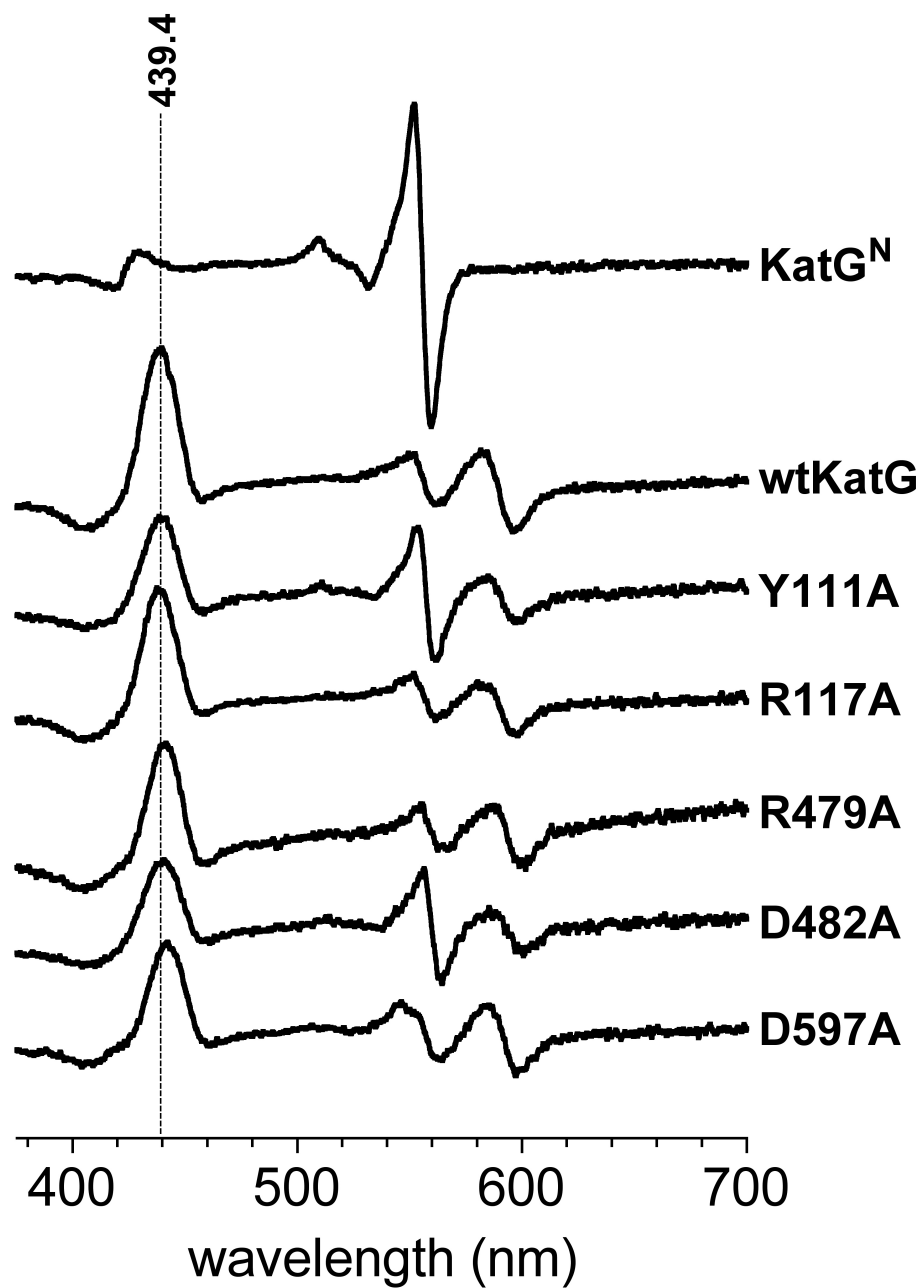


Figure 5.4: MCD Spectra of KatG^N, wtKatG, and Interdomain Interface Variants: Ferrous Heme.

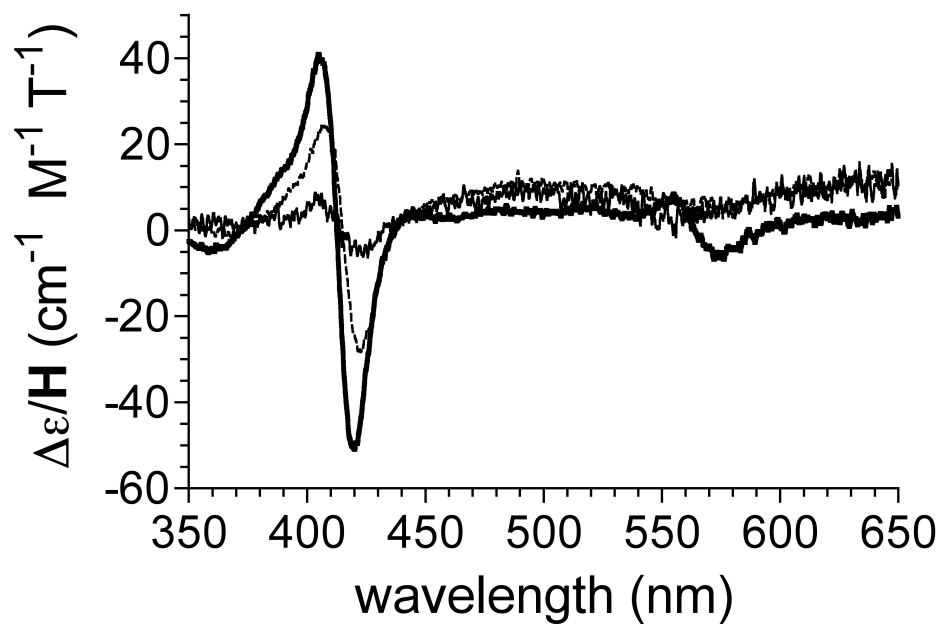


Figure 5.5: MCD Spectrum of R479A KatG Ferric Heme Compared to wtKatG and KatG^N. R479A (---), wtKatG (—), and KatG^N (—).

5.3.3 Magnetic Circular Dichroism

Distinction between high- and low-spin heme species in magnetic circular dichroism (MCD) is more facile in the ferrous heme state than ferric. Magnetic circular dichroism on the ferrous forms of the enzyme corroborated the evidence of low-spin heme observed in the ferrous UV-vis in Y111A and D482A, but R479A did not have any more low-spin contribution than the wild type or the other high-spin variants (Figure 5.4). The distant-network variants also appeared to be purely high-spin, like the wild type. Although R479A appeared high-spin after reduction with dithionite, the ferric MCD spectrum revealed a clear low-spin presence similar to KatG^N and unlike the wild type (Figure 5.5). The discrepancy between the ferric and ferrous MCD spectra is consistent with the precipitation of low-spin species upon addition of dithionite observed during the UV-vis studies.

5.3.4 Electron Paramagnetic Resonance

EPR spectra confirm the presence of low-spin heme iron in the ferric state of the near-network variants and the absence of low-spin in the distant-network variants (Figure 5.6). To quantify the relative proportion of each species, we simulated the spectra and integrated the individual signals. The best simulations required three high-spin signals and one low-spin. The high spin signals were a rhombic signal (RHS) with g-values approximately 6.64, 4.95, and 1.955, an axial signal (AHS1) with g-values approximately 5.95 and 1.995, and a second axial signal (AHS2) with g-values approximately 5.65 and 1.995. The two axial signals could also be treated as one rhombic signal, but not without less satisfactory simulations. The low-spin signal was rhombic (RLS) with approximate g-values of 2.93, 2.3, and 1.53. The amount of low-spin signal present in the distant-network variants was small enough that simulations could not be improved by adding in the RLS signal. The RLS in the near-network variants accounted for approximately twenty percent of the signal, two to three times that of wild type (Table 5.1). Y111A, as an example of a spectrum that includes substantial contribution of all four signals, is shown with its simulated spectrum overlain in Figure 5.7. Although all of the interface variants had more rhombic contribution to the

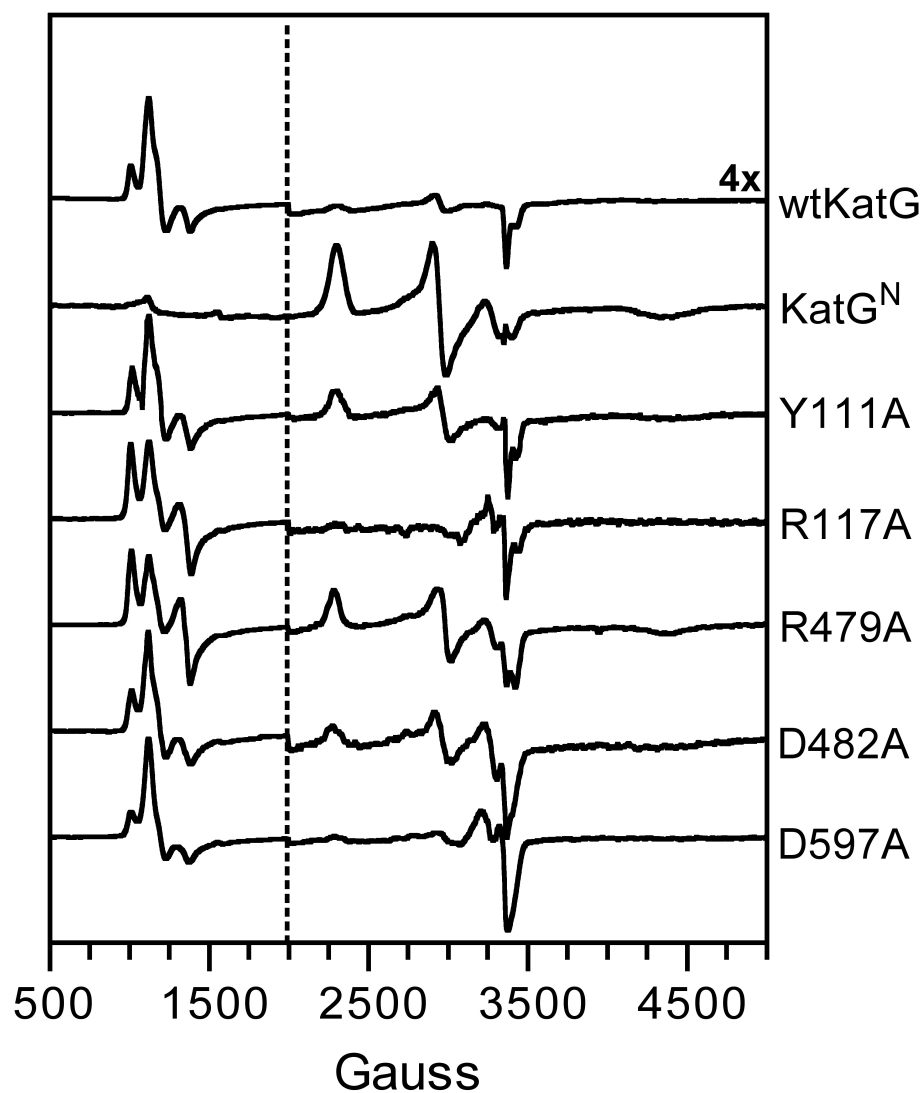


Figure 5.6: **EPR Spectra of wtKatG, KatG^N, and Interdomain Interface Variants.** All spectra, except KatG^N, magnified by four above 2000 Gauss. R117A and D597A spectra have had copper impurity signal subtracted.

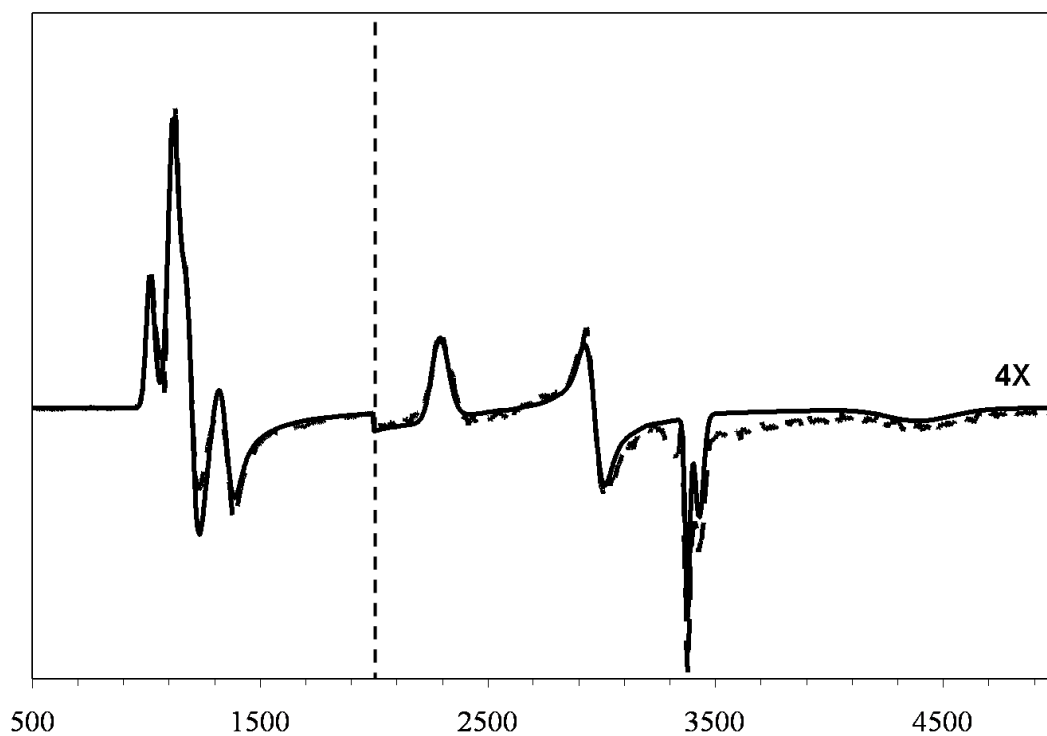


Figure 5.7: **Simulation of Y111A KatG Spectrum.** Y111A KatG(—) and simulated (—) spectra magnified by four above 2000 Gauss.

Species	HS : LS	RHS : AHS	AHS1 : AHS2	AHS1:AHS2:RHS:RLS
wt	91 : 9	60 : 40	51 : 49	28 : 27 : 36 : 9
KatG ^N	2 : 98	74 : 26	100 : 0	1 : 0 : 1 : 98
Y111A	80 : 20	50 : 50	55 : 45	22 : 18 : 40 : 20
R117A	100 : 0	73 : 27	52 : 48	14 : 13 : 73 : 0
R479A	78 : 22	75 : 25	49 : 51	10 : 10 : 58 : 22
D482A	84 : 16	53 : 47	54 : 46	21 : 19 : 44 : 16
D597A	100 : 0	40 : 60	55 : 45	33 : 27 : 40 : 0

Table 5.1: **Ratios of Various EPR Signals Observed in wtKatG and Variants.** Expressed as percentages.

overall signal than the wild type, only R117A and R479A had a greater RHS to AHS ratio than wild type. This corroborates the more prominent shoulder at 380 nm in UV-vis ferric spectra of these two variants.

5.3.5 Steady-state Kinetics

Substituting any of the residues along the interdomain interface resulted in a decrease in the apparent k_{cat} for catalase activity with the exception of D597, the residue most distant from the active site (Table 5.2). The apparent Michaelis constant was largely unaffected in the C-terminal residue variants (R479A, D482A, D597A), but was slightly elevated in the N-terminal residue variants (Y111A, R117A). Apparent peroxidase parameters are shown in Table 5.3. With the exception of the R117A ABTS-dependent k_{cat} , all variants showed a decrease in k_{cat} and k_{cat}/K_M to varying degrees.

5.4 Discussion

The non-heme binding C-terminal domain of KatG is crucial for proper active site configuration of the enzyme. Without it, the active site is collapsed due to the energetically favorable coordination of histidine 106 to the heme iron, but can be restored with the introduction of the separately expressed and isolated C-terminal domain [46, 130]. This suggests that the C-terminal domain is providing an architectural framework necessary for proper active site configuration. The strict conservation of the interdomain interacting residues suggests that the interactions are specific and crucial to the ability of the C-terminal domain to act as this framework. Therefore, disruption of these interdomain contacts offers an opportunity to understand the nature of how the C-terminal domain provides this support from such a great distance from the active site.

KatG^N is expressed in inclusion bodies and must be refolded before becoming soluble, signifying that the C-terminal domain is essential for structural stability. The single alanine variants of all of the interdomain interface residues were all soluble as expressed. This indicates that no single interaction is completely responsible for the structural stability

Protein	Catalase cycle parameters		
	k_{cat} (s^{-1})	K_M (mM H_2O_2)	k_{cat}/K_M ($10^6 \text{ M}^{-1} \text{ s}^{-1}$)
wtKatG	11000 ± 200	3.5 ± 0.2	3.2
Y111A	2140 ± 50	5.2 ± 0.3	0.41
R117A	3820 ± 230	4.2 ± 0.7	0.91
R479A	4370 ± 110	3.4 ± 0.3	1.3
D482A	5840 ± 120	3.7 ± 0.2	1.6
D597A	10000 ± 400	3.2 ± 0.4	3.1

Table 5.2: **Apparent Catalase Kinetic Parameters of wtKatG and Interdomain Interface Variants.** Assays included 20 nM wtKatG, R117A, D597A, 50 nM R479A, D482A, or 70 nM Y111A KatG, 100 mM phosphate buffer, pH 7.0, 23 °C

Protein	Peroxide-dependent peroxidase cycle parameters			
	k_{cat} (s ⁻¹)	K_M (mM H ₂ O ₂)	k_{cat}/K_M (10 ⁵ M ⁻¹ s ⁻¹)	K_N (mM H ₂ O ₂)
wtKatG	76 ± 9	0.22 ± 0.04	4.5	2.9 ± 1.1
Y111A	24.1 ± 0.8	0.081 ± 0.007	3.0	8.3 ± 2.2
R117A	30 ± 5	0.14 ± 0.05	2.1	5.8 ± 5.0
R479A	10.9 ± 0.4	0.19 ± 0.01	0.57	3.1 ± 0.3
D482A	28.4 ± 4	0.57 ± 0.13	0.49	2.1 ± 0.6
D597A	32 ± 5	0.8 ± 0.2	0.40	not detected
	ABTS-dependent peroxidase cycle parameters			
	k_{cat} (s ⁻¹)	K_M (mM ABTS)	k_{cat}/K_M (10 ⁵ M ⁻¹ s ⁻¹)	K_N (mM ABTS)
wtKatG	55.2 ± 1.3	0.087 ± 0.008	6.3	not detected
Y111A	33.3 ± 0.9	0.061 ± 0.004	5.5	1.6 ± 0.1
R117A	76 ± 4	0.13 ± 0.01	5.8	6.8 ± 3.0
R479A	8.7 ± 0.2	0.025 ± 0.001	3.5	0.92 ± 0.05
D482A	20.7 ± 1.0	0.046 ± 0.004	4.5	0.39 ± 0.04
D597A	33 ± 3	0.11 ± 0.04	3.0	not detected

Table 5.3: **Apparent Peroxidase Kinetic Parameters of wtKatG and Interdomain Interface Variants.** Assays included 20 nM wtKatG, R117A, D597A, 50 nM R479A, D482A, or 70 nM Y111A KatG, 50 mM acetate buffer, pH 5.0, 23 °C

that the C-terminal domain imparts to the enzyme. The tendency to precipitate upon addition of dithionite, however, suggests that some of the stability has been lost in the R479A and D482A variants.

The fact that no two variants had identical properties, despite four of the residues acting as single contact bridges (Y111-D482 and R117-D597), was surprising at first. The extensiveness of the hydrogen bonding networks, however, provides some explanation. In the available structures, Y111 is only within hydrogen bonding distance of D482. Similarly, D597 is only within hydrogen bonding distance of R117. However, D482 also is within hydrogen bonding distance with R479 and R484, which are also within hydrogen bonding distance of each other, and R117 is within hydrogen bonding distance of D115. This does not even consider the intradomain hydrogen bonds between these mentioned residues and backbone carbonyls. As such, it is impossible to make a single variation without possibly affecting multiple interdomain contacts simultaneously, and each residue must primarily be considered based on what it individually contributes to the whole network. In fact, it could be considered more surprising that the kinetic and spectroscopic characteristics of the variants *can* be grouped based on the proximity to the active site or on the domain on which they reside.

The distant-network variants remained spectroscopically similar to the wild type with the exception of rhombic contribution to the high spin signal observed in EPR (R117A appearing more rhombic, D597A less rhombic). The near-network variants all demonstrated a mixture of high- and low-spin heme in all spectroscopic evaluations, whereas the distant-network variants exhibited purely high-spin heme. This suggests that the nearer hydrogen bonding network is more crucial to the prevention of active site collapse, while the more distant hydrogen bonding network plays more of a fine-tuning role.

Concomitant with the shift to a greater relative population of low spin species in the near-network variants is a loss in overall activity due to inactive species. This makes direct kinetic comparison to wild-type difficult. To determine if the residue has a role in more than just active site configuration, we looked at the ratio of catalase to peroxidase

maximum activity (Table 5.4). Interestingly, none of the variants had the same ratio as the wild type. The N-terminal residue variants reduced catalase activity more substantially than peroxidase activity. Most KatG variants show the same behavior [117, 125, 128, 169]. This is expected, considering that the overall structure of KatG is more similar to a monofunctional peroxidase, and if a change was made that disrupted one activity more than another, the novel activity should be more affected than the original. Surprisingly, the substitution of the C-terminal residues reduced peroxidase activity more than catalase activity. The only other instance of a KatG variant selectively and substantially reducing peroxidase more than catalase activity was W321F in *M. tuberculosis* KatG, however specific activity of the W321F was measured for catalase and peroxidase at pH 7.2, well outside of the reasonable range for peroxidase activity measurements [170].

The transition of the population to mixed spin states and the loss of between 50 and 75% activity seen in most of these variants is quite substantial given their distance from the active site. In fact, these changes are comparable to variations made to the many active site residues in *Synechocystis* PCC 6803 [147, 171]. The Soret and CT2 band shifts in the ferric heme UV-vis spectra of H123E and R119A (H106 and R102 in *E. coli* numbering) in the distal cavity and D402N and D402E in the proximal triad (Trp341 - D402 - His290, *SynKatG* numbering) were similar to what is seen here in the near-network interface residues variants. The ferrous UV-vis spectra of R119N, R119A, H123E, and H123Q were also very similar to the ferrous spectra of the near-network interface variants having Soret peaks around 425 nm with a shoulder around 439 nm and three bands evident between 525 and 590 nm. With the exception of the proximal histidine, variants of the proximal triad retained at least 25% peroxidase activity, while R479A here lost 85% activity [147]. These comparisons demonstrate that the roles of the specific interactions along the interdomain interface are as substantial in proper active site configuration and functionality as many of the active site residues themselves, giving the C-terminal domain the same significance to KatG function as the proximal triad and distal catalytic residues.

Protein	ratio	relative to wtKatG
wtKatG	167.7	1
Y111A	74.6	0.445
R117A	71.7	0.428
R479A	445.9	2.659
D482A	239.8	1.43
D597A	307.7	1.835

Table 5.4: **Ratio of Catalase to Peroxidase Activity Relative to Wild Type.** Ratio is catalase k_{cat} divided by the average of peroxide- and ABTS-dependent k_{cat} .

CHAPTER 6

SUMMARY

The complicating features of the catalase-peroxidase system are numerous. With a single active site, the enzyme is able to catalyze at least two different reaction cycles. This active site is indistinguishable from the active site in monofunctional peroxidases which can catalyze only one reaction. Furthermore, the KatG active site bears little resemblance to catalase-active enzymes. Therefore, catalase catalytic capability is imparted to the enzyme from some non-active site structure or collection of structures, requiring an expansion from the typical active site-limited scrutiny.

The next complicating factor is that the catalytic mechanisms are not strictly Michaelis-Menten type reactions as they require multiple substrates. Each cycle on its own can easily be handled, as the kinetics have been worked out for the monofunctional equivalents in the past. Putting the two activities inside the same enzyme greatly complicates the kinetics, particularly with the two activities sharing the same first step. KatG seems to offer some relief in this in that pH and the availability of a peroxidatic reducing substrate can be used to differentiate between the two reaction cycles. The appropriateness of this approach, however is debatable. Is it safe to assume that the catalase cycle behaves the same when no reducing substrate is present? Are the two activities competitive? Have the pH effects been sufficiently characterized to know which pH is best to study each activity and why? These were questions that were overlooked during the attempts to simplify this system to a manageable level of complexity.

6.1 Assumption: pH-profiling at Saturating Substrate Concentrations

Instead, pH-profiling was carried out disregarding the kinetic complexity of the enzyme. Using saturating substrate concentrations, KatG was found to have maximal peroxidase activity between pH 4.5 and 5.0, maximal catalase activity near pH 6.5, and maximal NADH oxidase activity at pH 8.5. This information was then used to interpret structural information, such as an arginine that is oriented towards the hydrogen bonding near-network residues on the C-terminal domain at pH 4.5, oriented towards the tyrosine involved in the covalent crosslink at pH 8.5, and is split between the two orientations at pH 6.5. The conclusion was that this residue is responsible for “switching on” peroxidase activity. Knowing that a full-scale kinetic solution including protonation effects had not been carried out for KatG, we took this task on and found that these conclusions could not be the whole story since peroxidase is still not completely “turned on” at pH 4.5.

What we found was that the approach used to generate the pH-profiles overlooked a significant feature: ABTS-dependent inhibition. This led to highly skewed pH-profiles for peroxidase activity, with what was claimed to be maximum activity actually being inhibited catalysis. We found that by using sub-saturating conditions at pH 3.75, velocities could be achieved in great excess of those found using any substrate concentration at pH 4.5 or higher. In fact, it appeared that activity would be even much higher at lower pHs if not for the loss of structural stability and unfolding of the enzyme at pH 3.6. Although precise pK_a s could not be assigned for the peroxidase cycle, 4.5 could easily be established as an upper-limit. This would suggest that the arginine-switch either is less significant in the differentiation between activities, or is only one of multiple pH-dependent features (possibly independent or in cascade) involved in differentiation. The trends in affinity towards the reducing substrate and H_2O_2 suggest that differentiation may be closely linked to changes in binding.

Similarly, by using the mechanistic solution for pH-dependent catalase kinetics, we found it to be more complicated than just a simple 6.5 pH optimum. It revealed that even

though all single concentration pH-profiles had an optimum of 6.5, the actual optimum for maximum turnover was pH 5.75 or lower, and the optimum for efficiency was pH 7.0. Again, this information will be valuable in evaluating pH-based structural and spectroscopic changes.

6.2 Assumption: Catalysis Can Be Differentiated by pH and Substrate Availability

Simply from the classical representation of the catalase-peroxidase mechanistic scheme (Figure 1.13), it is obvious that the two catalytic cycles were assumed to be competitive. Compound I could react with either H_2O_2 or a reducing substrate. The simple way of studying the two cycles separately would be to only provide H_2O_2 to study catalase, and do so at a pH where catalase is optimal. Similarly, to study peroxidase shift to a pH where catalase is no longer optimal and provide the substrates necessary for peroxidase. As a result of the pH-optima being misidentified, peroxidase activity has been regularly evaluated between pH 4.5 and 5.0. Catalase activity, however, is still easily measurable down to pH 5.0 and peroxidase (as just discussed) is not very active until below pH 4.5. Furthermore, based on this more exhaustive analysis of pH-dependence, pH 4.5 to 5.5 seems to be a catalytic pH gap for KatG.

If at pH 5.0 both activities are present, it seemed beneficial to determine what fraction of the enzyme was utilizing the catalase cycle and what fraction was utilizing the peroxidase cycle. This would provide a framework for interpreting past (and future) work as well as being more biologically relevant in that it would require studying the enzyme while both cycles are available. What we found was that the presence of peroxidase reducing substrate did not act competitively with catalase activity, but enhanced it. The result of this synergistic effect is that KatG becomes a highly efficient catalase over an extremely broad pH range (4.5 to near 8.0), which can be used to suggest that its primary role is perhaps H_2O_2 detoxification.

The only way this synergy could occur would be if the classical scheme was a misrepresentation or oversimplification of the KatG catalytic cycles. After establishing that the presence of reducing substrate prevented the accumulation of an unreactive species during catalase turnover, we proposed a mechanism that has differentiation between catalase and peroxidase based on electron transfer occurring prior to binding of the second substrate. Direct evidence for this electron transfer and for part of our proposed mechanism came out in some of the most recent published literature [143].

6.3 Assumption: Global Features Play Structural Roles, Active Site Features Play Functional Roles

Overall, structure and function are intimately linked. Function arises from structure. However, much like the equipment inside a factory determines what it produces and not the shape of the factory itself, structure-function relationship studies in enzymes are usually limited to the active site while global features are treated as the building framework. Limiting consideration of functional players to active site features has been well-established to be a fallacy by KatG studies. Of the KatG activities, non-active site mutations can selectively knock out certain activities: the S315T substitution (and others) in *Mycobacterium tuberculosis* knocks out the isonicotinic acid hydrazide activation, and substitutions blocking formation of the covalent adduct knock out catalase activity. Absence of the C-terminal domain completely knocks out activity due to structural instability and active site collapse. Here, even the C-terminal domain's role is shown to be possibly functional based on the interdomain interface variants.

Maintaining the proper fold and active site architecture (established roles of the C-terminal domain) can still be considered primarily framework in nature. At first, this role was confirmed by the Y111A variant. This enzyme existed in a mixed population, with 64% resembling wild-type KatG and 36% resembling KatG^N. This ratio was consistent enough to allow prediction of the MCD ferrous spectra from stopped-flow kinetic data. The steady-state kinetics, however, revealed that catalase activity was decreased more than what could

be accounted for by only 36% having a collapsed active site. This foreshadowed some of the results found by evaluating all of the other alanine variants of the interdomain interface residues.

The near-network variants showed a population mixture similar to the Y111A variant. This was confirmed with UV-Vis, MCD, and EPR spectroscopy. The ratios of catalase to peroxidase activity, however, showed that function was affected in a way that could not correlate to the population mixtures. Instead, the C-terminal variants demonstrated an increase in the catalase:peroxidase ratio relative to wild-type, while the N-terminal variants demonstrated a decrease in that ratio. This actually serves to confirm that the arginine switch mentioned earlier in relation to pH-induced structural changes is involved in catalysis differentiation to some degree. It also serves to indicate that specific residues on the C-terminal domain (R479, D482) are involved in catalysis differentiation, as when those residues are modified peroxidase activity is decreased more substantially than catalase activity.

6.4 Conclusion

KatG has proved to be a superb model for evaluating some of the common assumptions made in enzymology. From attempts to transform enzyme kinetics into pseudo-first order through substrate concentration manipulation to how global features are treated in the scope of structure-function relationships, we have been able to evaluate the necessity of thorough parametric analysis and the significance of global protein structure. Even in these studies, however, not all assumptions could be eliminated. In the pH studies, pH and one substrate concentration were varied while the other substrate was held constant. The sheer volume of data involved in this collection alone proved to be both tedious and often elusive due to the time required to collect one data set. To have expanded this to include another variable would have created a data set that required more points than could be reasonably or even accurately collected in one sitting with current technology. In the interdomain interface variants, peroxidase data was still obtained at pH 5.0 in spite of the

results demonstrated by the pH studies. With no structural studies and very little literature involving kinetics carried out below pH 4.5, there would have been no reference point for the work. Furthermore, performing the same pH-based evaluation of all the variants would have been nearly as massive an undertaking as adding another variable. In the end, the complexity of enzymes necessitates simplifying assumptions that can often be detrimental, or at least misleading, in data interpretation. This emphasizes the need for technological developments in the realm of data acquisition as it pertains to speed of collection, volume of reagents, quantity of data, and number of variables. As these advancements are in progress, it is the responsibility of the researcher (as it has always been) to be aware of the pitfalls associated with making simplifications, eliminate them whenever possible and reasonable, and recognize how those simplifications might affect the data at hand and the interpretation of that data.

BIBLIOGRAPHY

- [1] A Fersht, *Structure and Mechanism in Protein Science*. W. H. Freeman and Company, New York, 1999, pp. 119-122, 164-215.
- [2] PCA Bruijninx, G van Koten, RJMK Gebbink, Mononuclear non-heme iron enzymes with the 2-His-1-carboxylate facial triad: recent developments in enzymology and modeling studies. *Chem. Soc. Rev.* 37 (2008) 2716-2744.
- [3] LJ Murray, R Garca-Serres, MS McCormick, R Davydov, SG Naik, SH Kim, BM Hoffman, BH Huynh, SJ Lippard, Dioxygen activation at non-heme diiron centers: oxidation of a proximal residue in the I100W variant of toluene/*o*-xylene monooxygenase hydroxylase. *Biochemistry* 46 (2007) 14795-14809.
- [4] JM Bollinger, W Jiang, MT Green, C Krebs, The manganese(IV)/iron(III) cofactor of *Chlamydia trachomatis* ribonucleotide reductase: structure, assembly, radical initiation, and evolution. *Curr. Opin. Struct. Biol.* 18 (2008) 650-657.
- [5] AH Saunders, AE Griffiths, KH Lee, RM Cicchillo, L Tu, JA Stromberg, C Krebs, SJ Booker, Characterization of quinolate synthases from *Escherichia coli*, *Mycobacterium tuberculosis*, and *Pyrococcus horikoshii* indicates that [4Fe-4S] clusters are common cofactors throughout this class of enzymes. *Biochemistry* 47 (2008) 10999-11012.
- [6] I Dance, The consequences of an interstitial N atom in the FeMo cofactor of nitrogenase. *Chem. Commun.* 3 (2003) 324-325.
- [7] A Battersby, Tetrapyrroles: the pigments of life. *Nat. Prod. Rep.* 17 (2000) 507-526.
- [8] GL Cantoni, The nature of the active methyl donor formed enzymatically from L-methionine and adenosinetriphosphate. *J. Am. Chem. Soc.* 74 (1952) 2942-2943.

- [9] S Roje, *S*-Adenosyl-L-methionine: Beyond the universal methyl group donor. *Phytochemistry* 67 (2006) 1686-1698.
- [10] T Urich, TM Bandejas, SS Leal, R Rachel, T Albrecht, P Zimmerman, C Scholz, M Teixeira, CM Gomes, A Kletzin, The sulphur oxygenase reductase from *Acidianus ambivalens* is a multimeric protein containing a low-potential mononuclear non-haem iron centre. *Biochem. J.* 381 (2004) 137-146.
- [11] SP de Visser, Elucidating enzyme mechanism and intrinsic chemical properties of short-lived intermediates in the catalytic cycles of cysteine dioxygenase and taurine/ α -ketoglutarate dioxygenase. *Coord. Chem. Rev.* 253 (2009) 754-768.
- [12] LE Grove, J Xie, E Yikilmaz, A Karapetyan, AF Miller, TC Brunold, Spectroscopic and computation insights into second-sphere amino-acid tuning of substrate analogue/active-site interactions in iron(III) superoxide dismutase. *Inorg. Chem.* 47 (2008) 3993-4004.
- [13] EN Brown, R Friemann, A Karlsson, JV Parales, MMJ Couture, LD Eltis, S Ramaswamy, Determining Rieske cluster reduction potentials. *J. Biol. Inorg. Chem.* 13 (2008) 1301-1313.
- [14] The PubChem Project. <http://pubchem.ncbi.nlm.nih.gov/>. Accessed June 2009.
- [15] SEJ Bowman, KL Bren, The chemistry and biochemistry of heme *c*: functional bases for covalent attachment. *Nat. Prod. Rep.* 25 (2008) 1118-1130.
- [16] CM DiCarlo, LB Vitello, JE Erman, Effect of active site and surface mutations on the reduction potential of yeast cytochrome *c* peroxidase and spectroscopic properties of the oxidized and reduced enzyme. *J. Inorg. Biochem.* 101 (2007) 603-613.
- [17] S Schneider, J Marles-Wright, KH Sharp, M Paoli, Diversity and conservation of interactions for binding heme in b-type heme proteins. *Nat. Prod. Rep.* 24 (2007) 621-630.

- [18] BC Finzel, TL Poulos, J Kraut, Crystal structure of cytochrome *c* peroxidase refined at 1.7Å resolution. *J. Biol. Chem.* 259 (1984) 13027-13036.
- [19] JRH Tame, B Vallone, The structures of deoxy human hemoglobin and the mutant Hb Tyr α 42His at 120 K. *Acta Crystallog., Section D: Biol. Crystallog.* D56 (2000) 805-811.
- [20] I Fita, MG Rossmann, The NADPH binding site on beef liver catalase. *Proc. Nat. Acad. Sci.* 82 (1985) 1604-1608.
- [21] M Meier, M Janosik, V Kery, JP Kraus, P Burkhard, Structure of human cystathionine β -synthase: a unique pyridoxal 5'-phosphate-dependent heme protein. *EMBO J.* 20 (2001) 3910-3916.
- [22] DH Sherman, S Li, LV Yermaliskaya, Y Kim, JA Smith, MR Waterman, LM Podust, The structural basis for substrate anchoring, active site selectivity, and product formation by P450 PikC from *Streptomyces venezuelae*. *J. Biol. Chem.* 281 (2006) 26289-26297.
- [23] F Arnesano, L Banci, I Bertini, J Faraone-Mennella, A Rosato, PD Barker, AR Fersht, The solution structure of oxidized *Escherichia coli* cytochrome b562. *Biochemistry* 38 (1999) 8657-8670.
- [24] M Paoli, BF Anderson, HM Baker, WT Morgan, A Smith, EN Baker, Crystal structure of hemopexin reveals a novel high-affinity heme site formed between two beta-propellor domains. *Nat. Struct. Biol.* 6 (1999) 926-931.
- [25] M Wirtz, V Oganessian, X Zhang, J Studer, M Rivera, Modulation of redox potentials in electron transfer proteins: Effects of complex formation on the active site microenvironment of cytochrome b5. *Faraday Discussions* 116 (2000) 221-234.
- [26] DB Goodin, DE McRee, The Asp-His-iron triad of cytochrome *c* peroxidase controls the reduction potential electronic structure, and coupling of the tryptophan free radical to the heme. *Biochemistry* 32 (1993) 3313-3324.

- [27] S Adachi, S Nagano, K Ishimori, Y Watanabe, I Morishima, T Egawa, T Kitagawa, R Makino, Roles of proximal ligand in heme proteins: replacement of proximal histidine of human myoglobin with cysteine and tyrosine by site-directed mutagenesis as models for P-450, chloroperoxidase, and catalase. *Biochemistry* 32 (1993) 241-252.
- [28] J Umbreit, Methemoglobin—it's not just blue: a concise review. *Amer. J. Hematol.* 82 (2007) 134-144.
- [29] CP Ponting, RR Russell, The natural history of protein domains. *Annu. Rev. Biophys. Biomol. Struct.* 31 (2002) 45-71.
- [30] RB Russell, Classification of protein folds. *Mol. Biotech.* 20 (2002) 17-28.
- [31] AD Moore, AK Björklund, D Ekman, E Bornberg-Bauer, A Elofsson, Arrangements in the modular evolution of proteins. *Trends Biochem. Sci.* 33 (2008) 444-451.
- [32] C Chothia, J Gough, Genomic and structural aspects of protein evolution. *Biochem. J.* 419 (2009) 15-28.
- [33] BC-H Lam, E Blumwald, Domains as functional building blocks of plant proteins. *Trends Plant Sci.* 7 (2002) 544-549.
- [34] SA Wolfe, L Nekludova, CO Pabo, DNA recognition by Cys₂His₂ zinc finger proteins. *Annu. Rev. Biophys. Biomol. Struct.* 3 (1999) 183-212.
- [35] J Nardelli, TJ Gibson, C Vesque, P Charnay, Base sequence discrimination by zinc-finger DNA-binding domains. *Nature* 349 (1991) 175-178.
- [36] KJ Brayer, DJ Segal, Keep your fingers off my DNA: protein-protein interactions mediated by C₂H₂ zinc finger domains. *Cell Biochem. Biophys.* 50 (2008) 111-131.
- [37] AH Fox, C Liew, M Holmes, K Kowalski, J Mackay, M Crossley, Transcriptional cofactors of the FOG family interact with GATA proteins by means of multiple zinc fingers. *EMBO J.* 18 (1999) 2812-2822.

- [38] SE Brenner, SCOP: Fold: TIM beta/alpha-barrel. <http://scop.mrc-lmb.cam.ac.uk/scop/data/scop.b.d.b.html>. Last updated November 2007. Accessed April 2009.
- [39] N Kannan, S Selvaraj, MM Gromiha, S Vishveshwara, Clusters in α/β barrel proteins: implications for protein structure, function, and folding: a graph theoretical approach. *PROTEINS: Struct. Funct. Genet.* 43 (2001) 103-112.
- [40] C Chu, Y Lai, H Huang, Y Sun, Kinetic and structural properties of triosephosphate isomerase from *Helicobacter pylori*. *PROTEINS: Struct. Funct. Bioinf.* 71 (2008) 396-406.
- [41] I Kursula, S Partanen, A Lambeir, RK Wierenga, The importance of the conserved Arg191–Asp227 salt bridge of triosephosphate isomerase for folding, stability, and catalysis. *FEBS Lett.* 518 (2002) 39-42.
- [42] B Schneider, T Knchel, B Darimont, M Hennig, S Deitrich, K Babinger, K Kirschner, R Sterner, Role of the N-terminal extension of the $(\beta\alpha)_8$ -barrel enzyme indole-3-glycerol phosphate synthase for its fold, stability, and catalytic activity. *Biochemistry* 44 (2005) 16405-16412.
- [43] K Suzuki, S Ito, A Shimizu-Ibuka, H Sakai, Crystal structure of pyruvate kinase from *Geobacillus stearothermophilus*. *J. Biochem.* 144 (2008) 305-312.
- [44] MS Jurica, A Mesecar, PJ Heath, W Shi, T Nowak, BL Stoddard, The allosteric regulation of pyruvate kinase by fructose-1,6-bisphosphate. *Structure* 6 (1998) 195-210.
- [45] S An, R Kumar, ED Sheets, SJ Benkovic, Reversible compartmentalization of de novo purine biosynthetic complexes in living cells. *Science* 320 (2008) 103-106.
- [46] RD Baker, CO Cook, DC Goodwin, Catalase-peroxidase active site restructuring by a distant and “inactive” domain. *Biochemistry* 45 (2006) 7113-7121.
- [47] CT Walsh, *Posttranslational Modifications of Proteins*. Roberts & Company Publishers, Greenwood Village, 2007.

- [48] AOW Stretton, The first sequence: Fred Sanger and insulin. *Genetics* 162 (2002) 527-532.
- [49] F Sanger, GM Air, BG Barrell, NL Brown, AR Coulson, CA Fiddes, CA Hutchison, PM Slocombe, M Smith, Nucleotide sequence of bacteriophage ϕ X174 DNA. *Nature* 265 (1977) 687-95.
- [50] SC Gill, PH von Hippel, Calculation of protein extinction coefficients from amino acid sequence data. *Anal. Biochem.* 182 (1989) 319-326.
- [51] CL Varnado, KM Hertwig, R Thomas, K Roberts, DC Goodwin, Properties of a novel periplasmic catalase-peroxidase from *Escherichia coli* O157:H7. *Arch. Biochem. Biophys.* 421 (2004) 166-174.
- [52] WR Hagen, EPR spectroscopy as a probe of metal centres in biological systems. *Dalton Trans.* (2006) 4415-4434.
- [53] S Basu, Whatever happened to...? Helium shortage • Cytokine Storm • Martian dust threat • Novel HIV drug. *Sci. Amer.* 297(4) (2007) 18.
- [54] WA Baase, WC Johnson, Circular dichroism and DNA secondary structure. *Nucleic Acids Res.* 6 (1979) 797-814.
- [55] MR Cheesman, C Greenwood, AJ Thomson, Magnetic Circular Dichroism of Hemoproteins. *Adv. Inorg. Chem.* 36 (1991) 203-255.
- [56] RC Bray, Sudden freezing as a technique for the study of rapid reactions. *Biochem. J.* 81 (1961) 189-193.
- [57] R Yalow, Development and proliferation of radioimmunoassay technology. *J. Chem. Ed.* 76 (1999) 767-768.
- [58] Scheering-Plough Animal Health Corp., Antibiotics, the basics. http://www.nuflo.com/_images/new/Antibiotic_Classes.pdf. Last updated June 2008. Accessed March 2009.

- [59] JD Buynak, Medicinal Outline. http://faculty.smu.edu/jbuynak/Medicinal_Outline_11_4_04.pdf. Last updated November 2004. Accessed March 2009.
- [60] MA Kohanski, DJ Dwyer, B Hayete, CA Lawrence, JJ Collins, A common mechanism of cellular death induced by bactericidal antibiotics. *Cell* 130 (2007) 797-810.
- [61] AR Zink, C Sola, U Reischl, W Grabner, N Rastogi, H Wolf, AG Nerlich, Characterization of *Mycobacterium tuberculosis* complex DNAs from Egyptian mummies by spoligotyping. *J. Clin. Microbiol.* 41 (2003) 359-367.
- [62] World Health Organization, Tuberculosis Fact Sheet. <http://www.who.int/mediacentre/factsheets/fs104/en/index.html>. Last updated March 2007. Accessed April 2009.
- [63] A Rattan, A Kalia, N Ahmad, Multidrug-resistant *Mycobacterium tuberculosis*: molecular perspectives. *Emerging Infectious Diseases* 4 (1998) 195-209.
- [64] Y Zhang, B Heym, B Allen, D Young, S Cole, The catalase-peroxidase gene and isoniazid resistance of *Mycobacterium tuberculosis*. *Nature* 358 (1992) 591-593.
- [65] B Heym, PM Alzari, N Honoré, ST Cole, Missense mutations in the catalase-peroxidase gene, *katG*, are associated with isoniazid resistance in *Mycobacterium tuberculosis*. *Mol. Microbiol.* 15 (1995) 235-245.
- [66] S Chouchane, I Lippai, R Magliozzo, Catalase peroxidase (*Mycobacterium tuberculosis*) catalysis and isoniazid activation. *Biochemistry* 39 (2000) 9975-9983.
- [67] B Lei, CJ Wei, SC Tu, Action mechanism of antitubercular isoniazid: Activation by *Mycobacterium tuberculosis* KatG, isolation and characterization of INH inhibitor. *J. Biol. Chem.* 275 (2000) 2520-2526.
- [68] GS Timmins, V Deretic, Mechanisms of action of isoniazid. *Mol. Microbiol.* 62 (2006) 1220-1227.

- [69] A Argyrou, MW Vetting, B Aladegbami, JS Blanchard, *Mycobacterium tuberculosis* dihydrofolate reductase is a target for isoniazid. *Nat. Struct. Mol. Biol.* 13 (2006) 408-413.
- [70] T Deemargan, X Carpena, R Singh, B Wiseman, I Fita, PC Loewen, Structural characterization of the Ser324Thr variant of the catalase-peroxidase (KatG) from *Burkholderia pseudomallei*, *J. Mol. Biol.* 345 (2005) 21-28.
- [71] S Yu, S Giroto, C Lee, RS Magliozzo, Reduced affinity for isoniazid in the S315T mutant of *Mycobacterium tuberculosis* KatG is a key factor in antibiotic resistance. *J. Biol. Chem.* 278 (2003) 14769-14775.
- [72] B Heym, Y Zhang, S Poulet, D young, S Cole, Characterization of the *katG* gene encoding a catalase-peroxidase required for the isoniazid susceptibility of *Mycobacterium tuberculosis*. *J. Bacteriol.* 175 (1993) 4255-4259.
- [73] VH Ng, JS Cox, AO Sousa, JD MacMicking, JD McKinney, Role of KatG catalase-peroxidase in mycobacterial pathogenesis: countering the phagocyte oxidative burst. *Mol. Microbiol.* 52 (2004) 1291-1302.
- [74] W Brunder, H Schmidt, H Karch, A novel catalase-peroxidase encoded by the large plasmid of enterohaemorrhagic *Escherichia coli* O157:H7. *Microbiology* 142 (1996) 3305-3315.
- [75] AM Junko, MA Sakurako, K Fumiaki, T Tomoko, W Haruo, Identification of a novel periplasmic catalase-peroxidase KatA of *Legionella pneumophila*. *FEMS Microbiol. Lett.* 176 (1999) 339-344.
- [76] P Bandyopadhyay, HM Steinman, Catalase-peroxidases of *Legionella pneumophila*: cloning of the *katA* gene and studies of KatA function. *J. Bacteriol.* 182 (2000) 6679-6686.

- [77] E Garcia, YA Nedialkov, J Elliott, VL Motin, RR Brubaker, Molecular characterization of KatY (antigen 5), a thermoregulated chromosomally encoded catalase-peroxidase of *Yersinia pestis*. *J. Bacteriol.* 181 (1999) 3114-3122.
- [78] BA Chromy, MW Choi, GA Murphy, AD Gonzales, CH Corzeett, BC Chang, JP Fitch, SL McCutchen-Maloney, Proteomic characterization of *Yersinia pestis* virulence. *J. Bacteriol.* 44 (2005) 15093-15105.
- [79] P Wojtaszek, Oxidative burst : an early plant response to pathogen infection. *Biochem. J.* 322 (1997) 681-692.
- [80] DE Heck, AM Vetrano, TM Mariano, JD Laskin, UVB light stimulates production of reactive oxygen species: unexpected role for catalase. *J. Biol. Chem.* 278 (2003) 22432-22436.
- [81] JM Wood, H Decker, H Hartmann, B Chavan, H Rokos, JD Spencer, S Hasse, MJ Thornton, M Shalhaf, R Paus, KU Schallreuter, Senile hair graying: H₂O₂-mediated oxidative stress affects human hair color by blunting methionine sulfoxide repair. *FASEB J* (2009) *In Press*.
- [82] P Chelikani, I Fita, PC Loewen, Diversity of structures and properties among catalases. *Cell. Mol. Life Sci.* 61 (2004) 192-208.
- [83] P Nicholls, I Fita, PC Loewen, Enzymology and structure of catalases. *Adv. Inorg. Chem.* 51 (2001) 51106.
- [84] P Jones, A Suggett, The catalase-hydrogen peroxide system: kinetics of catalatic action at high substrate concentrations. *Biochem. J.* 110 (1968) 617-620.
- [85] HB Dunford, JS Stillman, On the function and mechanism of action of peroxidases. *Coord. Chem. Rev.* 19 (1976) 187-251.
- [86] KG Welinder, Superfamily of plant, fungal and bacterial peroxidases. *Curr. Opin. Struct. Biol.* 2 (1992) 388-393.

- [87] V Fülöp, CJ Ridout, C Greenwood, J Hajdu, Crystal structure of di-haem cytochrome *c* peroxidase from *Pseudomonas aeruginosa*. *Structure* 3 (1995) 1225-1233.
- [88] LP Hager, PF Hollenberg, T Rand-Meir, R Chiang, D Doubek, Chemistry of peroxidase intermediates. *Ann New York Acad. Sci.* 244 (1975) 80-93.
- [89] GC Mills, Hemoglobin catabolism I. glutathione peroxidase, an erythrocyte enzyme which protects hemoglobin from oxidative breakdown. *J. Biol. Chem.* 229 (1957) 189-197.
- [90] JR Arthur, The glutathione peroxidases. *Cell. Mol. Life Sci.* 57 (2000) 1825-1835.
- [91] J Littlechild, Haloperoxidases and their role in biotransformation reactions. *Curr. Opin. Chem. Biol.* 3 (1999) 28-34.
- [92] R Floris, I Recio, B Berkhout, S Visser, Antibacterial and antiviral effects of milk proteins and derivatives thereof. *Curr. Pharm. Des.* 9 (2003) 1257-1275.
- [93] J Ruf, P Carayon, Structural and functional aspects of thyroid peroxidase. *Arch. Biochem. Biophys.* 445 (2006) 269-277.
- [94] G Nie, SD Aust, Effect of calcium on the reversible thermal inactivation of lignin peroxidase. *Arch. Biochem. Biophys.* 337 (1997) 225-231.
- [95] GRJ Sutherland, SD Aust, The effects of calcium on the thermal stability and activity of manganese peroxidase. *Arch. Biochem. Biophys.* 332 (1996) 128-134.
- [96] SJ George, M Kvaratskhelia, MJ Dilworth, RNF Thorneley, Reversible alkaline inactivation of lignin peroxidase involves the release of both the distal and proximal site calcium ions and bishistidine co-ordination of the haem. *J. Biochem.* 344 (1999) 237-244.
- [97] M Sundarmoothy, K Kishi, MH Gold, TL Poulos, The crystal structure of manganese peroxidase from *Phanerochaete chrysosporium* at 2.06-Å resolution. *J. Biol. Chem.* 269 (1994) 32759-32767.

- [98] R Margis, C Dunand, FK Texeira, M Margis-Pinheiro, Glutathione peroxidase family - an evolutionary overview. *FEBS J.* 275 (2008) 3959-3970.
- [99] J Lu, A Holmgren, Selenoproteins. *J. Biol. Chem.* 284 (2009) 723-727.
- [100] A Claiborne, JI Yeh, TC Mallett, J Luba, EJ Crane, V Charrier, D Parsonage, Protein-sulfenic acids: diverse roles for an unlikely player in enzyme catalysis and redox regulation. *Biochemistry* 38 (1999) 15407-15416.
- [101] SE Brenner, SCOP: Family: Di-heme cytochrome c peroxidase. <http://scop.mrc-lmb.cam.ac.uk/scop/data/scop.b.b.h.b.h.html>. Last updated November 2007. Accessed April 2009.
- [102] J Verdín, R Pogni, A Baeza, MC Baratto, R Basosi, R Vázquez-Duhalt, Mechanism of versatile peroxidase inactivation by Ca^{2+} depletion . *Biophys. Chem.* 121 (2006) 163-170.
- [103] N Kresge, RD Simoni, RL Hill, Classics: Britton Chance: olympian and developer of stop-flow methods. *J. Biol. Chem.* 279 (2004) 109-111.
- [104] B Chance, The kinetics of the enzyme-substrate compound of peroxidase. *J. Biol. Chem.* 151 (1943) 553-577.
- [105] A Claiborne, I Fridovich, Purification of the *o*-dianisidine peroxidase from *Escherichia coli* B. Physicochemical characterization and analysis of its dual catalytic and peroxidatic activities. *J. Biol. Chem.* 254 (1979) 4245-4252.
- [106] P Charalabous, J Risk, R Jenkins, A Birss, C Hart, J Smalley, Characterization of a bifunctional catalase peroxidase of *Burkholderia cenocepacia*. *FEMS Immunol. Med. Microbiol.* 50 (2007) 37-44.
- [107] M Fraaije, H Roubroeks, W Hagen, W van Berkel, Purification and characterization of an intracellular catalase-peroxidase from *Penicillium simplicissimum*. *Eur. J. Biochem.* 235 (1996) 192-198.

- [108] A Hochman, A Shemesh, Purification and characterization of a catalase-peroxidase from the photosynthetic bacterium *Rhodobacterium capsuata*. J. Biol. Chem. 262 (1987) 6871-6876.
- [109] C Jakopitsch, F Rüker, G Regelsberger, M Dockal, G Peschek, C Obinger, Catalase-peroxidase from the cyanobacterium *Synechocystis* PCC 6803: cloning, overexpression in *Escherichia coli*, and kinetic characterization. Biol. Chem. 380 (1999) 1087-1096.
- [110] K Johnsson, W Froland, P Schultz, Overexpression, purification, and characterization of the catalase-peroxidase KatG from *Mycobacterium tuberculosis*. J. Biol. Inorg. Chem. 272 (1997) 2834-2840.
- [111] SWM Kengen, FJ Bikker, WR Hagen, WM de Vos, J van der Oost, Characterization of a catalase-peroxidase from the hyperthermophilic archaeon *Archaeoglobus fulgidus*. Extremophiles 5 (2001) 323-332.
- [112] J Marcinkeviciene, R Magliozzo, J Blanchard, Purification and characterization of the *Mycobacterium smegmatis* catalase-peroxidase involved in isoniazid activation. J. Biol. Chem. 270 (1995) 22290-22295.
- [113] P Pongpon, CR Cooper, N Vanittanakom, Isolation and characterization of a catalase-peroxidase gene from the pathogenic fungus, *Penicillium marneffeii*. Med. Mycol. 43 (2005) 403-411.
- [114] H Youn, Y Yim, K Kim, YC Hah, S Kang, Spectral characterization and chemical modification of catalase-peroxidase from *Streptomyces* sp. J. Biol. Chem. 270 (1995) 13740-13747.
- [115] KG Welinder, Bacterial catalase-peroxidases are gene-duplicated members of the plant peroxidase superfamily. Biochim. Biophys. Acta 1080 (1991) 215-220.
- [116] Y Yamada, T Fujiwara, T Sato, N Igarashi, N Taanaka, The 2.0 Å crystal structure of catalase-peroxidase from *Haloarcula marismortui*. Nat. Struct. Biol. 9 (2002) 691-695.

- [117] X Carpena, S Loprasert, S Mongkolsuk, J Switala, PC Loewen, I Fita, Catalase-
peroxidase KatG of *Burkholderia pseudomallei* at 1.7 Å resolution . J. Mol. Biol. 327
(2003) 475-489.
- [118] T Bertrand, NAJ Eady, JN Jones, Jesmin, JM Nahgy, B Jamart-Gregoire, EL Raven,
KA Brown, Crystal Structure of *Mycobacterium tuberculosis* Catalase-Peroxidase. J.
Biol. Chem. 279 (2004) 38991-38999.
- [119] K Wada, T Tada, Y Nakamura, T Kinoshita, M Tamoi, S Shigeoka, K Nishimura,
Crystallization and preliminary x-ray diffraction studies of catalase-peroxidase from
Synechocystis PCC 7942. Acta Crystallogr. D Biol. Crystallogr. 58 (2002) 157-159.
- [120] W Blodig, AT Smith, WA Doyle, K Piontek, Crystal structure of prosthine and ox-
idatively processed lignin peroxidase expressed in *Escherichia coli* and of the W171F
variant that eliminates the redox active tryptophan 171. Implications for the reaction
mechanism. J. Mol. Biol. 305 (2001) 851-861.
- [121] M Gajhede, DJ Schuller, A Henriksen, AT Smith, TL Poulos, Crystal structure of
horseradish peroxidase C at 2.15 Å resolution. Nat. Struct. Biol. 4 (1997) 1032-1038.
- [122] MG Klotz, PC Loewen, The molecular evolution of catalatic hydroperoxidases: Evi-
dence for multiple lateral transfer of genes between prokaryota and from bacteria into
eukaryota. Molec. Biol. Evol. 20 (2003) 1098-1112.
- [123] Y Li, DC Goodwin, Vital roles of an interhelical insertion in catalase-peroxidase
bifunctionality. Biochem. Biophys. Res. Commun. 318 (2004) 970-976.
- [124] RA Ghiladi, KF Medzihradzky, PR Ortiz de Montellano, Role of the Met-Tyr-Trp
cross-link in *Mycobacterium tuberculosis* catalase-peroxidase (KatG) as revealed by
KatG(M255I). Biochemistry 44 (2005) 15093-15105.
- [125] G Smulevich, C Jakopitsch, E Droghetti, C Obinger, Probing the structure and bi-
functionality of catalase-peroxidases (KatG). J. Inorg. Biochem. 100 (2006) 568-585.

- [126] C Jakopitsch, M Auer, A Ivanvich, F R uker, PG Furtm uller, C Obinger, Total conversion of bifunctional catalase-peroxidase (KatG) to monofunctional peroxidase by exchange of a conserved distal side tyrosine. *J. Biol. Chem.* 278 (2003) 20185-20191.
- [127] X Carpena, B Wiseman, T Deemagarn, R Singh, J Switala, A Ivancich, I Fita, PC Loewen, A molecular switch and electronic circuit modulate catalase activity in catalase peroxidases. *EMBO J.* 6 (2005) 1156-1162.
- [128] X Carpena, B Wiseman, T Deemagarn, B Herguedas, A Ivanvich, R Singh, PC Loewen, I Fita, Roles for Arg426 and Trp111 in the modulation of NADH oxidase activity of the catalase-peroxidase KatG from *Burkholderia pseudomallei* inferred from pH-induced structural changes. *Biochemistry* 45 (2006) 5171-5179.
- [129] M Zamocky, G Regelsberger, C Jakopitsch, C Obinger, The molecular peculiarities of catalase-peroxidases. *FEBS Lett.* 492 (2001) 177-182.
- [130] RD Baker, CO Cook, DC Goodwin, Properties of catalase-peroxidase lacking its C-terminal domain. *Biochem. Biophys. Res. Commun.* 320 (2004) 833-839.
- [131] C Jakopitsch, M Auer, G Regelsberger, W Jantschko, PG Furtm uller, F R uker, C Obinger, Distal site aspartate is essential in the catalase activity of catalase-peroxidases. *Biochemistry* 42 (2003) 5292-5300.
- [132] C Jakopitsch, M Auer, G Regelsberger, W Jantschko, PG Furtm uller, F R uker, C Obinger, The catalytic role of the distal site asparagine-histidine couple in catalase-peroxidases. *Eur. J. Biochem.* 270 (2003) 1006-1013.
- [133] C Jakopitsch, E Droghetti, F Schmuckenschlager, PG Furtm uller, G Smulevich, C Obinger, Role of the main access channel of catalase-peroxidase in catalysis. *J. Biol. Chem.* 280 (2005) 42411-42422.

- [134] E Santoni, C Jakopitsch, C Obinger, G Smulevich, Comparison between catalase-peroxidase and cytochrome *c* peroxidase. The role of the hydrogen-bond networks for protein stability and catalysis. *Biochemistry* 43 (2004) 5792-5802.
- [135] Y Li, Ph.D. thesis (2004) Auburn University.
- [136] C Jakopitsch, D Kolarich, G Petutschnig, PG Furtmüller, C Obinger, Distal side tryptophan, tyrosine, and methionine in catalase-peroxidases are covalently linked in solution. *FEBS Lett.* 552 (2003) 135-140.
- [137] C Varnado, Ph.D. thesis (2006) Auburn University.
- [138] LJ Donald, OV Krokhin, HW Duckworth, B Wiseman, T Deemagarn, R Singh, J Switala, X Carpena, I Fita, PC Loewen, Characterization of the catalase-peroxidase KatG from *Burkholderia pseudomallei* by mass spectrometry. *J. Biol. Chem.* 278 (2003) 35687-35692.
- [139] S Yu, S Giroto, X Zhao, R Magliozzo, Rapid formation of compound II and a tyrosyl radical in the Y229F mutant of *Mycobacterium tuberculosis* catalase-peroxidase disrupts catalase but not peroxidase function. *J. Biol. Chem.* 278 (2003) 44121-44127.
- [140] C Jakopitsch, A Ivancich, F Schmuckenschlager, A Wanasinghe, G Pörtl, P Furtmüller, F Rüker, C Obinger, Influence of unusual covalent adduct on the kinetics and formation of radical intermediates in *Synechocystis* catalase-peroxidase. A stopped-flow and EPR characterization of the met²⁷⁵, tyr²⁴⁹, and arg⁴³⁹ variants. *J. Biol. Chem.* 279 (2004) 46082-46095.
- [141] RA Ghiladi, GM Knudsen, KF Medzihradzky, PR Montellano, The Met-Tyr-Trp cross-link in *Mycobacterium tuberculosis* catalase-peroxidase (KatG): autocatalytic formation and effect on enzyme catalysis and spectroscopic properties. *J. Biol. Chem.* 280 (2005) 22651-22663.

- [142] K Rangelova, S Giroto, G Gerfen, S Yu, J Suarez, L Metlitsky, R Magglio, Radical sites in *Mycobacterium tuberculosis* KatG identified using electron paramagnetic resonance spectroscopy, the three-dimensional crystal structure, and electron transfer couplings. *J. Biol. Chem.* 282 (2007) 6255-6264.
- [143] J Suarez, K Rangelova, A Jarzecki, J Manzerova, V Krymov, X Zhao, S Yu, L Metlitsky, G Gerfen, R Magglio, An oxyferrous heme/protein-based radical intermediate is catalytically competent in the catalase reaction of *M. tuberculosis* catalase-peroxidase (KatG). *J. Biol. Chem.* 284 (2009) 7017-7029.
- [144] R Singh, J Switala, PC Loewen, A Ivancich, Two [Fe(IV)=O Trp*] intermediates in *M. tuberculosis* catalase-peroxidase discriminated by multifrequency (9-285 GHz) EPR spectroscopy: reactivity toward isoniazid. *J. Am. Chem. Soc.* 129 (2007) 15954-15963.
- [145] A Ivancich, C Jakopitsch, M Auer, S Un, C Obinger, Protein-based radicals in the catalase-peroxidase of *Synechocystis* PCC 6803: a multifrequency EPR investigation of wild-type and variants on the environment of the heme active site. *J. Am. Chem. Soc.* 125 (2003) 14093-14102.
- [146] R Singh, B Wiseman, T Deemagarn, LJ Donald, HW Duckworth, X Carpena, I Fita, PC Loewen, Catalase-peroxidases (KatG) exhibit NADH oxidase activity. *J. Biol. Chem.* 279 (2004) 43098-43106.
- [147] C Jakopitsch, G Regelsberger, P Furtmüller, F Rüker, G Peschek, C Obinger, Engineering the proximal heme cavity of catalase-peroxidase. *J. Inorg. Biochem.* 91 (2002) 78-86.
- [148] SL Scott, WJ Chen, A Bakac, JH Espenson, Spectroscopic parameters, electrode potentials, acid ionization constants, and electron exchange rates of the 2,2'-azinobis(3-ethylbenzothiazoline-6-sulfonate) radicals and ions. *J. Phys. Chem.* 97 (1993) 6710-6714.

- [149] DP Nelson, LA Kiesow, Enthalpy of decomposition of hydrogen peroxide by catalase at 25°. (with molar extinction coefficients of H₂O₂ solutions in the uv). Anal. Biochem. 49 (1972) 474-478.
- [150] HB Dunford, *Heme Peroxidases*, John Wiley & Sons, Inc., New York, 1999, pp. 73-85.
- [151] C Jakopitsch, J Vlastis, B Wiseman, PC Loewen, C Obinger, Redox intermediates in the catalase cycle of catalase-peroxidases from *Synechocystis* PCC 6803, *Burkholderia pseudomallei*, and *Mycobacterium tuberculosis*. Biochemistry 46 (2007) 1183-1193.
- [152] JN Rodríguez-López, MA Gilabert, J Tudela, RNF Thorneley, F García-Cánovas, Reactivity of horseradish peroxidase compound II towards substrates: kinetic evidence for a two-step mechanism. Biochemistry 39 (2000) 13201-13209.
- [153] A Claiborne, I Fridovich, Chemical and enzymatic intermediates in the peroxidation of *o*-dianisidine by horseradish peroxidase. 1. Spectral properties of the products of dianisidine oxidation. Biochemistry 18 (1979) 2324-2329.
- [154] F Bosco, A Capolongo, B Ruggeri, Effect of temperature, pH, ionic strength, and sodium nitrate on activity of LiPs: Implications for bioremediation. Biorem. J. 6 (2002) 65-76.
- [155] DC Goodwin, T Grover, SD Aust, Roles of efficient substrates in enhancement of peroxidase-catalyzed oxidations. Biochemistry 36 (1997) 139-147.
- [156] E Derat, S Shaik, An efficient proton-coupled electron-transfer process during oxidation of ferulic acid by horseradish peroxidase: coming full cycle. J. Am. Chem. Soc. 128 (2006) 13940-13949.
- [157] R Marjaana, A Lambeir, N Ellfolk, B Dunford, A rapid-scan spectrometric and stopped-flow study of Compound I and Compound II of *Pseudomonas* cytochrome c peroxidase. Arch. Biochem. Biophys. 236 (1985) 714-719.

- [158] V Ximenes, L Catalani, A Campa, Oxidation of melatonin and tryptophan by an HRP cycle involving compound III. *Biochem. Biophys. Res. Commun.* 287 (2001) 130-134.
- [159] R Singh, B Wiseman, T Deemagarn, V Jha, J Switala, PC Loewen, Comparative study of catalase-peroxidases (KatGs). *Arch. Biochem. Biophys.* 471 (2008) 207-214.
- [160] C Jakopitsch, C Obinger, S Un, A Ivancich, Identification of Trp106 as the tryptophanyl radical intermediate in *Synechocystis* PCC 6803 catalase-peroxidase by multifrequency Electron Paramagnetic Resonance spectroscopy. *J. Inorg. Biochem.* 100 (2006) 1091-1099.
- [161] JK Falk, in KM Smith (Ed.), *Porphyrins and Metalloporphyrins*, Elsevier Publishing, New York, 1964, pp. 804-807.
- [162] S Chouchane, S Girotto, S Kapetanaki, JP Schelvis, S Yu, RS Magliozzo, Analysis of Heme Structural Heterogeneity in *Mycobacterium tuberculosis* Catalase-Peroxidase (KatG). *J. Biol. Chem.* 278 (2003) 8154-8162.
- [163] EW Svastits, JH Dawson, Models for ferrous cytochrome b₅: Sign inversions in the magnetic circular dichroism spectra of bis-imidazole ferrous porphyrin systems. *Inorg. Chim. Acta* 123 (1986) 83-86.
- [164] J Cheek, D Mendelman, TL Poulos, JH Dawson, A study of the K⁺-site mutant of ascorbate peroxidase: mutations of protein residues on the proximal side of the heme cause changes in iron ligation on the distal side. *J. Biol. Inorg. Chem.* 4 (1999) 64-72.
- [165] AE Pond, M Sono, EA Elenkova, DB Goodin, AM English, JH Dawson, Influence of protein environment on magnetic circular dichroism spectral properties of ferric and ferrous ligand complexes of yeast cytochrome c peroxidase. *Biospectroscopy* 5 (1999) S42-S52.

- [166] L Vickery, T Nozawa, K Sauer, Magnetic circular dichroism studies of low-spin cytochromes. Temperature dependence and effects of axial coordination on the spectra of cytochrome c and cytochrome b₅. *J. Am. Chem. Soc.* 98 (1976) 351-357.
- [167] MK Johnson, in L Que (Ed.), *Physical Methods in Bioinorganic Chemistry: Spectroscopy and Magnetism*, University Science Books, Sausalito, 2000, pp. 233-285.
- [168] W Hagen, TU Delft – Biomolecular EPR Spectroscopy. <http://www.bt.tudelft.nl/biomolecularEPRspectroscopy>.
- [169] T Deemagarn, B Wiseman, X Carpena, A Ivancich, I Fita, PC Loewen, Two alternative substrate paths for compound I formation and reduction in catalase-peroxidase KatG from *Burkholderia pseudomallei*. *PROTEINS: Struct. Funct. Bioinf.* 66 (2007) 219-228.
- [170] S Yu, S Chouchane, R Magliozzo, Characterization of the W321F mutant of *Mycobacterium tuberculosis* catalase peroxidase KatG. *Prot. Sci.* 11 (2002) 58-64.
- [171] H Heering, C Indiani, G Regelsberger, C Jakopitsch, C Obinger, G Smulevich, New insights into the heme cavity structure of catalase-peroxidase: A spectroscopic approach to the recombinant *Synechocystis* enzyme and selected distal cavity mutants. *Biochemistry* 41 (2002) 9237-9247.